TECHNICAL REPORT STANDARD TITLE PAGE

1. Report No.	2. Government Accession No.	3. Recipient's Catalog No.
FHWA/TX-83/8+247-4		

4. Title and Subtitle	5. Report Date
ESTIMATION OF THE FATIGUE LIFE OF A TEST BRIDGE FROM TRAFFIC DATA	May 1983
	6. Performing Organization Code

7. Author(s)	8. Performing Organization Report No.
Peter W. Hoadley, Karl H. Frank, and Joseph A. Yura	Research Report 247-4

9. Performing Organization Name and Address	10. Work Unit No.
Center for Transportation Research The University of Texas at Austin Austin, Texas 78712-1075	11. Contract or Grant No. Research Study 3-5-79-247
	13. Type of Report and Period Covered Interim
12. Sponsoring Agency Name and Address Texas State Department of Highways and Public Transportation; Transportation Planning Division P. O. Box 5051 Austin, Texas 78763	14. Sponsoring Agency Code

15. Supplementary Notes

Study conducted in cooperation with the U. S. Department of Transportation, Federal Highway Administration. Research Study Title: "Estimation of the Fatigue Life of Structural Steel Bridge Details"

16. Abstract

Fatigue studies were conducted on a twin-girder, multilaned highway bridge. Two types of stress histories were measured at several locations on the bridge. One type of stress history was measured during the passage of a test truck of known weight. Stress histories were measured for velocities of the test truck of 5, 35, and 50 m.p.h. The second type of stress history was measured under normal traffic conditions.

An effective stress range, S_{RE}, and number of cycles were computed from each measured stress history using the Rainflow Cycle Counting method in conjunction with Miner's linear damage rule. Other cycle counting methods are considered and compared with the Rainflow Cycle Counting method. The values of S_{RE} and number of cycles are used to compute fatigue-life estimates for the bridge. The fatigue-life estimates were computed as a function of the amount of fatigue damage occurring per hour and per day, and future increases in traffic and axle loads were considered.

The longitudinal-transverse stiffener intersection, LTSI, detail was found to control the fatigue life of the bridge. The estimated fatigue life for this detail was 50 to 85 years. A modified LTSI detail increased the fatigue life by a factor of three.

17. Key Words	18. Distribution Statement
fatigue studies, twin girder highway bridge, stress histories, test load, normal traffic, longitudinal-transverse stiffener intersection, service life	No restrictions. This document is available to the public through the National Technical Information Service, Springfield, Virginia 22161.

19. Security Classif. (of this report)	20. Security Classif. (of this page)	21. No. of Pages	22. Price
Unclassified	Unclassified	140	

Form DOT F 1700.7 (8-69)

ESTIMATION OF THE FATIGUE LIFE OF A TEST BRIDGE FROM TRAFFIC DATA

by

Peter W. Hoadley
Karl H. Frank
and
Joseph A. Yura

Research Report Number 247-4

"Estimation of the Fatigue Life of Structural Steel Bridge Details"

Research Project 3-5-79-247

Conducted for

Texas
State Department of Highways and Public Transportation
in cooperation with the
U. S. Department of Transportation
Federal Highway Administration

by the

CENTER FOR TRANSPORTATION RESEARCH
BUREAU OF ENGINEERING RESEARCH
THE UNIVERSITY OF TEXAS AT AUSTIN

May 1983

The contents of this report reflect the views of the authors who are responsible for the facts and accuracy of the data presented herein. The contents do not necessarily reflect the views or policies of the Federal Highway Administration. This report does not constitute a standard, specification or regulation.

P R E F A C E

The study reported herein was conducted at the Phil M. Ferguson Structural Engineering Laboratory, Department of Civil Engineering, The University of Texas at Austin. This project, "Estimation of the Fatigue Life of Structural Steel Bridge Details," was sponsored by the Texas Department of Highways and Public Transportation and the Federal Highway Administration and administered through the Center for Transportation Research under Study Number 3-5-79-247.

Sincere thanks are due various support personnel of the Phil M. Ferguson Structural Engineering Laboratory. Mr. Richard Marshall and Mr. Dan Perez supervised and assisted in the operation of the electronic data acquisition equipment and related components. Mrs. Laurie Golding aided in the purchasing of the items required for field testing. Mr. Gorham Hinckley and Mr. George Moden assisted in the preparations of the field tests. Mr. Frank Endres developed the computer software needed to reduce the large amounts of field test data. Mrs. Tina Robinson carefully typed the manuscript.

Special thanks are given to Research Assistants Antonio Leite, Ashok Gupta, Dave Platten, and John Pass for their assistance in the areas of computer work, laboratory work, and field testing.

Liaison with the Texas Department of Highways and Public Transportation was maintained through contact representatives Bob Reed and Gerry Fox. Their cooperation in the field testing was invaluable. Mr. Randy Losch was the contact representative for the Federal Highway Administration.

S U M M A R Y

Fatigue studies were conducted on a twin-girder, multilaned highway bridge. Two types of stress histories were measured at several locations on the bridge. One type of stress history was measured during the passage of a test truck of known weight. Stress histories were measured for velocities of the test truck of 5, 35, and 50 m.p.h. The second type of stress history was measured under normal traffic conditions.

An effective stress range, S_{RE}, and number of cycles were computed from each measured stress history using the Rainflow Cycle Counting method in conjunction with Miner's linear damage rule. Other cycle counting methods are considered and compared with the Rainflow Cycle Counting method. The values of S_{RE} and number of cycles are used to compute fatigue-life estimates for the bridge. The fatigue-life estimates were computed as a function of the amount of fatigue damage occurring per hour and per day, and future increases in traffic and axle loads were considered.

The longitudinal-transverse stiffener intersection, LTSI, detail was found to control the fatigue life of the bridge. The estimated fatigue life for this detail was 50 to 85 years. A modified LTSI detail increased the fatigue life by a factor of three.

I M P L E M E N T A T I O N

The results of the analysis contained in this report indicate that the service life of the bridge is controlled by fatigue behavior of the longitudinal-transverse stiffener intersection (LTSI). The estimated fatigue life of this detail is 50 to 85 years. Given the uncertainties of the prediction of future traffic densities, vehicle weights, and the scatter in fatigue test results, the actual fatigue life may be even smaller.

A simple retrofit procedure, documented in the project's final report, improves the fatigue life considerably. The increase in fatigue life is at least a factor of 3. Therefore, it is recommended that this retrofit be applied to the bridge studied and to other bridges with similar details.

TABLE OF CONTENTS

Chapter Page

L I S T O F T A B L E S

Table Page

L I S T O F F I G U R E S

Figure Page

N O T A T I O N

A = constant which is a function of detail geometry

ADT = average daily traffic

ADTT = average daily truck traffic

D = number of days in the service life of a bridge

L = fatigue life in units of time

m = years to failure

n = material constant

n_i = number of cycles at a particular stress range, S_{Ri}

N = number of cycles

N_i = fatigue life in cycles at a particular stress range, S_{Ri}

N_L = fatigue life in minutes

N_{LT} = fatigue life in number of test trucks

N_M = cycles per minute

N_T = cycles per test truck

N_Y = cycles per year

q = decimal equivalent of the annual percentage increase in axle loads

r = decimal equivalent of the annual percentage increase in cycles

S_R = stress range, ksi

S_{Ri} = stress range for the interval in a stress histogram, ksi

S_{RD} = design stress range, ksi

$\frac{S_{RD}}{S_{RM}}$ = dispersion ratio

S_{RE} = effective stress range, ksi

T = fatigue life in terms of number of test trucks

TTD = number of test trucks per day

Y = fatigue life in years

γ_i = fraction of the total number of cycles at S_{Ri}

CHAPTER 1

INTRODUCTION

1.1 History of the Fatigue of Welded Structures

The early fatigue specifications for welded structures were based on allowable maximum stresses expressed in terms of the stress ratio, R, which is defined as the algebraic ratio of the minimum and maximum stress. Until 1965, the American Association of State Highway Officials, AASHO, used the allowable maximum stress concept as a basis for the fatigue specifications of welded steel bridges. New steel bridge fatigue provisions were adopted by AASHO in 1965 where the allowable fatigue stress was still based on the allowable stress with provisions for stress ratio and steel yield strength. A major revision of the AASHO fatigue specifications occurred in 1973. The new provisions were based on a comprehensive study on steel beams with various weld details.[1,2] The study was designed to determine the significance of the parameters believed to be important in fatigue behavior. Results from these studies have shown that the fatigue life, N, is related to the applied stress range, S_R, as follows:

$$N = A \times S_R^{-n} \tag{1.1}$$

where A and n are empirical constants. The value of A is a function of the fatigue behavior of a detail and n was found to approximately equal 3 for welded steel details. The study showed the effect of R was not significant for welded details. These fatigue studies were used to develop design curves relating stress range to fatigue life.

1.2 AASHTO Design Curves

The American Association of State Highway and Transportation Officials, AASHTO, developed design curves, shown in Fig. 1.1, which divide welded details into six categories.[3] In order to use the design curves an engineer would determine the design stress range for a particular detail and use the appropriate S_R - N curve to determine the fatigue life.

The AASHTO design curves were developed from fatigue tests using a constant amplitude stress history as shown in Fig. 1.2. Bridge details, however, are subject to variable amplitude stress histories caused by traffic loading. Figure 1.3 is the stress history of a flange in a longitudinal girder of a typical highway bridge described and studied in this report, and it illustrates the variable amplitude stress histories experienced by bridge details. Bridge details subjected to variable amplitude stress histories are designed with curves developed from constant amplitude stress histories. Therefore, a relationship needs to be developed between variable amplitude stress histories and constant amplitude stress histories so the AASHTO design curves can be applied in the design of bridge details.

1.3 Derivation of Effective Stress Range

One method of relating variable amplitude stress histories to a constant amplitude stress history is to assume fatigue damage accumulates in a linear fashion as suggested by Miner.[4] Miner's linear damage equation is given as follows:

$$\sum \frac{n_i}{N_i} = 1.0 \qquad (1.2)$$

where n_i is the number of cycles at a stress range S_{Ri} in a variable amplitude stress range spectrum and N_i is the fatigue life at S_{Ri}.

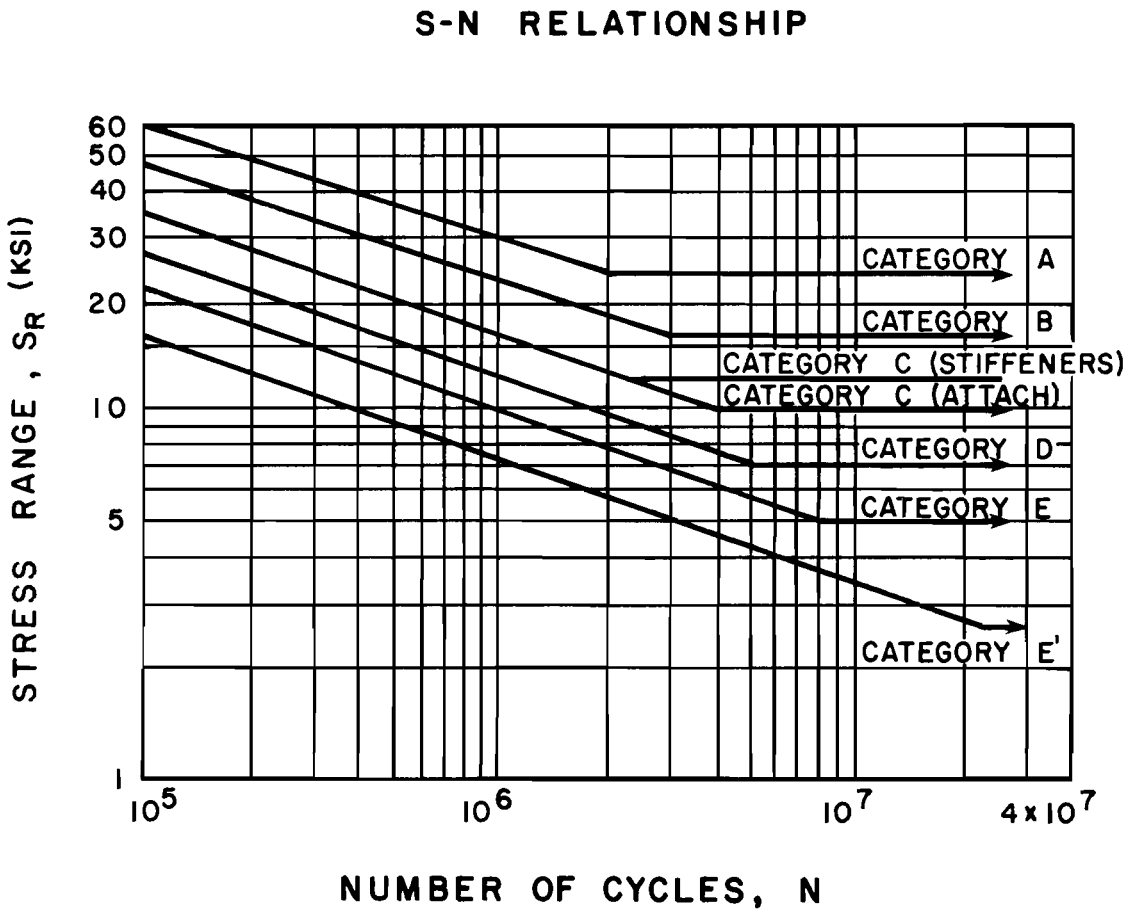

Fig. 1.1 Design stress range curves for Categories A through E′

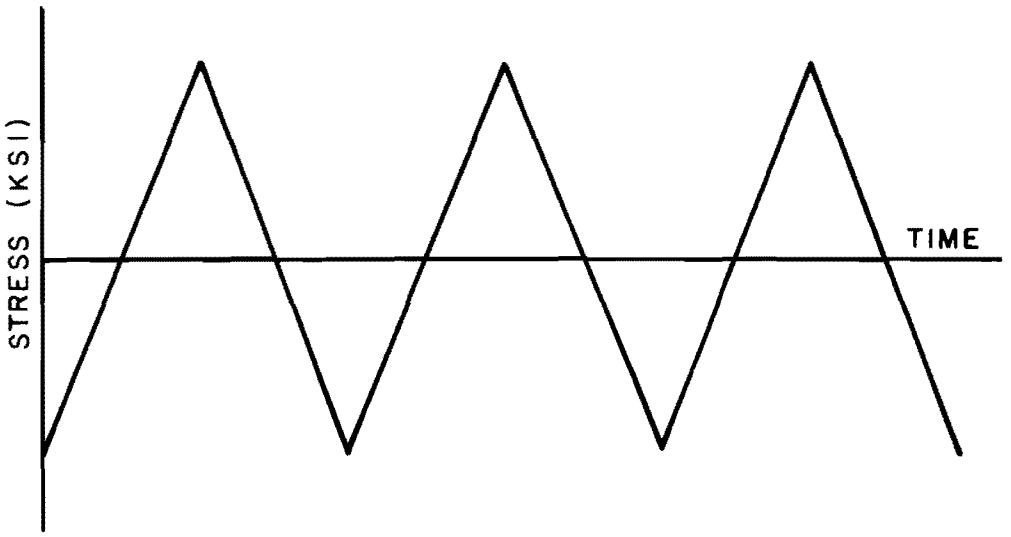

Fig. 1.2 Constant amplitude stress history

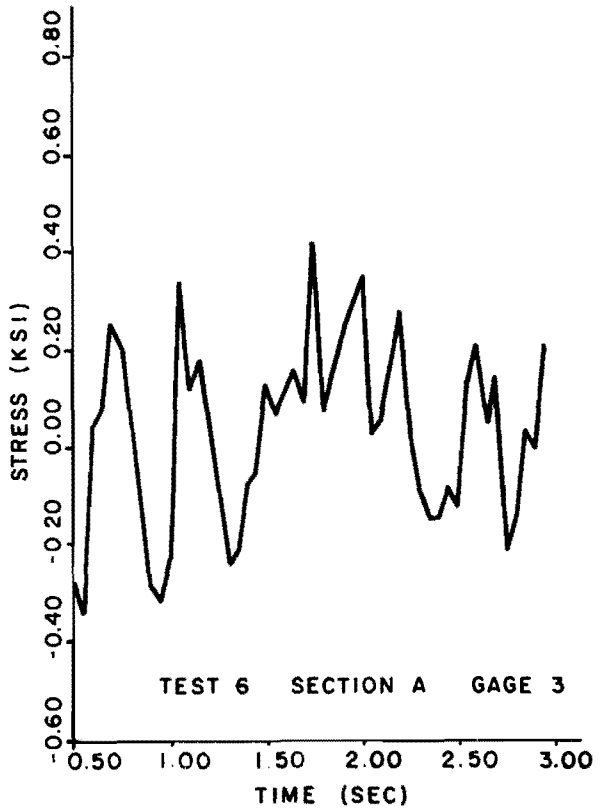

Fig. 1.3 Variable amplitude stress history

The fatigue life N_i may be written in terms of the stress range S_{Ri} as follows:

$$N_i = AS_{Ri}^{-n} \tag{1.3}$$

Substituting Eq. (1.3) into Eq. (1.2) yields:

$$\sum \frac{n_i}{AS_{Ri}^{-n}} = 1.0 \tag{1.4}$$

The variable n_i may be written as a function of the total number of cycles to failure, N, in the following manner:

$$n_i = \gamma_i \times N \tag{1.5}$$

where γ_i equals the fraction of the total number of cycles at S_{Ri}. Substituting the equation for n_i into Eq. (1.4) and rearranging yields:

$$\frac{N}{A} \sum \gamma_i S_{Ri}^n = 1.0 \tag{1.6}$$

A new parameter called the effective stress range can be defined as follows:

$$S_{RE}^n = \sum \gamma_i S_{Ri}^n \tag{1.7}$$

where S_{RE} is the effective stress range. Substituting S_{RE} into Eq. (1.6) and rearranging yields:

$$N = AS_{RE}^{-n} \tag{1.8}$$

where N is the total number of variable amplitude stress range cycles.

Equation (1.8) is in the same form as Eq. (1.1) relating constant amplitude stress range, S_R, to N. Therefore, the effective stress range is defined as the constant amplitude stress range which

would produce the same fatigue life as the variable stress history from which it was derived.

A study was conducted by U.S. Steel to determine the reliability of the effective stress range as it relates variable amplitude stress histories to a constant amplitude stress range.[5] Test specimens were subjected to various distributions of stress range and tested to failure. The effective stress range and cycles to failure for each test were compared to data collected at constant amplitude stress ranges. Figure 1.4 presents a portion of the data collected from these tests.

Figure 1.4 presents data from tests performed on welded steel beams. The steel beams were subjected to three distributions of stress range. Figure 1.4 shows the stress range distributions used in these tests. The parameter S_{RD}/S_{RM} is called the dispersion ratio and describes the variation of the stress range. A value of S_{RD}/S_{RM} equal to 0 implies a constant amplitude stress range while values of S_{RD}/S_{M} greater than 0.0 imply a variable amplitude stress range spectrum. The solid line in Fig. 1.4 is a linear fit to the constant amplitude data. The graph shows that the effective stress range is a reasonable method of relating variable amplitude data with constant amplitude data.

A stress range histogram must be developed from a variable amplitude stress history in order to compute the effective stress range. To obtain the cycles and stress ranges from a variable amplitude stress history needed for a stress range histogram, some type of cycle counting scheme must be employed. Several cycle counting methods are available and the major methods are discussed in Chapter 2.

1.4 Objectives of This Study

The purpose of this study is to estimate the fatigue life of an in-service welded steel girder bridge using stress histories measured under normal traffic conditions and under a known load.

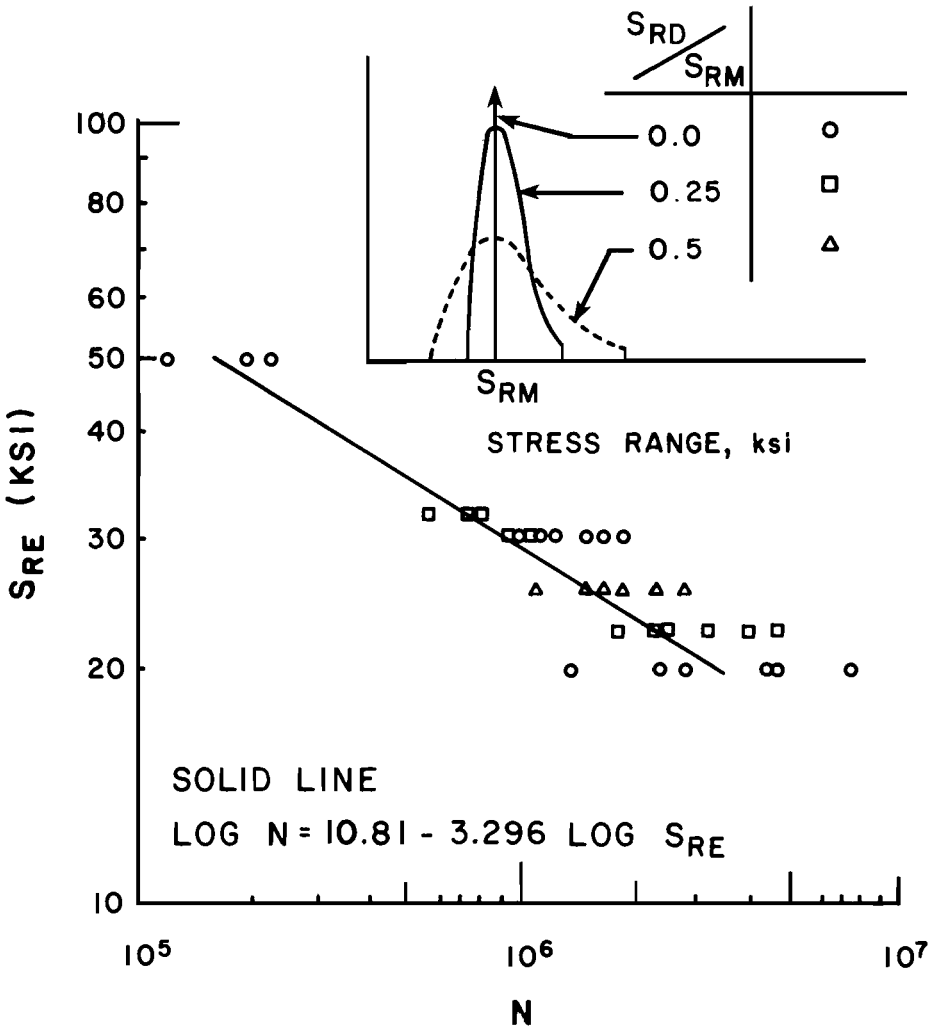

Fig. 1.4 Data from U.S. Steel tests relating constant amplitude data with variable amplitude data

Several cycle counting methods may be used to analyze the measured stress histories. The reliability of these cycle counting methods in predicting fatigue life when used in conjunction with Miner's law is discussed in Chapter 2. The Rainflow Cycle Counting method is used with the measured stress histories to compute effective stress ranges and the number of stress range cycles associated with each stress history, and is presented in Chapter 3. The effective stress ranges and corresponding number of cycles are used to compute a fatigue-life estimate for particular welded details. These fatigue-life estimates are presented and discussed in Chapter 4.

Two types of stress histories were obtained from the highway bridge. The first type was produced by the passage of a test truck over the bridge and the second was produced by traffic loading. Fatigue-life estimates computed from these two types of stress histories are expressed in terms of the number of trucks and of years of normal traffic required for a fatigue failure.

Application of the results is included in Chapter 4 and final conclusions from the study are presented in Chapter 5.

CHAPTER 2

CYCLE COUNTING METHODS

Several cycle counting methods have been developed which may be used to count stress cycles in complicated stress histories.[9,10,11,12,13,14,15] In general, each method has been developed in response to a particular problem. Cycle counting methods are used to correlate variable amplitude stress histories, similar to the one shown in Fig. 2.1, with constant amplitude stress histories. Cycle counting methods tend to fall into three categories: peak counting, range counting and level crossing methods. Each type of method has its advantages and disadvantages. Generally the Range Pair, Rainflow and Reservoir cycle counting methods are the most popular.[9] These, as well as other cycle counting methods, will be discussed in detail later in this chapter.

2.1 Peak Counting Methods

All of the peak counting methods are concerned with the peaks of a stress history.[11,14,15] The Peak Count method identifies all the maximum and minimum points of a stress history. This method reduces a stress history to full-cycle stress ranges which are a series of deviations from a datum level. Given the stress history in Fig. 2.2a, the Peak Count method yields the full-cycle stress ranges shown in Fig. 2.2b. The Peak Count method tends to magnify some small stress ranges. Peak numbers 2 and 4 in Fig. 2.2a become full-cycle stress ranges of 4 and 5 ksi, respectively, which are exaggerations of the actual stress ranges.

The Zero Crossing Peak Count method is a modification of the Peak Count method.[11,15] This method considers only the

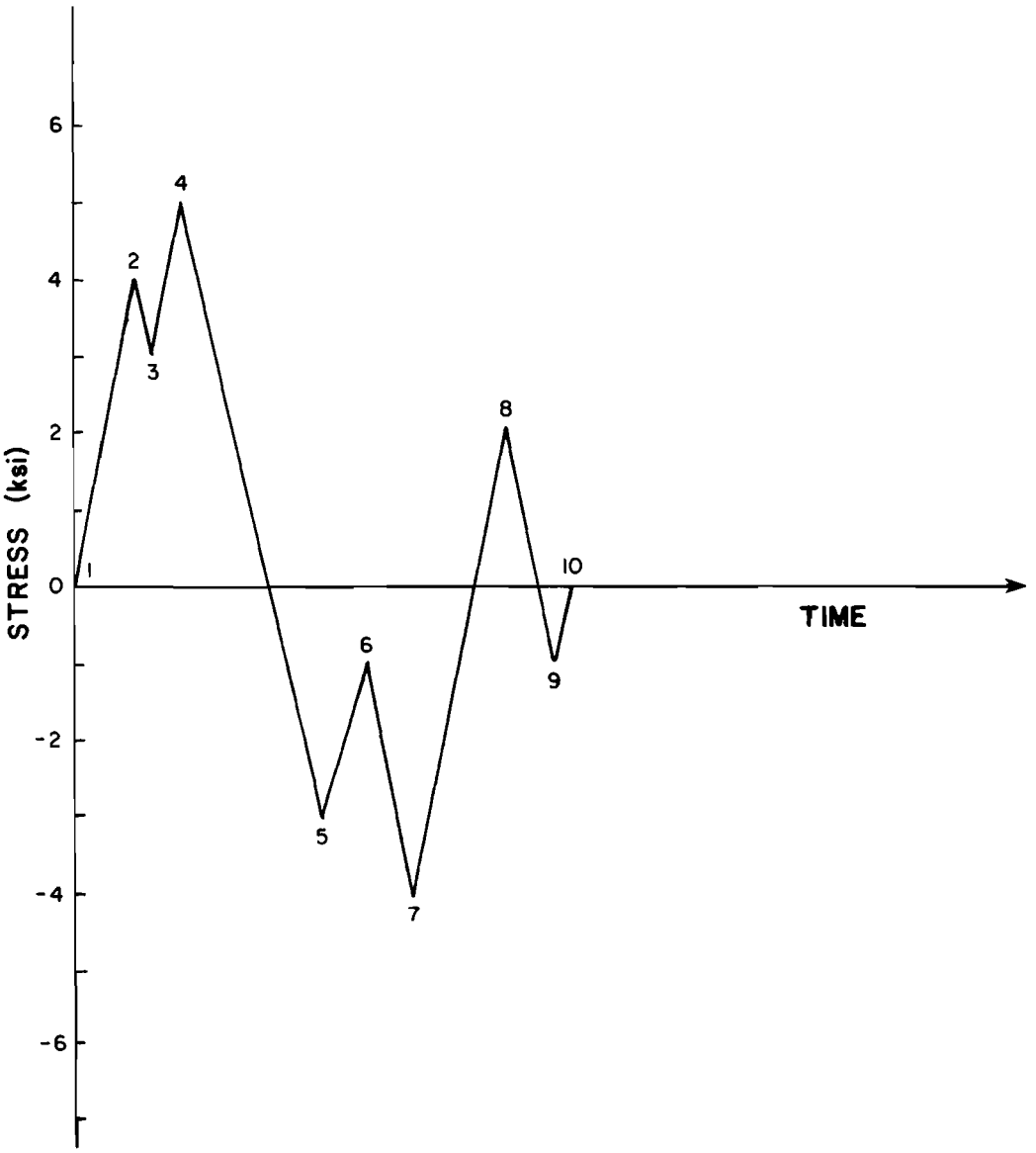

Fig. 2.1 Typical variable amplitude stress history

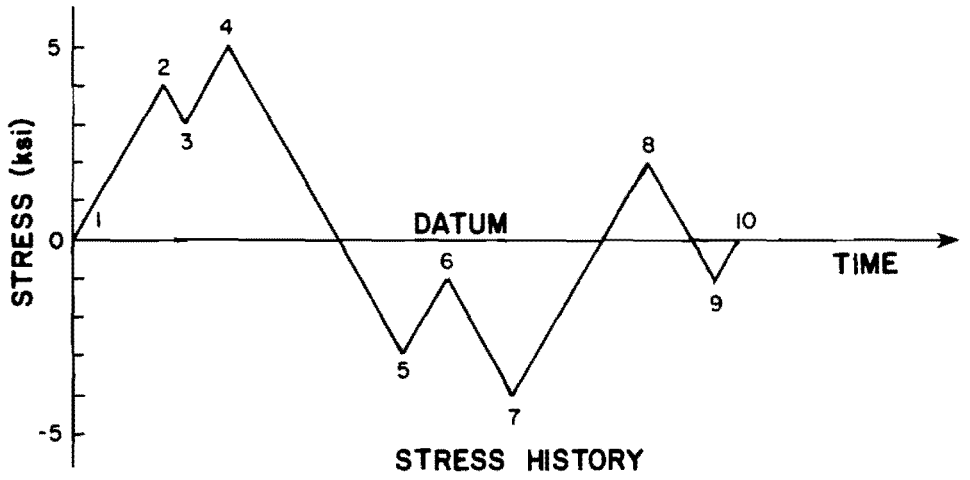

(a)

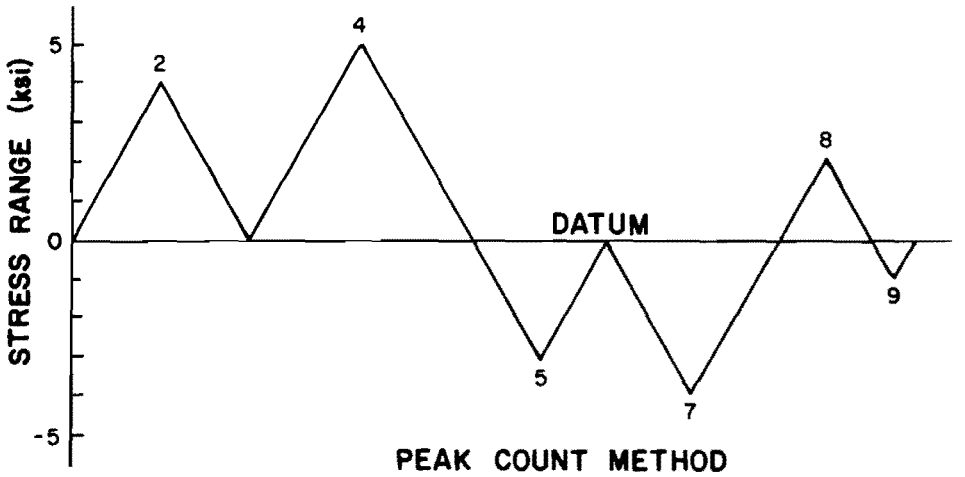

(b)

Fig. 2.2 Peak Count method on variable amplitude stress history

absolute maximum or minimum points between two successive zero level crossings. The stress history shown in Fig. 2.3a yields the full-cycle stress ranges shown in Fig. 2.3b by the Zero Crossing Peak Count method. One shortcoming with this cycle counting method is that interruptions of the main cycle between zero level crossings are not counted even though these cycles may be significant. The small cycles between points 1 and 4 and points 5 and 7 in Fig. 2.3 are not counted by this method.

Both of the above methods provide results which are not consistent with laboratory data using a sinusoidal load history. For example, n cycles of a constant amplitude stress history with a stress range of S_R would be counted as 2n cycles of a stress range $S_R/2$. This incorrectly predicts fatigue performance when used in conjunction with the Miner cumulative damage rule.

2.2 Range Counting Methods

The Range Count method identifies half-cycle stress ranges between relative maximum and minimum points.[11,14,15] Each range is paired with a range of equal value, but in the opposite direction, to form complete cycles. Table 2.1 contains the half-cycle stress ranges and the complete cycles for the stress history shown in Fig. 2.4. One problem with range count methods is that many ranges cannot be paired with others to form complete cycles. The half-cycle stress range between points 1 and 2 cannot be paired with another half-cycle stress range because there are no stress ranges of the same magnitude. The half-cycle stress range between points 3 and 4 cannot be paired with the stress range between points 5 and 6 because they are acting in the same direction. Half-cycle stress ranges cannot be used in conjunction with Miner's cumulative damage rule.

Large stress ranges may not be recognized by the Range Count method. Consider a stress history consisting of small load cycles at a high frequency superimposed on a large cycle of lower frequency

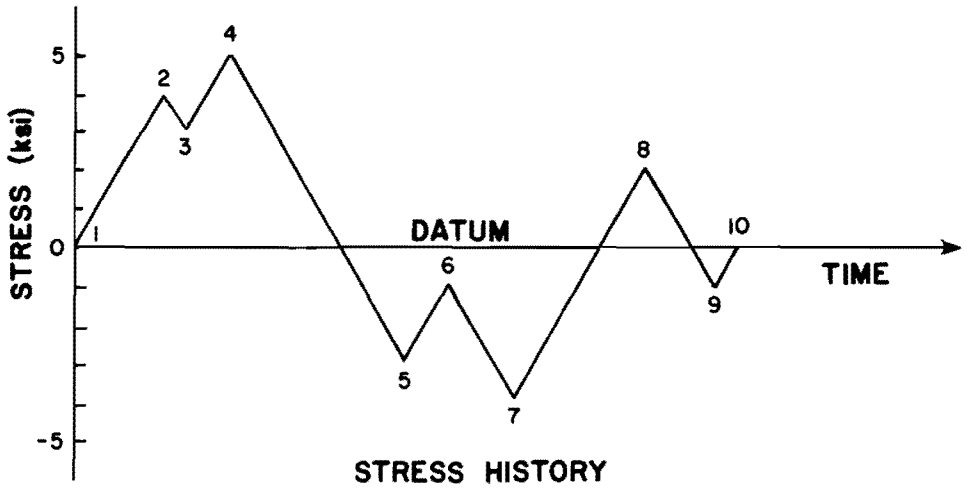

(a)

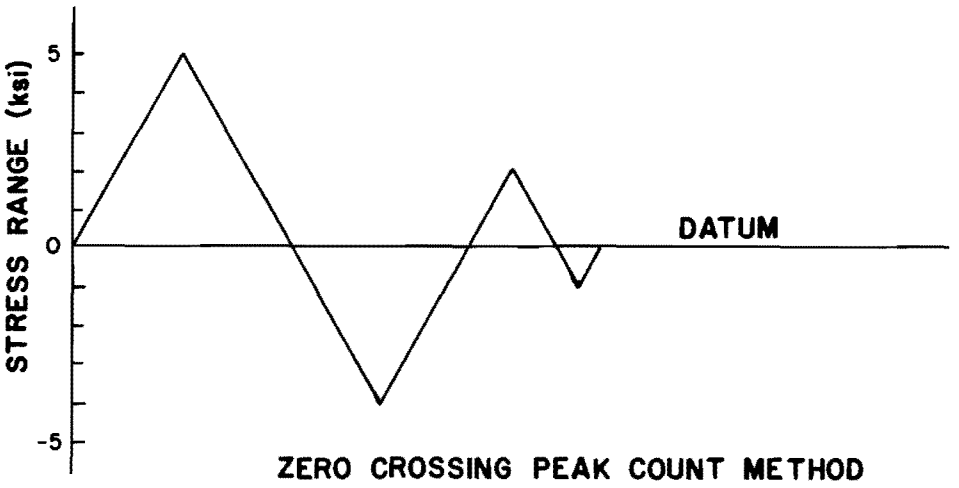

(b)

Fig. 2.3 Zero Crossing Peak Count method on variable amplitude stress history

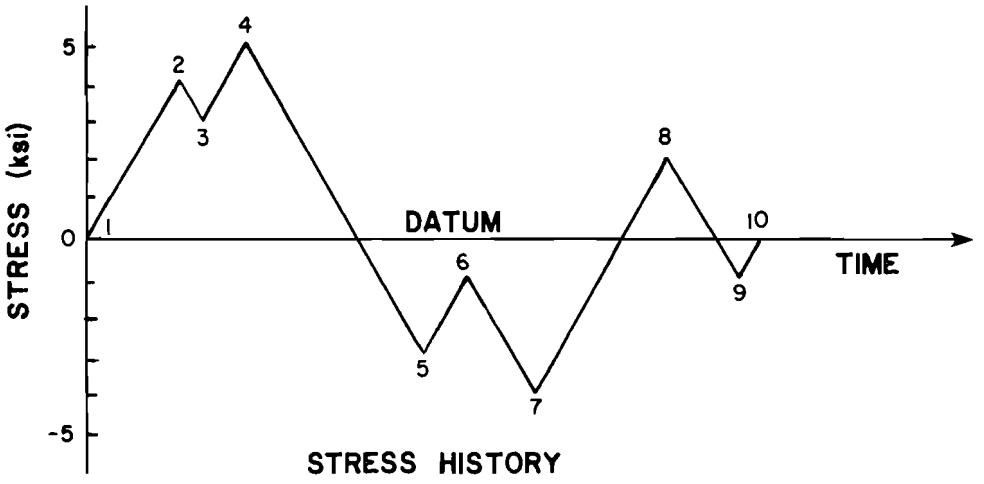

Fig. 2.4 Variable amplitude stress history

TABLE 2.1 CYCLES COUNTED BY THE RANGE COUNT METHOD

Half Cycles	Range (ksi)	Completed Cycles
1-2	4	--
2-3	1	2-3, 9-10
3-4	2	--
4-5	8	--
5-6	2	--
6-7	3	6-7, 8-9
7-8	6	--
8-9	3	--
9-10	1	--

as shown in Fig. 2.5. Such a stress history may occur in a member vibrating at its natural frequency while being subjected to a sinusoidal load at a lower frequency. The Range Count method would count ranges between successive maximum and minimum points therefore neglecting the large range between points 1 and 2.

2.3 Level Crossing Methods

The Level Crossing method involves the establishment of several stress levels or boundaries.[11,14,15] The number of times a stress history crosses these predetermined stress levels in an increasing direction is recorded. Mean levels and the number of peaks cannot be deduced from this method.

2.4 Range Pair Method

The Range Pair method is in the family of range counting methods.[11,14,15] This method, illustrated in Fig. 2.6, counts a half-cycle stress range if it can be paired with a subsequent half-cycle stress range of equal magnitude in the opposite direction. Each peak of the stress history, taken in subsequent order, is considered the initial peak of a stress range. If the initial peak is a minimum, a half-cycle is counted between this minimum and the absolute maximum which occurs between it and the next lower minimum. For example, a half-cycle stress range is counted between minimum point 1 and maximum point 4 in Fig. 2.6a. Likewise, if the initial peak of a stress range is a maximum, a half-cycle is counted between this maximum and the absolute minimum which occurs before the next greater maximum. For example, a half-cycle stress range is counted between maximum point 2 and minimum point 3. Each half-cycle stress range counted is paired with the next stress range of equal magnitude and in the opposite direction to form one complete cycle. For example, part of the stress history between points 3 and 4 is paired with the initial stress range between 2 and 3. All initial stress ranges are outlined with solid lines in Fig. 2.6b while all stress ranges paired with initial ranges

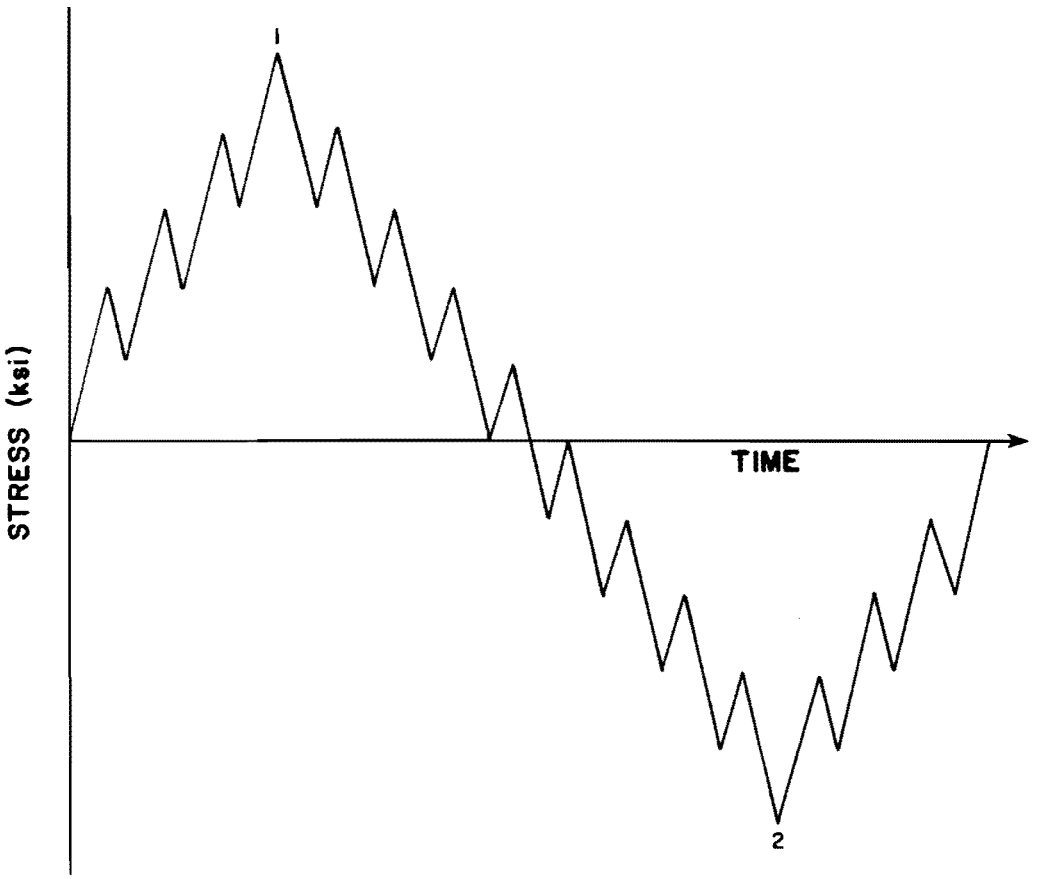

Fig. 2.5 Low frequency loading with superimposed high frequency vibrations

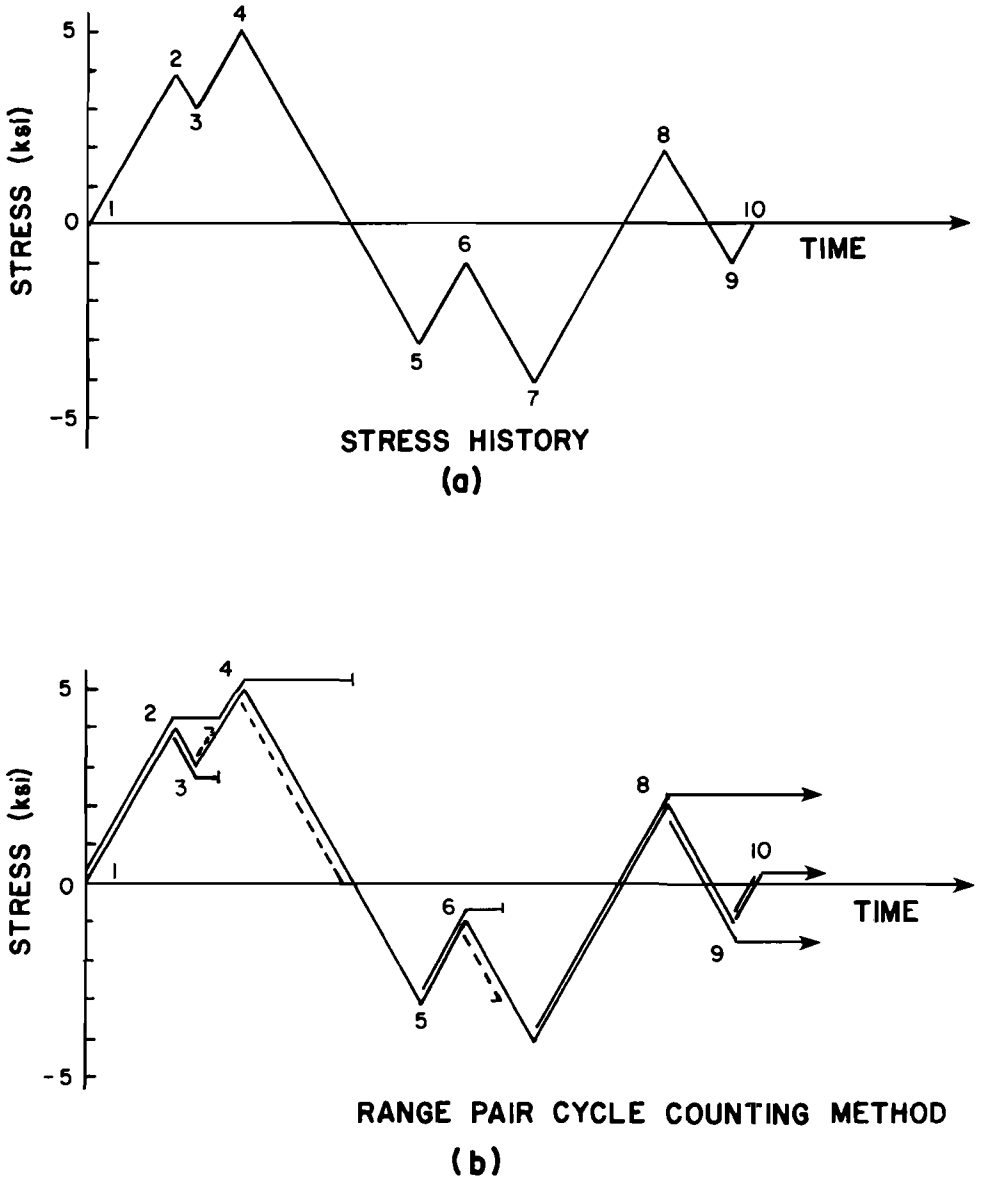

Fig. 2.6 Range Pair cycle counting method on a variable amplitude stress history

are outlined with dotted lines. A peak cannot be considered as an initial point in a range if the history immediately following has been paired with a previously counted stress range. For example, point 3 cannot be used as the initial point of a half cycle stress range because the history immediately following has been paired with the initial range between points 2 and 3. Some parts of the stress history are not considered in forming complete cycles and some half-cycles cannot be paired with others to form complete cycles.

2.5 Rainflow Counting Method

The Rainflow Cycle Counting method counts cycles using "raindrops" which roll down the stress history to define stress ranges.[9] In order to apply the Rainflow Counting method to a specific stress history, the stress history must first be rotated ninety degres so the horizontal axis points down, as shown in Fig. 2.7b. A raindrop is placed at each peak and is allowed to roll down the stress history much like rain rolling down a series of corrogations in a wall. A raindrop which begins at a minimum point is allowed to roll down the stress history until it falls opposite another minimum less than the minimum at which it started. For example, a raindrop which begins at point 1 rolls down the stress history to point 2. At point 2 the raindrop falls onto the sloping part of the stress history between points 3 and 4, and continues to roll down the stress history to point 4. At point 4, the raindrop falls and stops opposite point 5 since point 5 is a minimum less than initial point 1. In the same way, a raindrop which begins at a maximum point is allowed to roll down the stress history until it falls opposite a maximum point greater than the maximum at which it started. For example, a raindrop which begins at point 2 rolls down the stress history to point 3. At point 3 the raindrop falls off and stops opposite point 4 since point 4 is a greater maximum than the initial point 2. A raindrop cannot continue to roll down the stress history when it comes in contact

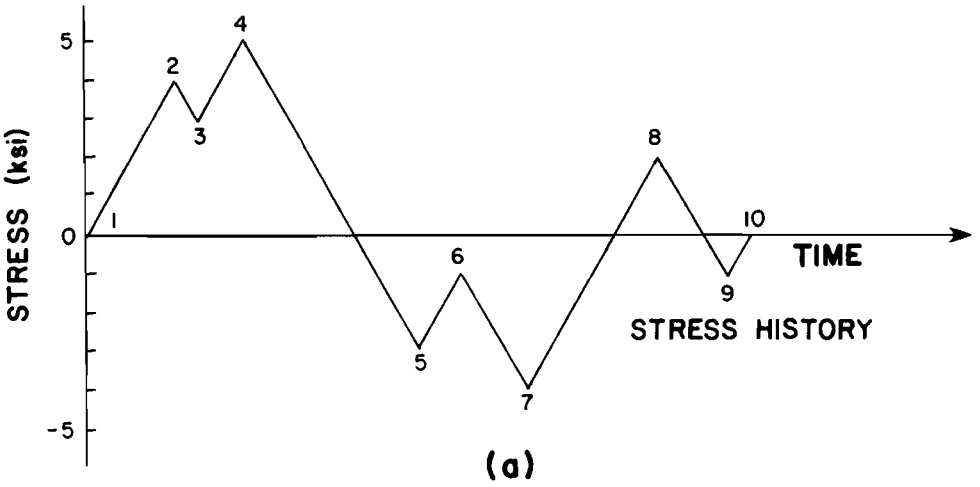

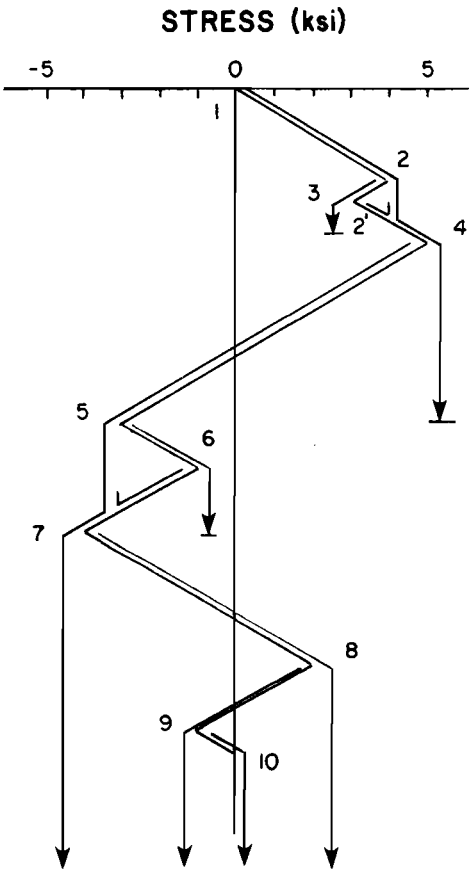

(b)

RAINFLOW CYCLE COUNTING METHOD

Fig. 2.7 Rainflow Counting method or variable amplitude stress history

with a part of the stress history which is already "wet" as a result of a raindrop from a preceding peak. A stress range which corresponds to one-half of a cycle is counted between the peak where a raindrop begins and where it ends. For example, a half-cycle stress range is counted between points 2 and 3. Complete cycles are created by combining half-cycles of equal stress range and opposite sense. For example, the half-cycle between points 2 and 3 is paired with the half-cycle between points 3 and 2′.

2.6 Modification to Counting Scheme to Eliminate Half Cycles

The Rainflow counting method yields a set of complete cycles and a set of half cycles which cannot be paired. The Range Pair method does not use all of the stress history when pairing half cycles. The Rainflow method, however, does use all parts of the stress history. Half cycles cannot be used in conjunction with Miner's linear damage rule, and it is desired that all parts of the stress history should be used to define stress ranges and corresponding cycles.

The shortcomings of these two counting methods may be solved by modifying the stress history. A modified stress history is obtained by moving the portion of the stress history before the absolute maximum to the end of the stress history. This modification is illustrated in Fig. 2.8b for the stress history in Fig. 2.8a. The portion of the stress history preceding the absolute maximum is removed and added to the end of the stress history. The cycle counting begins at the absolute maximum of the stress history. Both the Rainflow method and the Range Pair method yield complete cycles when applied to the modified stress history. Figure 2.9 illustrates how the Rainflow and Range Pair cycle counting methods are applied to the modified stress history. Notice that both methods recognize the same cycles and stress ranges.

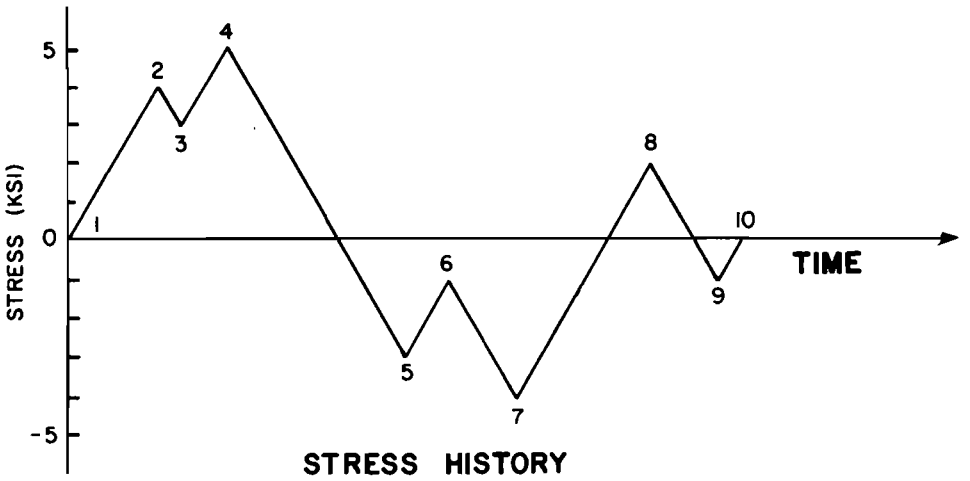

(a)

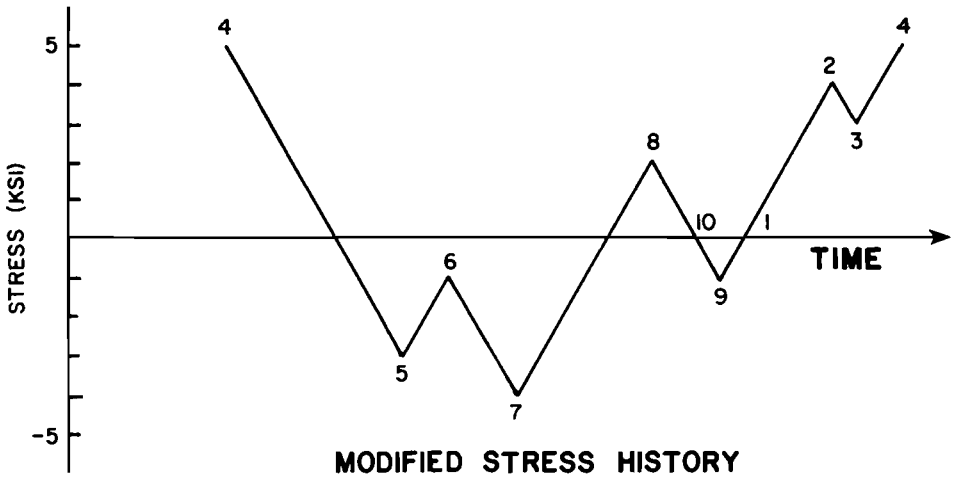

(b)

Fig. 2.8 Modified variable amplitude stress history

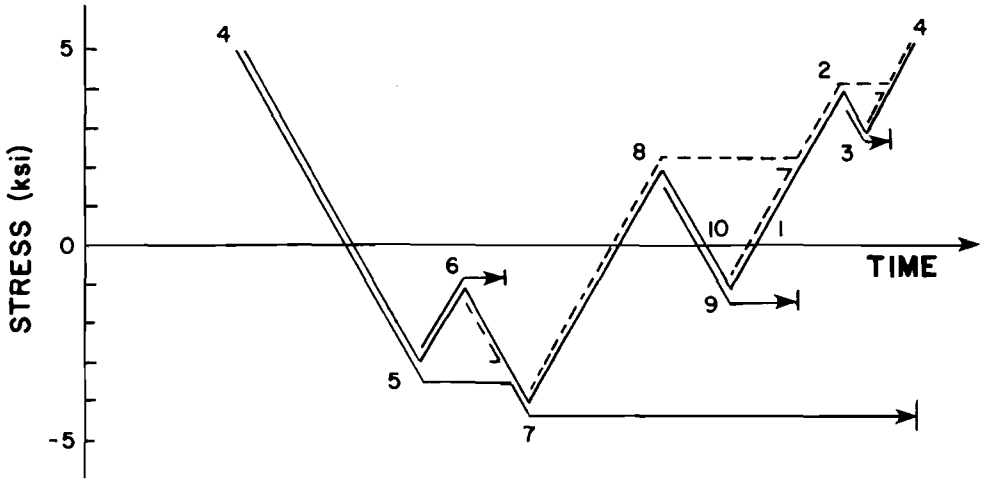

Fig. 2.9a Range Pair Count on modified stress history

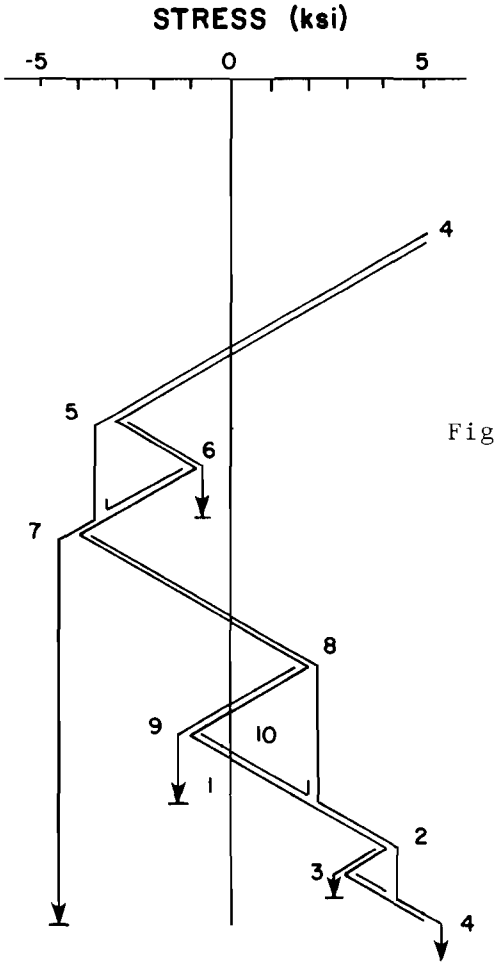

Fig. 2.9b Rainflow method on modified stress history

The technique of modifying a stress history before applying a counting method is used in the Reservoir Cycle counting method.[12,13] The stress history is first modified and is treated like a reservoir filled with water. The reservoir is drained from the lowest point in the stress history, leaving behind the water which cannot escape. One cycle is counted having a stress range equal to the vertical height of the water drained. This process is repeated until the whole reservoir is drained of water. One cycle is counted for each section drained. The Reservoir method is illustrated in Fig. 2.10. First, the stress history is modified. Next the reservoir is drained from point 7 and one cycle is counted with a stress range equal to the vertical distance between points 7 and 4. The reservoir is subsequently drained from points 5, 9 and 3 until the reservoir is emptied. The Reservoir method yields the same results on the modified stress history as the Rainflow and Range Pair methods. Therefore, these three methods are identical.

2.7 Critical Illustrative Examples of Counting Schemes

Six cycle counting methods are compared by applying them to the three stress histories shown in Figs. 2.11a, 2.13a, and 2.15a. The examples begin with a simple constant amplitude stress history and become progressively more complicated.

In order to compare each cycle counting method, the effective stress range S_{RE}, and the total number of cycles are computed using the cycles and stress ranges counted by each method. Since the Rainflow, Range Pair and Reservoir methods yield identical results on a modified stress history, only the Rainflow method is shown for each example. Only full cycles were used when computing S_{RE}.

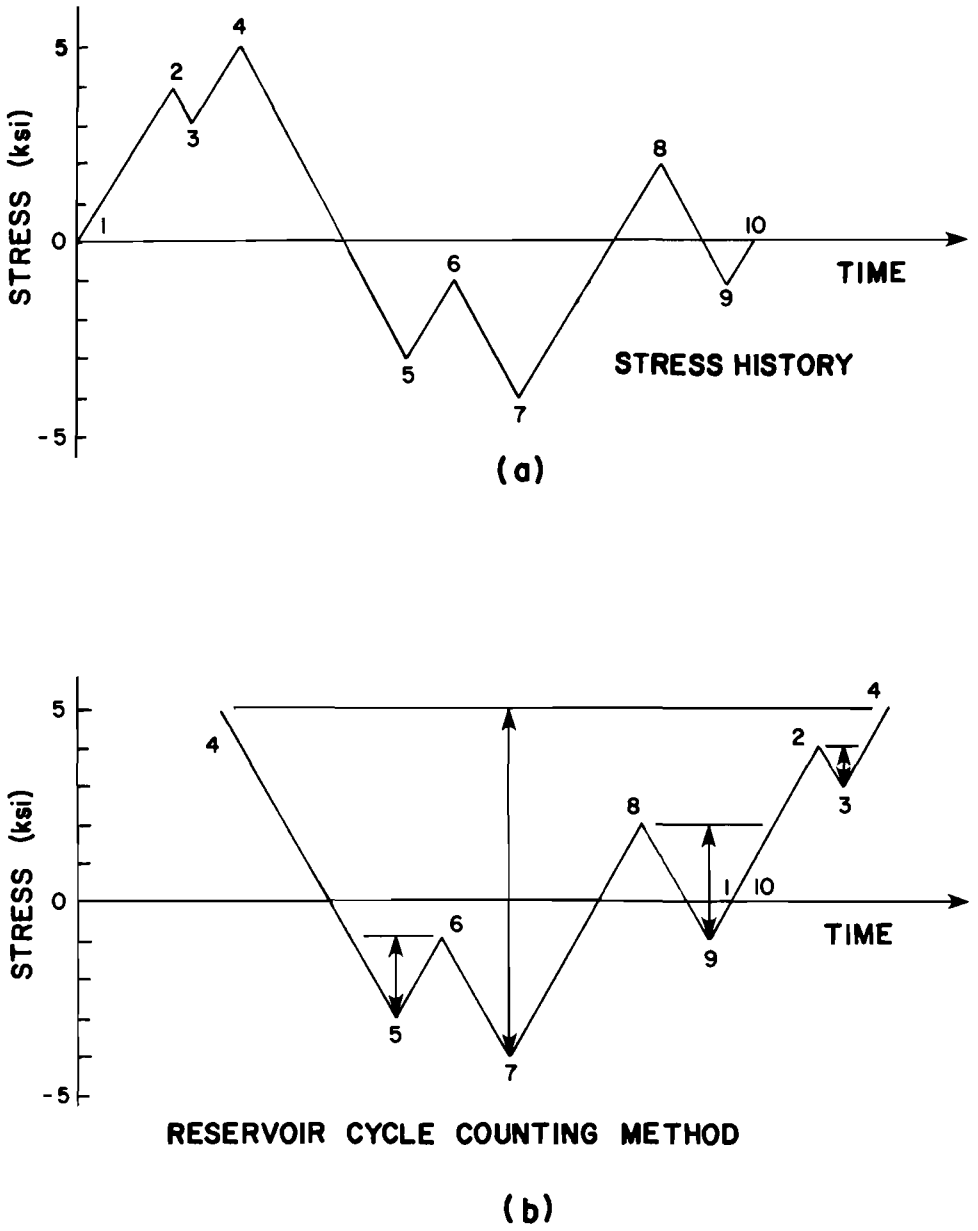

Fig. 2.10 Reservoir cycle counting method on the modified stress history

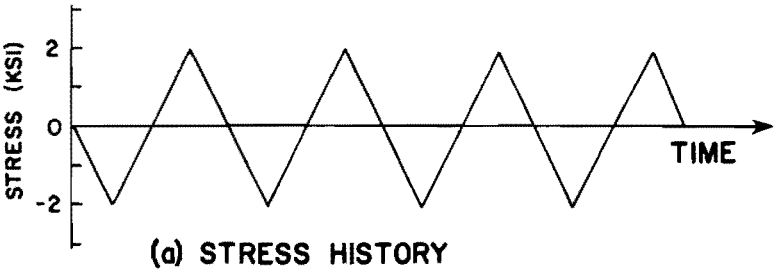

S_R = 4 ksi

N = 4 cycles

(a) STRESS HISTORY

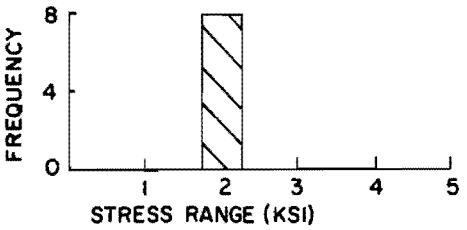

S_{RE} = 2 ksi

N = 8 cycles

(b) STRESS RANGE HISTOGRAM FROM PEAK COUNT METHOD

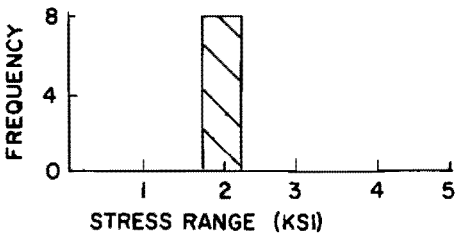

S_{RE} = 2 ksi

N = 8 cycles

(c) STRESS RANGE HISTOGRAM FROM ZERO CROSSING PEAK COUNT METHOD

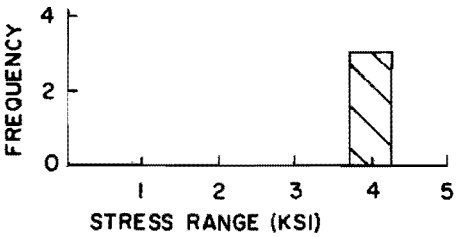

S_{RE} = 4 ksi

N = 3 cycles

(d) STRESS RANGE HISTOGRAM FROM RANGE COUNT METHOD

Fig. 2.11 Example 1

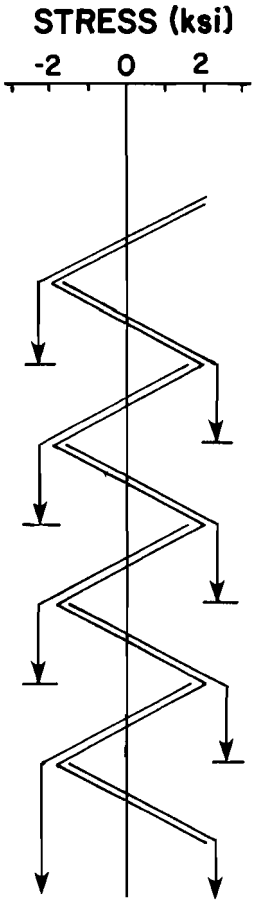

(e) RAINFLOW METHOD ON MODIFIED STRESS HISTORY

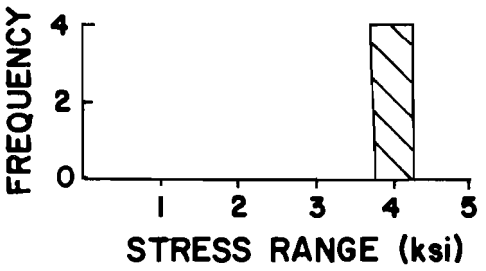

S_{RE} = 4 ksi

N = 4 cycles

(f) STRESS RANGE HISTOGRAM FROM RAINFLOW METHOD

Fig. 2.12 Example 1 (cont.)

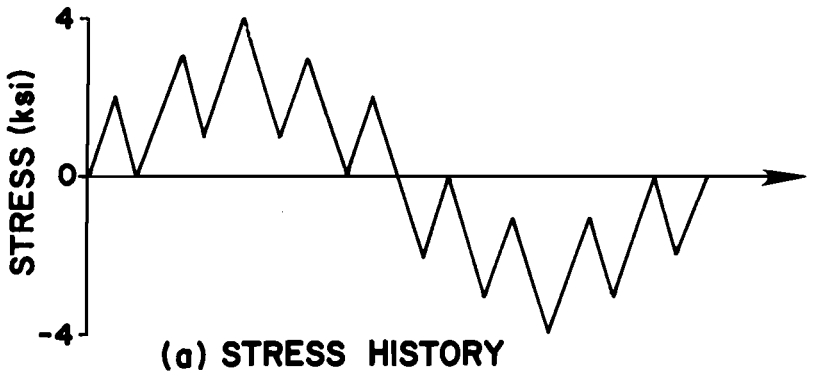

(a) STRESS HISTORY

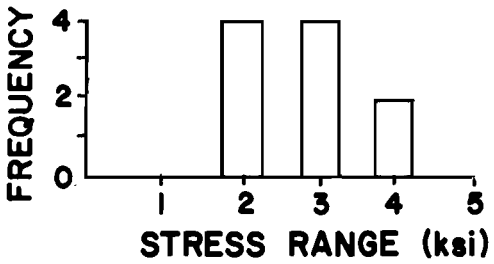

S_{RE} = 2.99 ksi

N = 10 cycles

(b) STRESS RANGE HISTOGRAM FROM PEAK COUNT METHOD

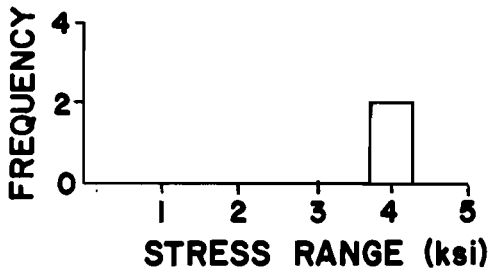

S_{RE} = 4.0 ksi

N = 2 cycles

(c) STRESS RANGE HISTOGRAM FROM ZERO CROSSING PEAK COUNT METHOD

S_{RE} = 2.6 ksi

N = 10 cycles

(d) STRESS RANGE HISTOGRAM FROM RANGE COUNT METHOD

(continued)

Fig. 2.13 Example 2

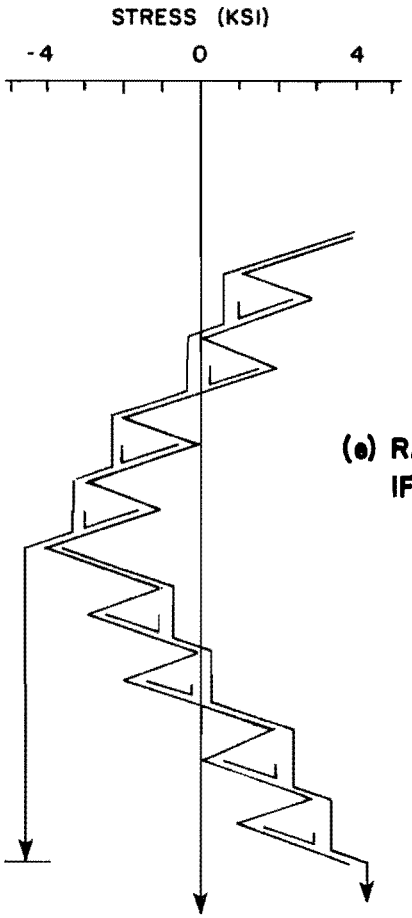

(e) RAINFLOW METHOD ON MODIFIED STRESS HISTORY

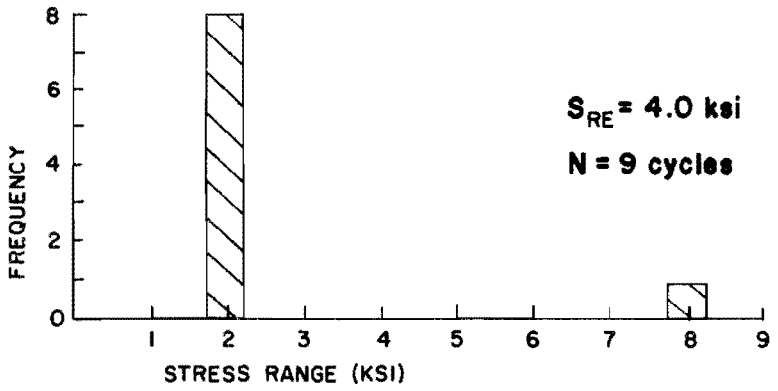

(f) STRESS RANGE HISTOGRAM FROM RAINFLOW METHOD

Fig. 2.14 Example 2 (cont.)

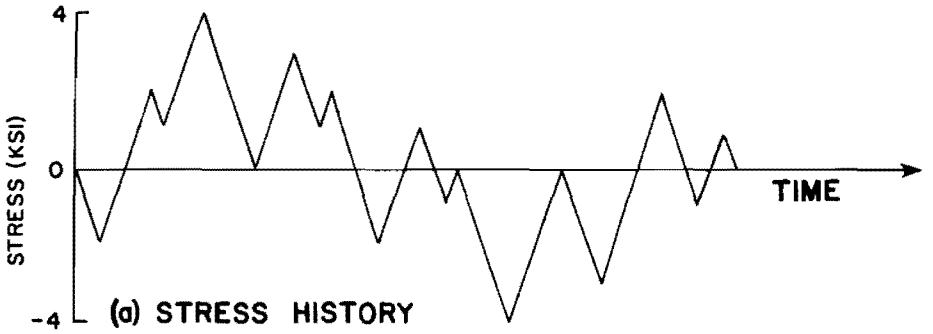

(a) STRESS HISTORY

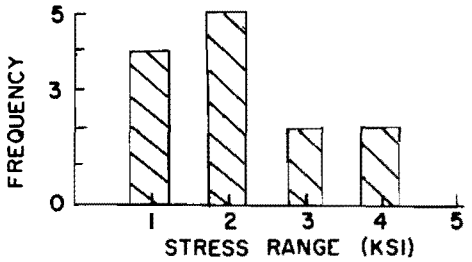

S_{RE} = 2.59 ksi

N = 13 cycles

(b) STRESS RANGE HISTOGRAM FROM PEAK COUNT METHOD

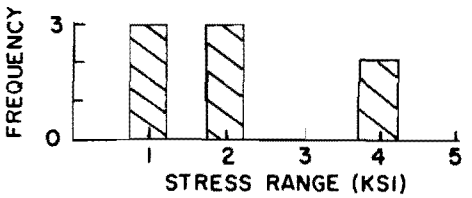

S_{RE} = 2.68 ksi

N = 8 cycles

(c) STRESS RANGE HISTOGRAM FROM ZERO CROSSING PEAK COUNT METHOD

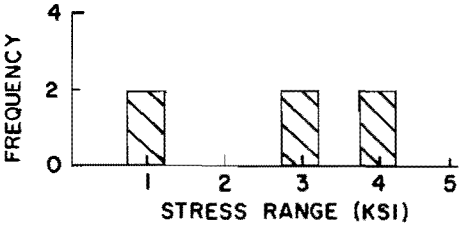

S_{RE} = 3.13 ksi

N = 6 cycles

(d) STRESS RANGE HISTOGRAM FROM RANGE COUNT METHOD

(continued)

Fig. 2.15 Example 3

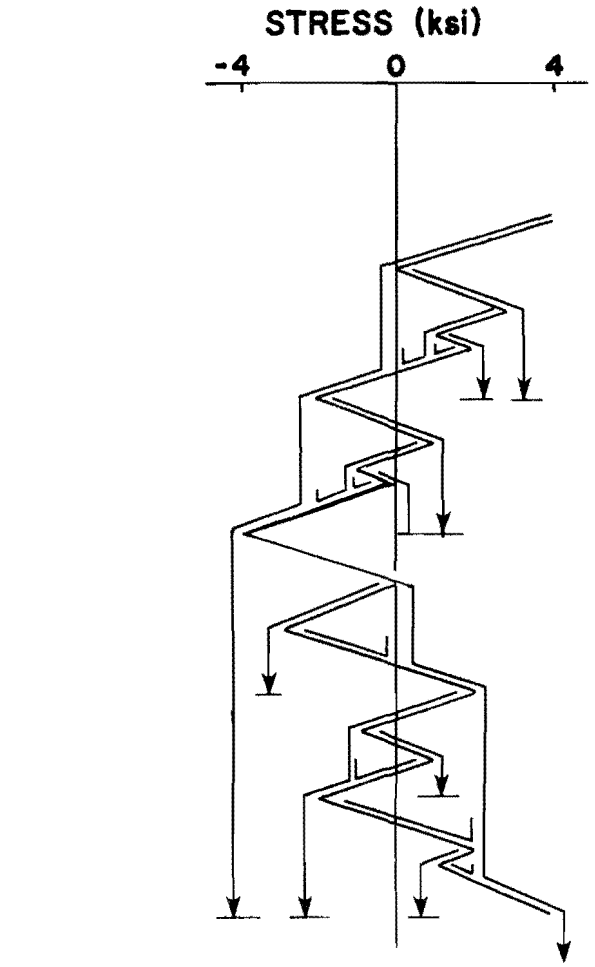

(e) RAINFLOW METHOD ON MODIFIED STRESS HISTORY

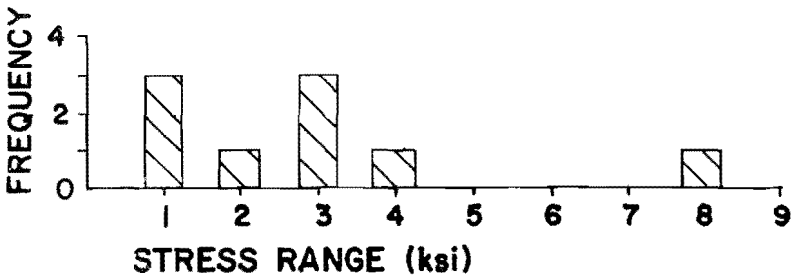

S_{RE} = 4.20 ksi

N = 9 cycles

(f) STRESS RANGE HISTOGRAM FROM RAINFLOW METHOD

Fig. 2.16 Example 3 (cont.)

The effective stress range for a constant amplitude stress history, Fig. 2.11a, should be equal to the constant amplitude stress range. The Peak Count and the Zero Crossing methods yield values of S_{RE} lower than the expected level. The Range Count method yields the expected value of S_{RE}, but loses one cycle from the constant amplitude stress history.

The Peak Count and Range Count methods fail to recognize the cycle with the large stress range in Fig. 2.13a, while the Zero Crossing Peak Count method fails to recognize the smaller cycles. Since these methods do not yield acceptable results from the simpler stress histories, then good results should not be expected from more complicated stress histories.

In order for a cycle counting method to be an acceptable means of counting cycles in a complicated stress history, it must first yield an S_{RE} and number of cycles which correlate with a simple constant amplitude stress history. The cycle counting method should also include all parts of the stress history in order to yield acceptable results. The Rainflow method yields an S_{RE} which correlates well with the S_R of the constant amplitude stress history in Fig. 2.11a. The Rainflow method does not add or drop any of the stress range cycles for the stress histories in Fig. 2.11a and Fig. 2.13a. In all the examples, the total stress history is used in the Rainflow cycle counting method. Since the Rainflow method correlates well with simple stress histories, then this method is used in this study on complicated stress histories in conjunction with Miner's law in order to determine effective stress ranges.

CHAPTER 3

TEST PROCEDURE AND PRESENTATION OF RESULTS

3.1 Bridge Description and Instrumentation

The bridge under study in this report is part of a four-lane, heavily traveled highway in Dallas, Texas. The structure consists of two longitudinal steel girders with transverse floor beams and a post-tensioned concrete deck. Figure 3.1a is a side view of the bridge and Fig. 3.1b is a view of the longitudinal girder and floor beam intersection which constitute the supporting elements of the bridge. A plan and elevation view of the two five-span continuous longitudinal girders is shown in Fig. 3.2. The longitudinal girders rest on concrete columns. The floor beams frame into the longitudinal girders and support the concrete deck. Figure 3.3 illustrates a typical cross section of the bridge.

The southernmost span (span EF in Fig. 3.2) was instrumented for study. This span is 72 ft. long supported by pinned hangers at one end with an interior support at the other. One-hundred twenty ohm strain gages, with a 3/8 in. gage length, were mounted on the flanges of the longitudinal girders at four sections, two sections on each girder. Figure 3.4 shows the location of the sections instrumented while Fig. 3.5 shows the location and numbering system of the strain gages on the flanges of the girders. The dimensions of the girder cross sections at the gage locations are shown in Fig. 3.6. Sections C and D were chosen for this study because they lie in a maximum live load moment region of the span. Reference 17 contains a more detailed discussion of the location of gaged sections.

(a)

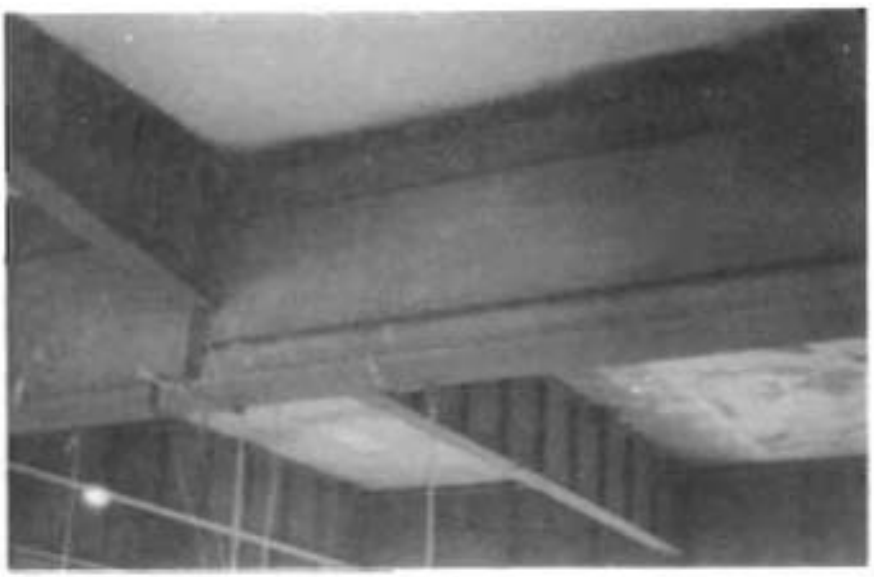

(b)

Fig. 3.1 Two views of the test bridge

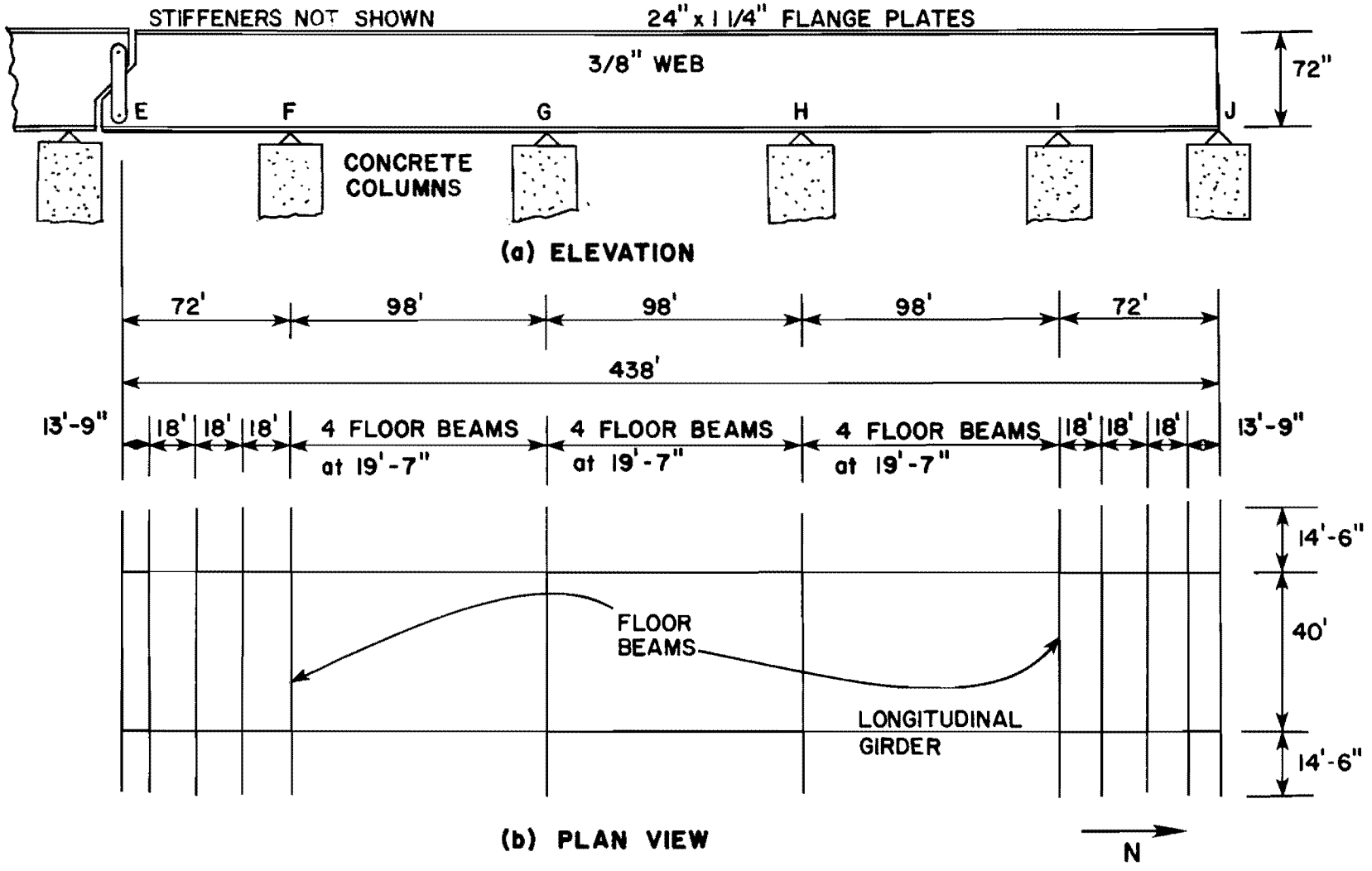

Fig. 3.2 Elevation and plan view of test bridge

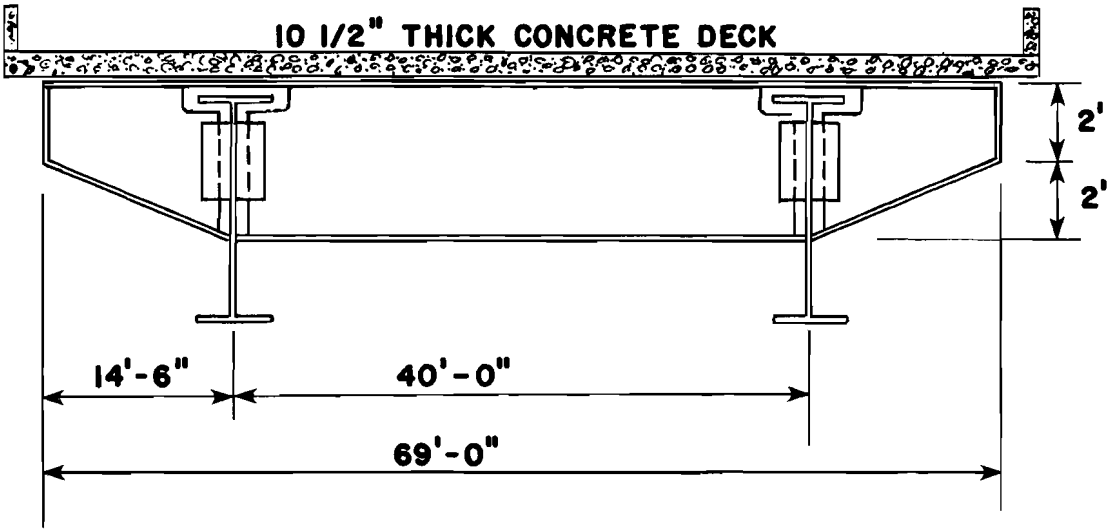

Fig. 3.3 Typical cross section of the test bridge

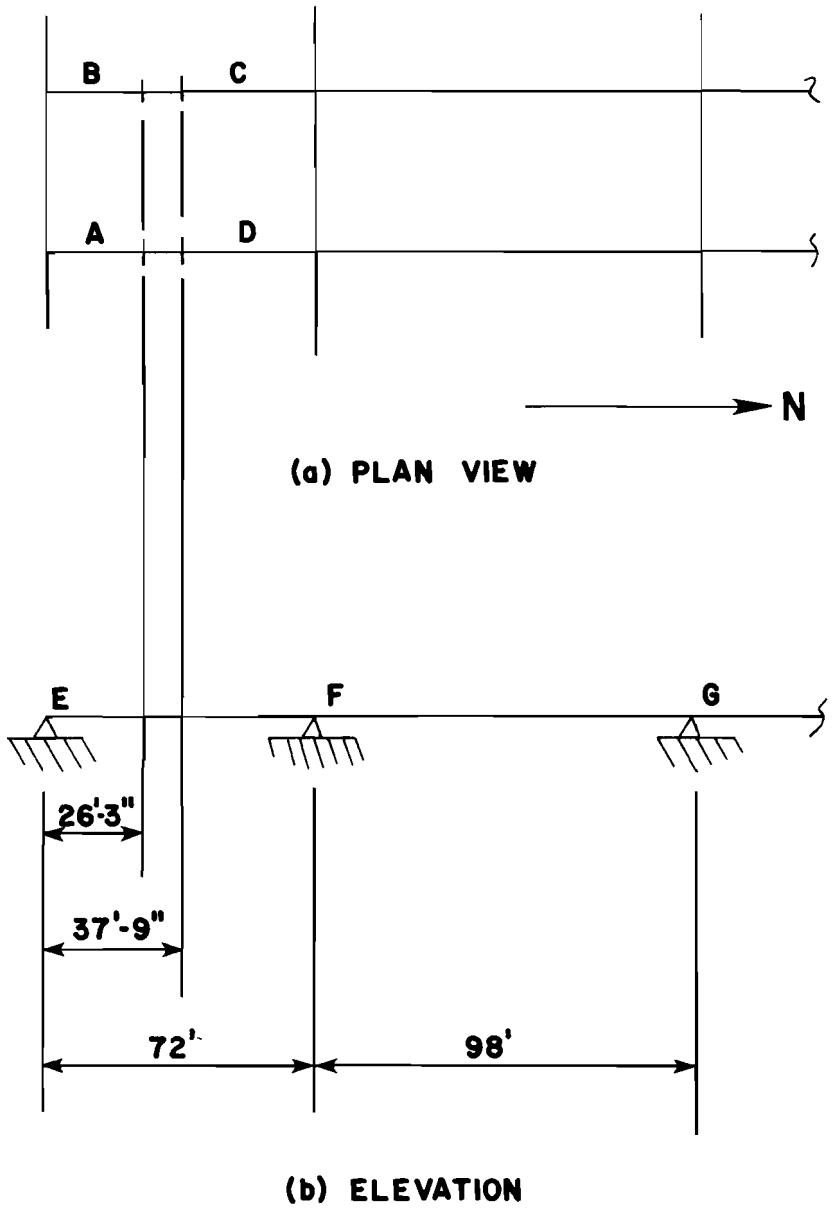

Fig. 3.4 Location of gaged sections on test bridge

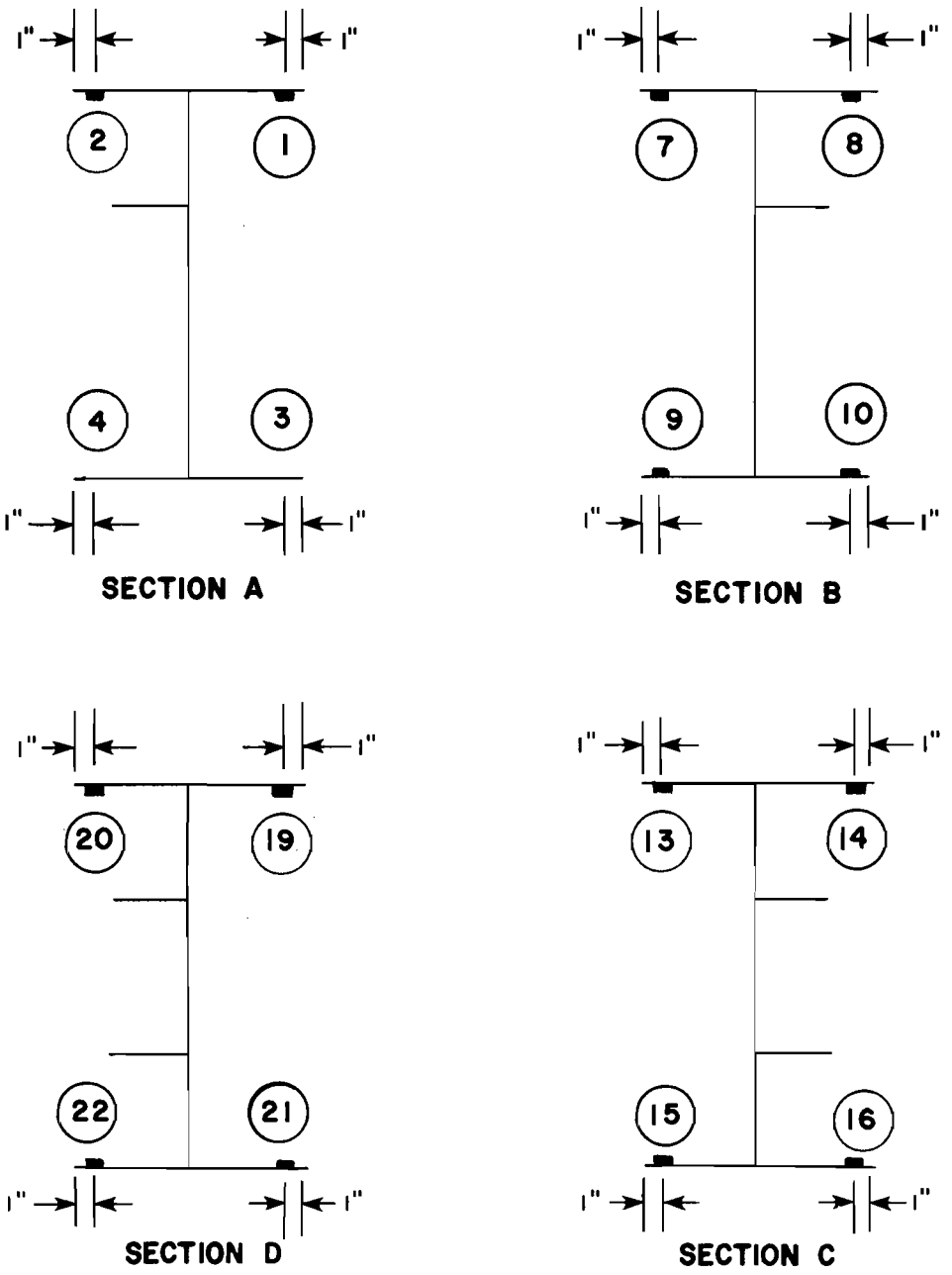

Fig. 3.5 Location of strain gages

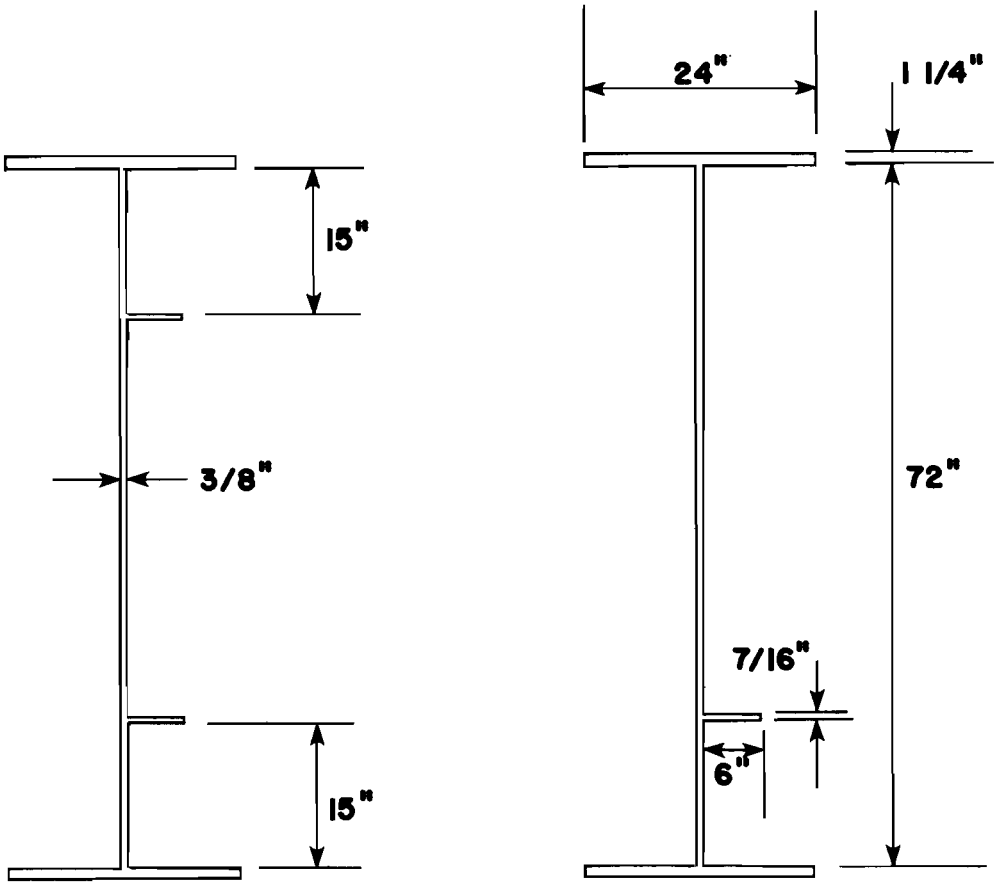

Fig. 3.6 Cross section of longitudinal girder

3.2 Data Acquisition

A VIDAR high-speed data acquisition system was used in this study to collect the data from the highway bridge. The VIDAR collects analog data from strain gages and converts it into binary coded data. The binary coded data is stored on magnetic tape. Figure 3.7 shows the path of the input data as it flows through the VIDAR data acquisition system. Voltage signals which originate from strain gages mounted on the bridge structure are fed into the VIDAR through the signal input panel. The signal is amplified and conditioned. The output of the individual gage amplifiers is sent to the VIDAR multiplexer and also to the signal output panel. An analog recorder connected to the output panel may be used by the operator to monitor the input signal. The VIDAR multiplexer is simply a highly sophisticated voltmeter. The multiplexer reads analog voltages at high rates of speed (up to 12000 input signals per second) and converts the voltages to binary coded data. The VIDAR controller allows the operator to initiate access to the data from the multiplexer and to write the data on magnetic tape. The controller may be operated manually or an electronic timer may be used in conjunction with the controller to establish a time interval between successive scans of input. A high-speed computer is used to convert the binary coded data on the magnetic tape into engineering units for general use.

3.3 Evaluation of Data

Certain adjustments were made to the data collected by the VIDAR data acquisition system to reduce experimental error. Before the measurements from a gage were considered in fatigue calculations, the measurements were analyzed to ensure the reliability of the data. The stress history of each gage location was compared with corresponding stress histories of other gages at the same cross section

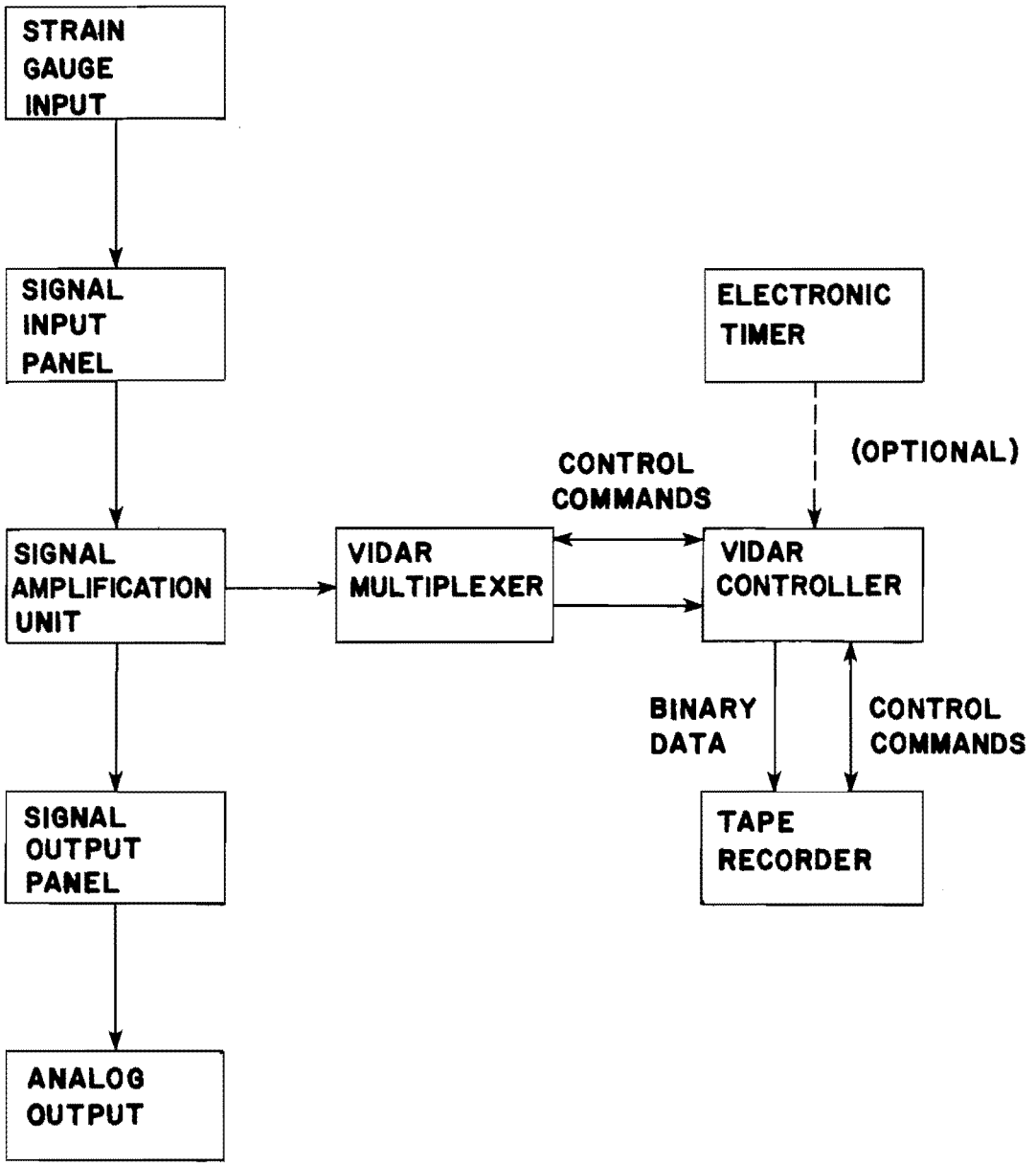

Fig. 3.7 VIDAR system block diagram

to determine if the data were valid. If the data did not seem reasonable, then the measurements from that particular gage were not considered in subsequent calculations.

A certain amount of random signal noise is inherent within the VIDAR data acquisition system. If the noise is truly random, then averaging data from gages measuring similar strains will partially eliminate the random noise. Figure 3.8 shows partial stress histories at gage locations 1, 3 and 4 under normal traffic conditions. Gage 1 measures stress in the top flange of the longitudinal girder while gages 3 and 4 measure stress in the bottom flange. Stresses at gage location 1 are of opposite sign than corresponding stresses at gage locations 3 and 4. This indicates that the data are reliable since this behavior is consistent with the normal behavior of a bending member. Notice also that the stress for all three gages is of the same magnitude which indicates that the neutral axis is near the centerline of the girder. Since the neutral axis is near the center of the girder, gages 1, 3 and 4 may be used to calculate an average value of stress in the flange. Averaging the measurements from these three gages will help to eliminate the random noise associated with the measurements. Figure 3.8d is the average stress history at Section A for gages 1, 3 and 4. Notice that averaging the data tends to smooth out the stress history by eliminating small variations of stress which occur in each gage. The small stress variations, which are circled in Figs. 3.8a, 3.8b, and 3.8c do not occur in the averaged data.

The VIDAR data acquisition system is capable of accurately measuring stresses much less than 0.1 ksi. However, to eliminate any extraneous data caused by experimental error, stress ranges less than 0.1 ksi were not considered when calculating the effective stress range and other fatigue parameters. Neglecting stress ranges less than 0.1 ksi changed the effective stress range by less than 2 percent. Therefore, neglecting the smaller stress ranges did not significantly affect the calculation of fatigue parameters.

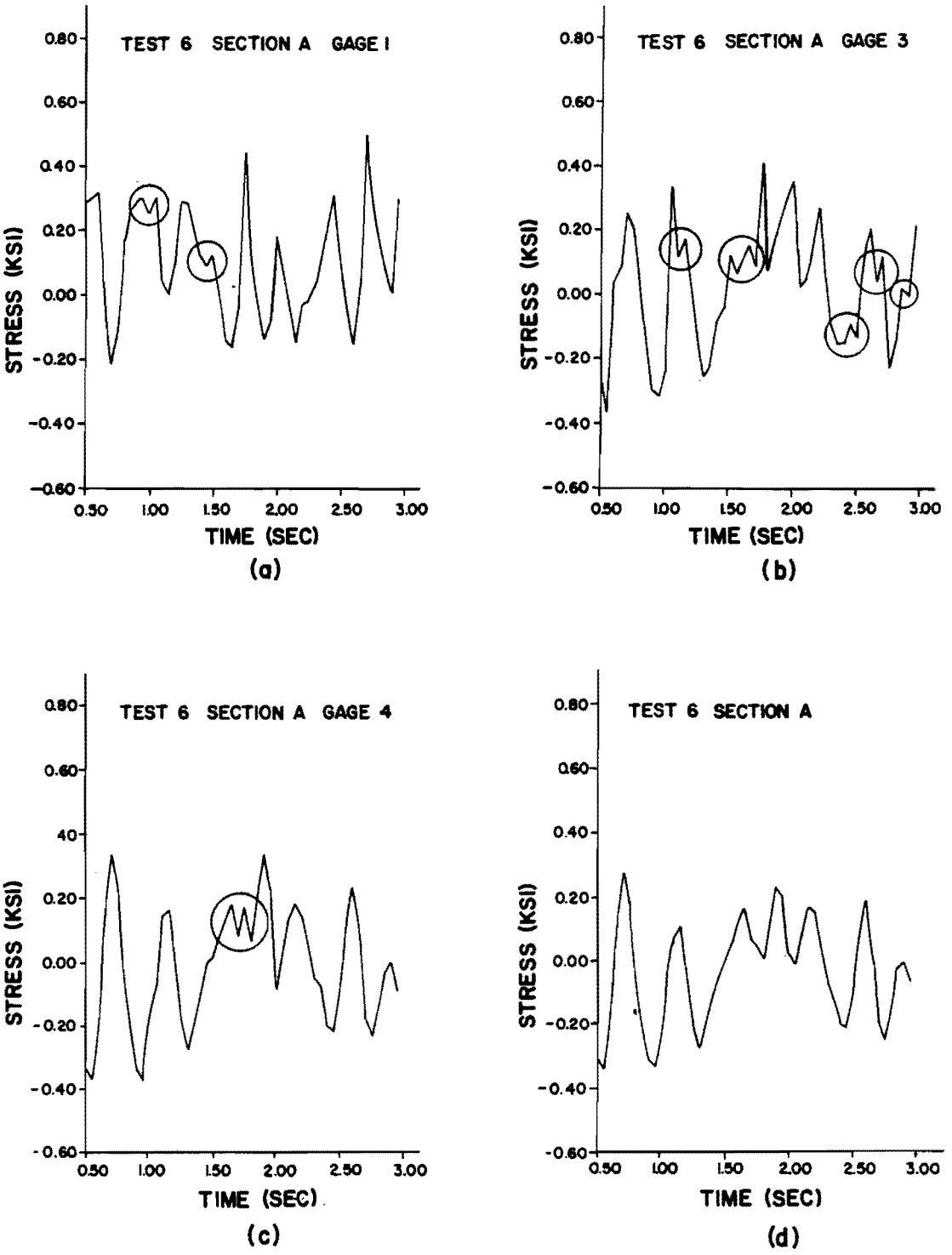

Fig. 3.8 Stress histories at Section A under normal traffic (Test 6)

In summary, three adjustments were made to the data to reduce experimental error. Each gage was first analyzed to determine if the measurements were consistent with the other gages at the cross section. Second, gages at each section were averaged to help eliminate random noise. Finally, only those stress ranges greater than 0.1 ksi were considered in the calculation of fatigue parameters.

3.4 Test Procedure and Presentation of Data

3.4.1 Vehicle Velocity Tests. Two sets of tests were performed in this investigation. The first set consisted of tests conducted with a truck of known dimension and weight which traveled across the bridge at three different speeds. The test truck, shown in Fig. 3.9, was a dump truck loaded with sand. The total weight of the truck for each test is given in Table 3.1. The truck traveled directly over the east longitudinal girder at three different speeds, 5, 35 and 50 m.p.h. One test was conducted with the truck traveling at 5 m.p.h., one test was conducted at 35 m.p.h., and four tests were conducted at 50 m.p.h. Data were collected by the VIDAR data acquisition unit from sections A and D of the east longitudinal girder (see Figs. 3.4 and 3.5) at a rate of 33.3 scans per second. Data were not collected from sections B and C of the west longitudinal girder because this girder was not directly loaded by the test truck. The data were analyzed using the procedures listed in Section 3.3, and Table 3.2 lists the gages which were finally used in fatigue calculations. The data collected represent stress histories at each gage location due to the passage of the test truck. Figures 3.10, 3.11 and 3.12 are the stress histories at gage location 1, section A for the three speeds. The stress history shown in Fig. 3.12 is typical for all 50 m.p.h. tests.

The velocity of the truck had considerable effect upon the stresses in the bridge. The maximum and minimum stresses increased with increasing speed as shown in Figs. 3.10, 3.11, and 3.12.

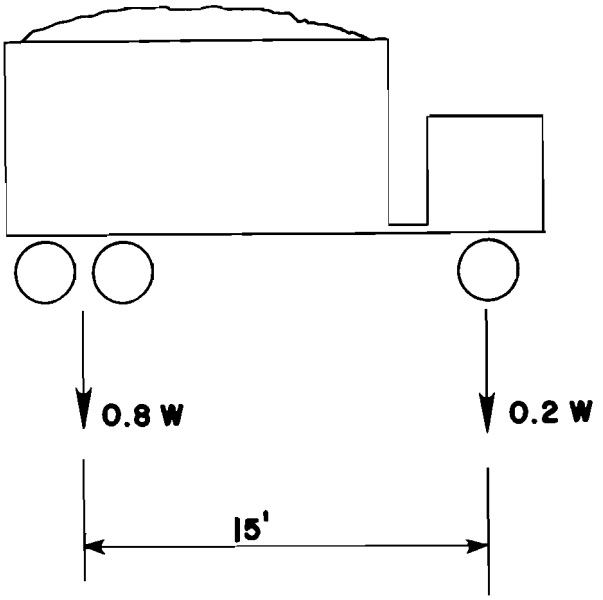

W = TOTAL WEIGHT OF TRUCK

Fig. 3.9 Axle load distribution on test truck

TABLE 3.1 TOTAL TEST TRUCK WEIGHT FOR EACH TEST

Test	W (kips)
5 mph	54.6
35 mph	54.6
50 mph	52.0

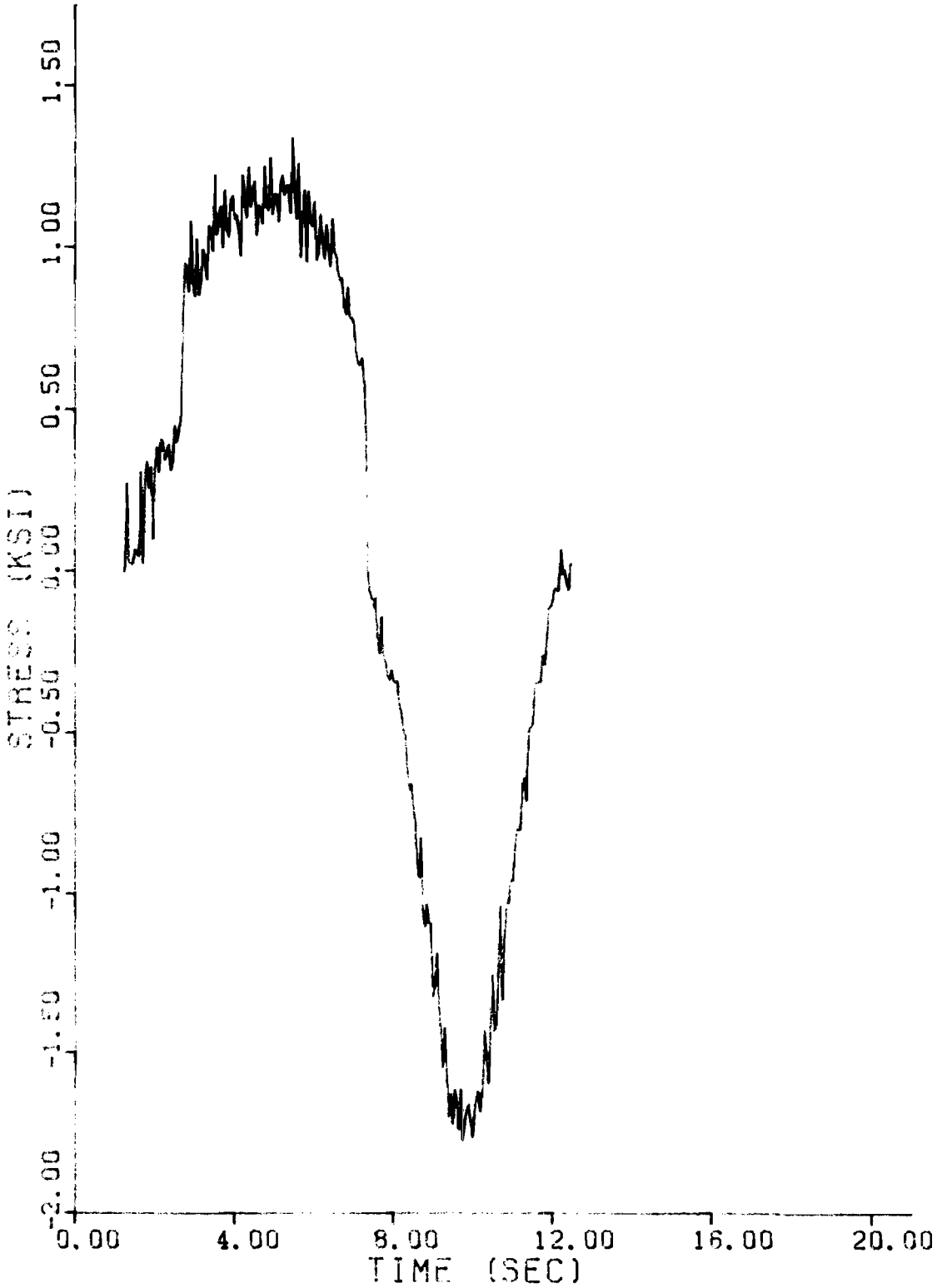

Fig. 3.10 Stress history at gage 1, section A, for a truck velocity of 5 mph

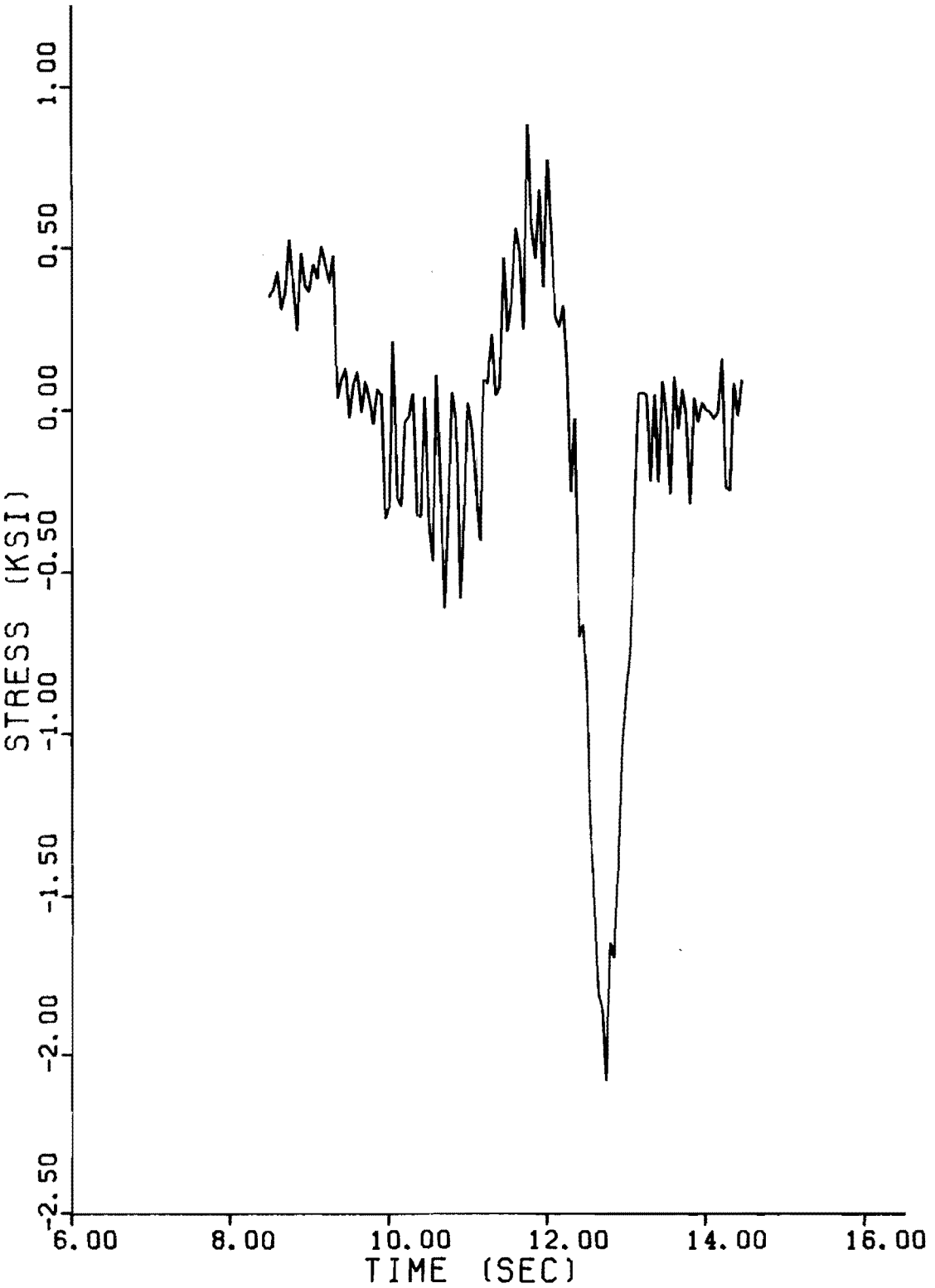

Fig. 3.11 Stress history at gage 1, section A, for a truck velocity of 35 mph

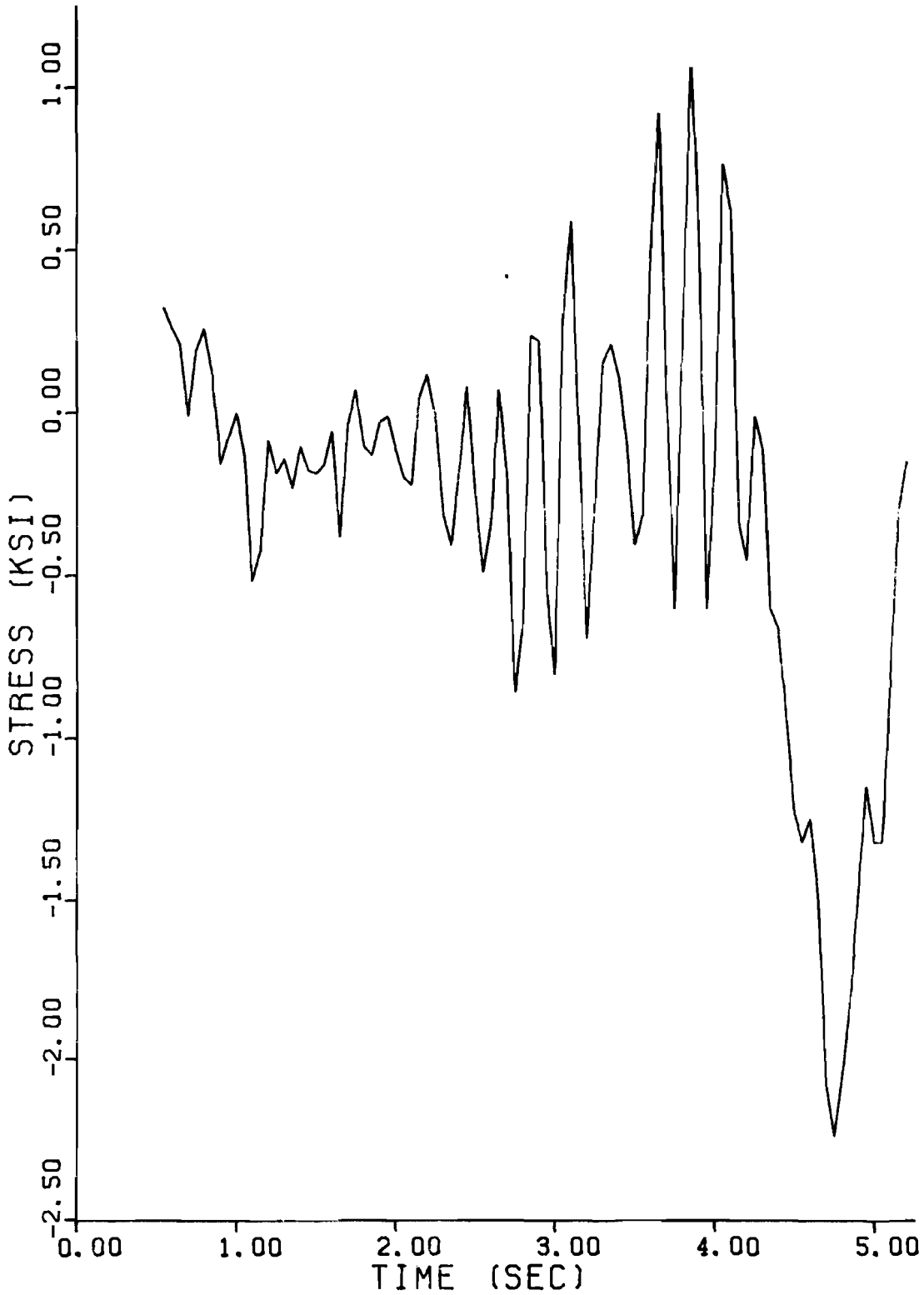

Fig. 3.12 Stress history at gage 1, section A, for a truck velocity of 50 mph

TABLE 3.2 GAGES USED IN THE COMPUTATION OF FATIGUE PARAMETERS

	Gages Used in Fatigue Calculations	
Test \ Section	A	D
5 m.p.h.	1,2,3,4	19,20,21,22
35 m.p.h.	1,2,3,4	19,20,21,22
50 m.p.h.	1,2,3,4	20

The magnitude of the secondary stresses caused by the vibration of the bridge and truck also increased with increasing speed. The effect of velocity on the fatigue life of the structure is discussed later in this chapter.

A computer program was written to reduce the stress histories derived from the data collected to stress ranges and corresponding cycles. The Rainflow Cycle Counting algorithm described in Chapter 2 was used in the program. A stress range histogram was developed from the stress ranges and cycles determined by the rainflow counting algorithm. Figure 3.13 shows examples of stress range histograms developed from the data collected at Section A, gage 1, for each speed. The histograms show an increase in the distribution of stress ranges with increasing speed. The histograms for the 5 and 35 m.p.h. tests show several small stress ranges which are produced by the vibration of the bridge and truck along with one large stress range which corresponds to the stress range from a static influence line at Section A for the passage of the test truck. A clear distinction between a major stress range and secondary vibrational stress ranges does not exist for the 50 m.p.h. test. There exists a greater distribution of stress ranges for the 50 m.p.h. tests than for tests conducted at lower speeds.

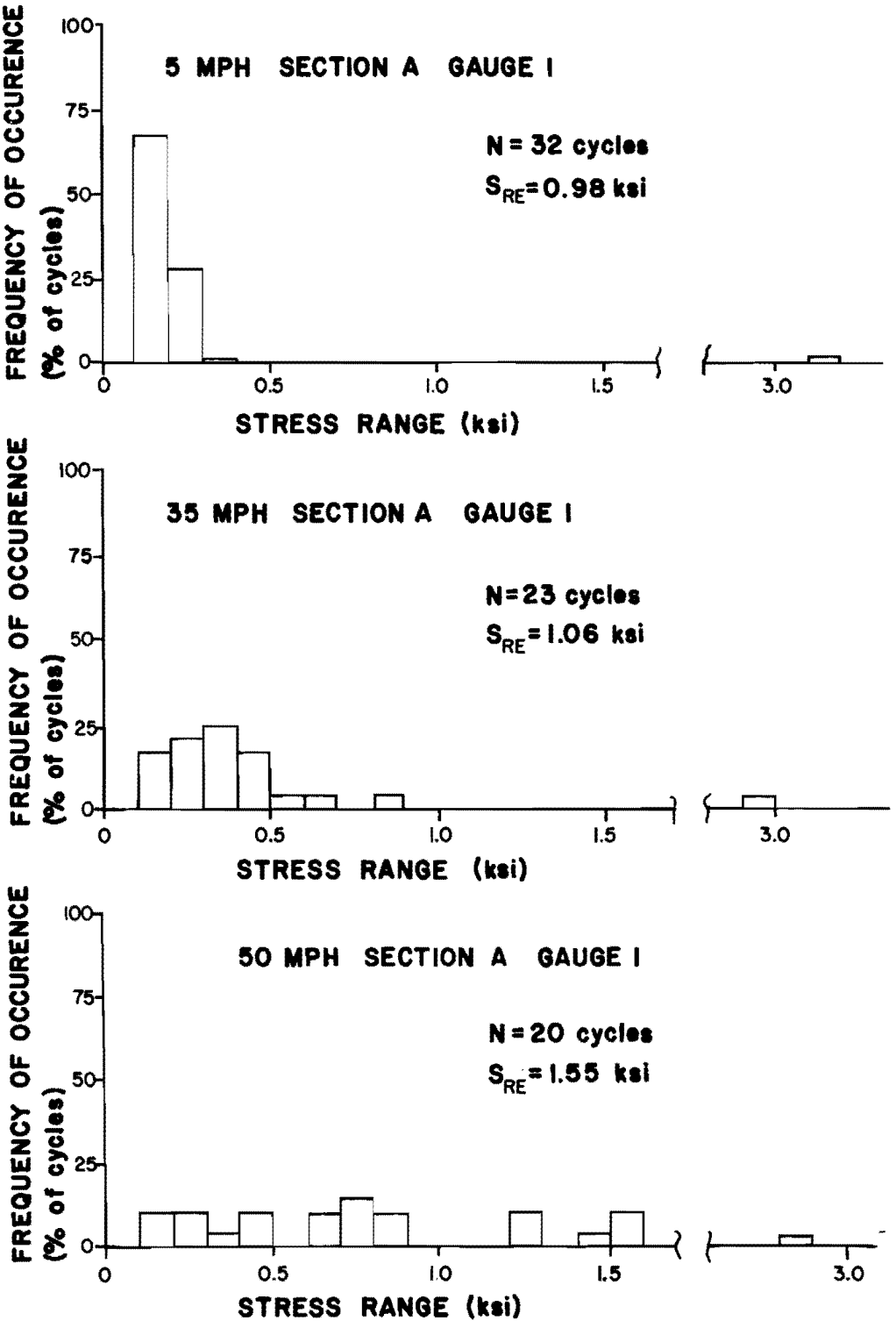

Fig. 3.13 Histograms of stress ranges from test truck data

An effective stress range, described in Chapter 2, can be calculated from the stress histograms using the following equation:

$$S_{RE} = \left[\sum_i \gamma_i \, S_{Ri}^3 \right]^{\frac{1}{3}} \tag{3.1}$$

where

S_{RE} = effective stress range

γ_i = frequency of occurrence of S_{Ri}

S_{Ri} = stress range at ith interval

Studies have shown that the fatigue life of a structure is related to the effective stress range as follows:[1,2]

$$N = AS_{RE}^n \tag{3.2}$$

where

N = cycles to failure

S_{RE} = effective stress range

A = function of weldment geometry

n = -3 for welded details

The stress range histograms indicate the number of cycles caused by the passage of the test truck. Dividing Eq. (3.2) by the number of cycles counted in the passage of the test truck, N_T, yields

$$N_{LT} = \frac{N}{N_T} = \frac{AS_{RE}^n}{N_T} \tag{3.3}$$

where

N_{LT} = the number of test truck passages required for fatigue failure

The parameter N_{LT} represents the number of times the test truck may pass over the bridge at a certain speed before failure occurs. Table 3.3 is a summary of S_{RE}, N_T, and N_{LT} for the tests conducted with a test truck.

The parameter N_{LT} was computed as a function of A. The parameter A is a function of welded detail and fabrication. Therefore, the parameter N_{LT} can be used to predict the fatigue life of different details. For example, according to the AASHTO specifications, the value of A for a web-to-flange filet weld is 1.04×10^{10}. The number of test trucks required for the fatigue failure of a web-to-flange filet weld is obtained by multiplying N_{LT} by 1.04×10^{10}. A further discussion of fatigue-life estimates using the parameter N_{LT} is presented in Chapter 4.

Figure 3.14b shows the changes in S_{RE} with increasing truck velocity at Section D. The increase in S_{RE} with increasing truck velocity was due to the dynamic amplification of stresses at higher truck velocities as discussed previously in this chapter. A decrease in the total number of cycles, N_T, also occurred with increasing truck velocity as shown in Fig. 3.14a. The number of stress-range cycles for the 5 and 35 m.p.h. tests is greater than those for the 50 m.p.h. tests partly because the test truck was on the bridge a longer period of time. Vibratory stress range cycles caused by other traffic on the bridge can also increase the number of stress range cycles. For the 50 m.p.h. tests the vibratory stress range cycles caused by the test truck tend to mask those caused by other traffic. Therefore, vibrations caused by other traffic did not affect the cycle counts for the 50 m.p.h. tests as much as they affect those for the 5 and 35 m.p.h. tests.

Figure 3.14c shows that changes in S_{RE} and N_T combine to produce a decrease in the estimated fatigue life, N_{LT}, with increasing speed. An increase in S_{RE} yields a decrease in estimated fatigue life while a decrease in the total number of

TABLE 3.3 SUMMARY OF DATA FOR VELOCITY TESTS

MPH	5	35	50	50	50	50
Section A:						
S_{RE} (ksi)	1.01	1.07	1.74	1.78	1.78	1.82
$N_T \left(\frac{\text{cycles}}{\text{truck}}\right)$	32	23	18	17	18	19
$\frac{N_{LT}}{A}\left(\frac{\text{trucks}}{\text{life}}\right)$	0.0300	0.0352	0.0104	0.0104	0.0099	0.0088
Section D:						
S_{RE} (ksi)	1.15	1.35	1.75	2.10	1.86	1.90
$N_T \left(\frac{\text{cycles}}{\text{life}}\right)$	33	21	20	11	14	15
$\frac{N_{LT}}{A}\left(\frac{\text{trucks}}{\text{life}}\right)$	0.0197	0.0192	0.0093	0.0098	0.0110	0.0097

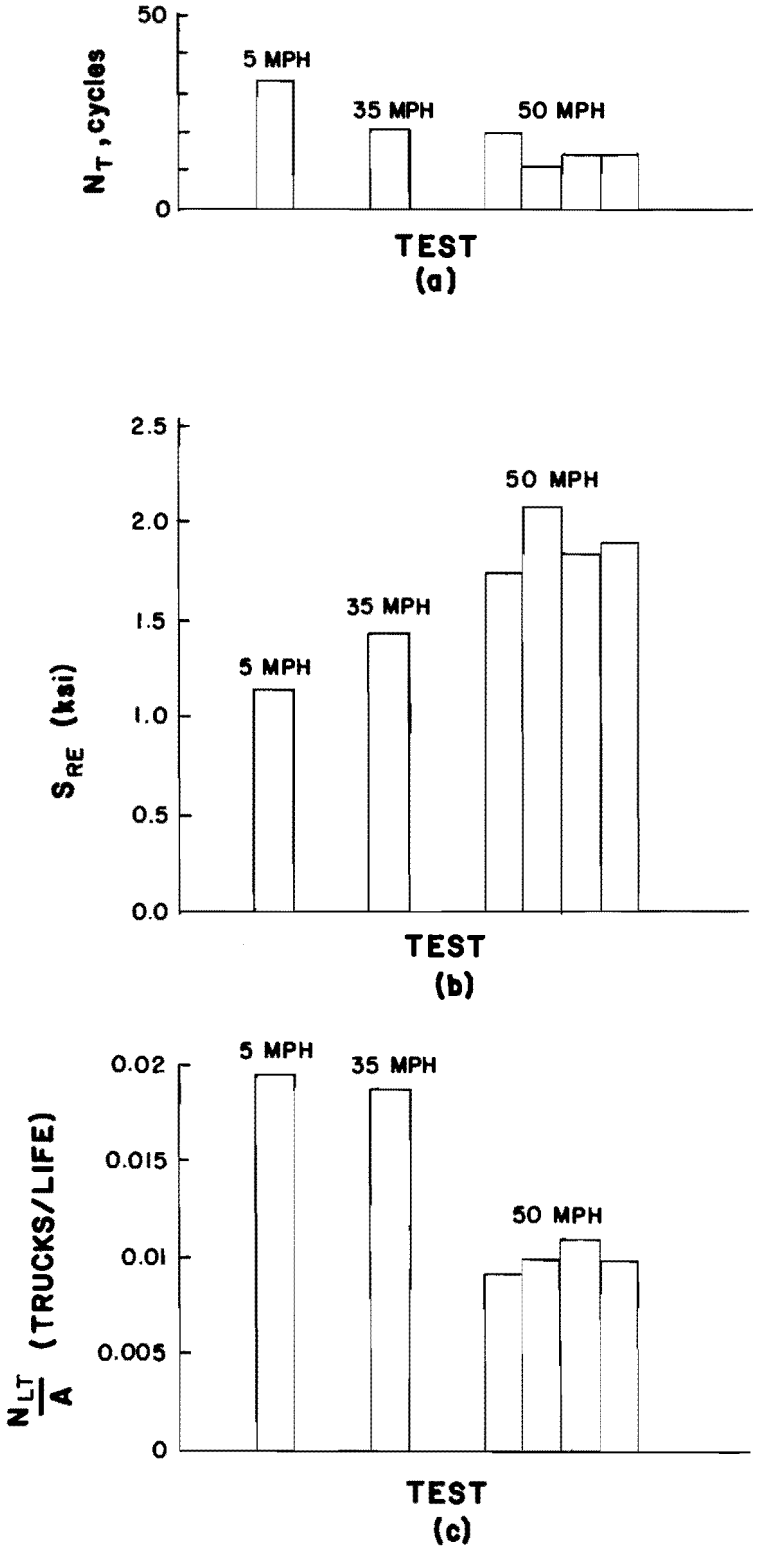

Fig. 3.14 Test truck data at section D

cycles yields an increase in N_{LT}. The estimated fatigue life is inversely proportional to S_{RE} raised to the third power; therefore, changes in S_{RE} have a greater influence on the fatigue life than changes in N_T. The data presented in Table 3.3 and Fig. 3.14 show fatigue-life estimates are dominated by S_{RE}. Fatigue-life estimates decrease with increasing truck velocity because S_{RE} increases even though corresponding decreases in the number of cycles tend to increase fatigue-life estimates.

The parameter, N_{LT}, in Table 3.3 at sections A and D are similar for the 50 m.p.h. tests, but differ for the lower speeds. Values of N_{LT} for section A are nearly double those for section D for the 5 and 35 m.p.h. tests. The number of cycles for each section are similar, so differences in the fatigue life are due to differences in S_{RE}. The effective stress range is a function of the secondary stress ranges caused by the vibration of the bridge and test truck and the main stress range caused by the static weight of the test truck. The major stress range is much larger than the secondary stress ranges for the 5 and 35 m.p.h. tests. Therefore, the effective stress range is affected largely by the major stress range. The effective stress range at section D is higher than at section A because live load stress are higher at section D. Therefore, fatigue-life estimates are lower for section D.

The data for the 50 m.p.h. tests is consistent and repeatable. Fatigue-life estimates for section A are similar to those at section D for the 50 m.p.h. tests. The vibratory stress range cycles have a major effect on S_{RE} and N_T. Effective stress ranges are higher for section D than for section A, but the number of cycles is higher for section A than for section D. Similarities in fatigue-life estimates between the two sections are due to the variation in S_{RE} and N_T. These variations are due to the vibratory stress ranges caused by the passage of the test truck.

On the average, section D yields lower fatigue-life estimates than section A for all tests.

3.4.2 Traffic Tests. The second set of tests performed in this study was conducted under normal traffic conditions. Data for the second set of tests were collected from sections A, B, C, and D (Figures 3.4 and 3.5). Eight tests were conducted over a period of two days. The tests were conducted at different times during the day and varied in duration from 10 to 20 minutes. Table 3.4 lists the time, day and date of each test. The VIDAR data acquisition system collected data at a rate of 20 scans per second. The data were examined using the procedures outlined in Section 3.3. Table 3.5 lists the gages which were finally used when computing fatigue-life estimates. The data represent stress histories at each gage location under traffic conditions. Figure 3.15 is an example of the stress history at gage 21 under traffic loading. Computer analysis is required because of the complexity of the stress history.

The computer program described earlier was used to reduce the stress histories to stress histograms using the rainflow cycle counting algorithm. Appendix A contains stress histograms for sections C and D for each test. Stress histograms for sections A and B are not included in Appendix A because sections C and D control fatigue-life estimates for each girder.

The effective stress range was calculated from the stress histories. An estimate of the fatigue life of a welded steel detail may be calculated from the equivalent stress range using Eq. (3.2). The number of cycles per minute under traffic conditions, N_M, may be computed by dividing the total number of cycles counted from a stress history by the record length of the stress history. Dividing Eq. (3.2) by the number of cycles per minute, N_m, yields:

TABLE 3.4 DAY, DATE, AND TIME OF TESTS CONDUCTED UNDER TRAFFIC CONDITIONS

Test	Date	Day	Time
1	10-2-80	TH	10:30 AM
2	10-2-80	TH	1:40 PM
3	10-2-80	TH	3:10 PM
4	10-2-80	TH	4:20 PM
5	10-3-80	FR	10:50 AM
6	10-3-80	FR	1:35 PM
7	10-3-80	FR	3:00 PM
8	10-3-80	FR	4:20 PM

TABLE 3.5 GAGES USED IN THE COMPUTATIONS OF FATIGUE PARAMETERS

Test \ Section	A	B	C	D
1	--	--	13,16	20,21
2	1,4	8	--	21,22
3	1,4	8,9,10	13,16	20,21,22
4	1	8,9	13,16	21
5	1,3,4	8,9,10	13,16	20,21,22
6	1,3,4	8,9,10	13,15,16	20,21,22
7	1,3,4	8,9,10	13,15,16	20,21,22
8	1,3,4	8,9,10	13,15,16	20,21,22

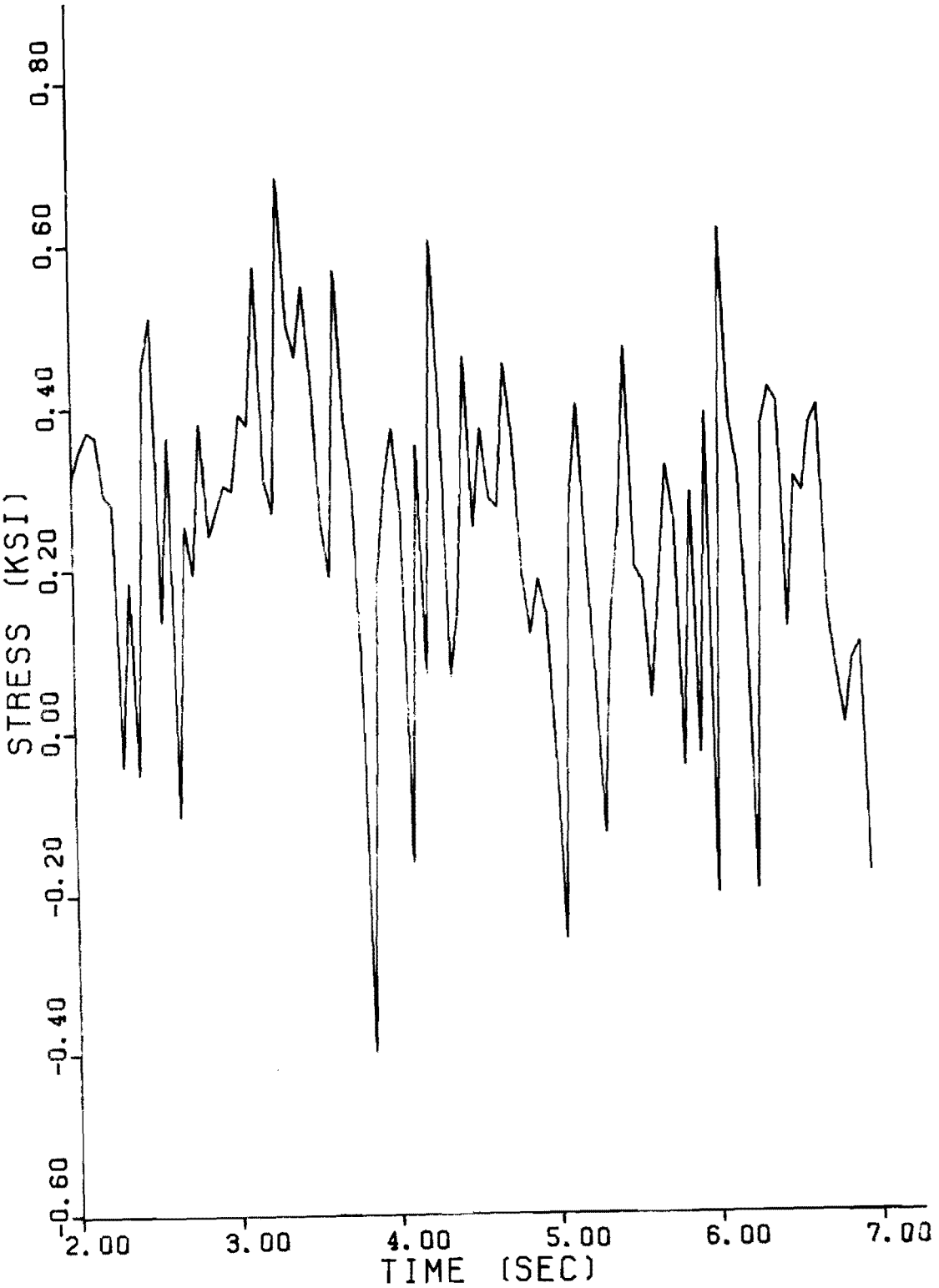

Fig. 3.15 Sample stress history at gage 21, section D for traffic test 5

$$N_L = \frac{N}{N_M} = \frac{AS_{RE}^n}{N_M} \tag{3.4}$$

where

N_L = fatigue life in minutes

The parameter N_L represents the estimated fatigue life in minutes of a detail subjected to repeated applications of the stress history from which S_{RE} and N_M were derived. Tables 3.6 through 3.16 summarize the parameters, S_{RE}, N_M, and N_L for each test. The parameter N_L is computed as a function of A so fatigue-life estimates of different welded details can be predicted as discussed in Section 3.4.

Tables 3.6 through 3.16 are divided into three sections. Tables 3.6 and 3.7 are summaries of the data at each section for all the tests. The data were examined using the process discussed in Section 3.3. The data at sections A and B for test 1 and at section C for test 2 did not satisfy the requirements stated in Section 3.3. Figure 3.16 is a comparison of a portion of the data at section C and section A for test 2. The stresses measured by gage 15 at section C are many times greater than the yield stress of the steel. This data are not acceptable; therefore, data from gage 15 were not used in further calculations. The stresses measured by gage 4 at section A are reasonable as opposed to those measured by gage 15 and can be used in further computations if this data meet the other standards stated in Section 3.3. All gages were examined in a similar manner to determine which gages should be used in the calculation of fatigue-life estimates.

Tables 3.6 and 3.7 show higher values for S_{RE} and N_M at the maximum live load moment regions, sections C and D, than for those at sections A and B. Consequently, the estimated fatigue life is

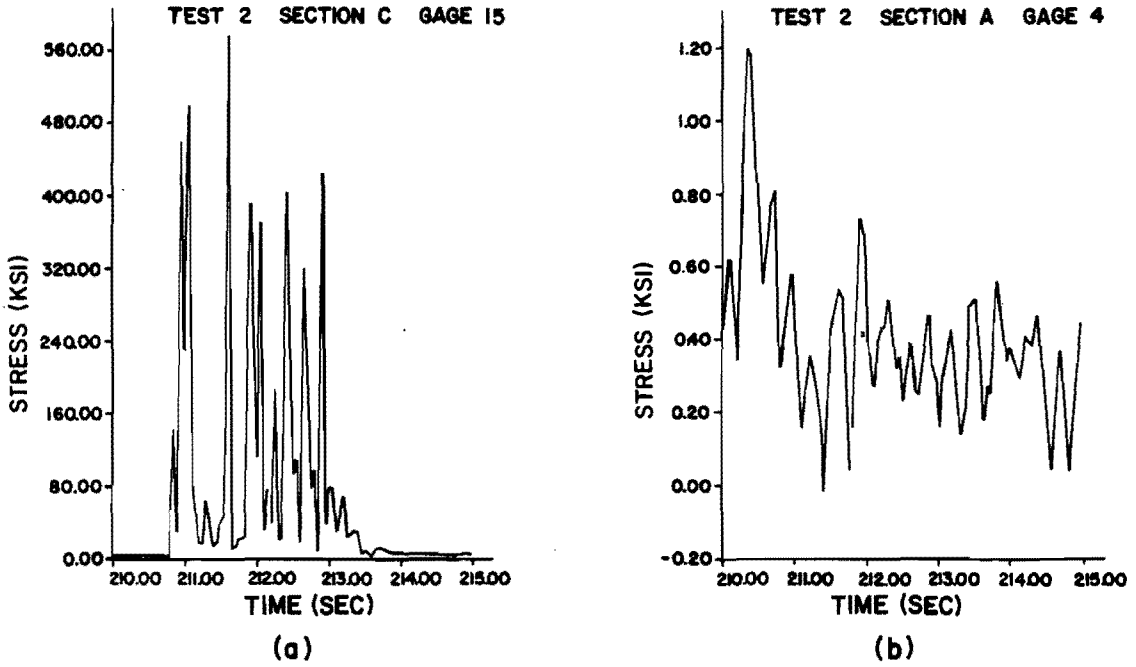

Fig. 3.16 Comparison of a bad strain gage and a good strain gage

TABLE 3.6 SUMMARY OF DATA AT SECTIONS A AND D FOR TESTS 1 THROUGH 8

Tests	1	2	3	4	5	6	7	8
Section A:								
Record Length (min.)	--	20.0	20.0	20.0	10.0	10.0	20.0	10.0
S_{RE} (ksi)	--	0.502	0.524	0.441	0.524	0.720	0.440	0.510
$N_M \left(\frac{\text{cycles}}{\text{min.}}\right)$	--	88.7	74.4	72.1	94.5	106.8	103.4	137.7
$\frac{N_L}{A}$ (min.)	--	0.0890	0.0932	0.1614	0.0735	0.0251	0.1130	0.0546
Section D:								
Record Length (min.)	15.0	20.0	20.0	20.0	10.0	10.0	20.0	10.0
S_{RE} (ksi)	0.587	0.831	0.831	0.681	0.847	0.911	0.700	0.859
$N_M \left(\frac{\text{cycles}}{\text{min.}}\right)$	124.0	249.0	157.5	261.7	154.7	106.3	195.5	210.8
$\frac{N_L}{A}$ (min.)	0.0399	0.0070	0.0111	0.0121	0.0106	0.0124	0.149	0.0075

TABLE 3.7 SUMMARY OF DATA AT SECTIONS B AND C FOR TESTS 1 THROUGH 8

Tests	1	2	3	4	5	6	7	8
Section B:								
Record Length (min.)	--	20.0	20.0	20.0	10.0	10.0	20.0	10.0
S_{RE} (ksi)	--	0.522	0.586	0.454	0.537	0.609	0.538	0.541
$N_M \left(\frac{\text{cycles}}{\text{min.}}\right)$	--	171.3	104.5	72.4	126.4	161.9	180.4	188.3
$\frac{N_L}{A}$ (min.)	--	0.0410	0.0476	0.1477	0.0511	0.0274	0.0356	0.0335
Section C:								
Record Length (min.)	15.0	--	20.0	20.0	10.0	10.0	20.0	10.0
S_{RE} (ksi)	0.621	--	0.627	0.422	0.529	0.646	0.534	0.528
$N_M \left(\frac{\text{cycles}}{\text{min.}}\right)$	102.0	--	84.1	73.5	102.0	171.8	192.0	200.8
$\frac{N_L}{A}$ (min.)	0.0408	--	0.0484	0.1812	0.0664	0.0216	0.0340	0.0338

shorter at sections C and D than at sections A and B. For all tests, section D yields shorter fatigue-life estimates than section C. Section D is located on the girder underneath the left-most traffic lane. It follows that a majority of the traffic uses the left-most traffic lane since the fatigue-life estimates are consistently lower at section D than at other sections. For most highways, the traffic usually uses the right traffic lane, however, for this bridge a major portion of the traffic is routed to the left further down the highway. The direction which the major portion of the traffic is routed may explain the lower fatigue-life estimates computed at section D.

A comparison of the data for different record lengths at sections C and D for each test is given in Tables 3.8 through 3.15. Only sections C and D are shown because these sections are in a maximum live-load moment region, and therefore control the fatigue life.

Figure 3.17 compares the estimated fatigue life and effective stress range as a function of record length at section D for each test. The effective stress range increases between record lengths at 5 and 10 minutes for most tests. After 10 minutes, S_{RE} tends to remain constant. The estimated fatigue life decreases between record lengths of 5 and 10 minutes for most tests. After 10 minutes, N_L tends to remain constant.

The effective stress range and estimated fatigue life are dependent on the stress range histograms for a particular record length. The behavior of S_{RE} and N_L with record length depends upon when the major stress ranges occur. If the major stress ranges occur in the first 5 minutes of a 20-minute record, then S_{RE} and N_L will tend to remain constant after approximately 10 minutes. Figure 3.18 shows stress range histograms for test 4 at section D. The major stress-range cycles occur within the first 5 minutes. As the record length increases, small stress-range cycles are added to

TABLE 3.8 COMPARISON OF DATA WITH VARIABLE RECORD LENGTH FOR TEST 1

Record Length (min.)	5	10	15	20
Section C:				
S_{RE} (ksi)	0.641	0.614	0.621	0.662
$N_M \left(\frac{\text{cycles}}{\text{min.}}\right)$	109.6	104.1	102.1	103.0
$\frac{N_L}{A} \left(\frac{\text{min.}}{A}\right)$	0.0346	0.0415	0.0408	0.0334
Section D:				
S_{RE} (ksi)	0.670	0.570	0.587	--
$N_M \left(\frac{\text{cycles}}{\text{min.}}\right)$	153.0	139.0	124.0	--
$\frac{N_L}{A} \left(\frac{\text{min.}}{A}\right)$	0.0217	0.0339	0.0399	--

TABLE 3.9 COMPARISON OF DATA WITH VARIABLE RECORD LENGTH FOR TEST 2

Record Length (min.)	5	10	15	20
Section D:				
S_{RE} (ksi)	0.871	0.794	0.821	0.831
$N_M \left(\frac{\text{cycles}}{\text{min.}}\right)$	259.0	267.9	250.6	249.0
$\frac{N_L}{A} \left(\frac{\text{min.}}{A}\right)$	0.00585	0.00759	0.00720	0.00700

TABLE 3.10 COMPARISON OF DATA WITH VARIABLE RECORD LENGTH FOR TEST 3

Record Length (min.)	5	10	15	20
Section C:				
S_{RE} (ksi)	0.748	0.625	0.661	0.627
$N_M \left(\frac{\text{cycles}}{\text{min.}}\right)$	80.0	82.9	90.6	84.1
$\frac{N_L}{A}\left(\frac{\text{min.}}{A}\right)$	0.02985	0.0494	0.0382	0.484
Section D:				
S_{RE} (ksi)	0.991	0.855	0.857	0.831
$N_M \left(\frac{\text{cycles}}{\text{min.}}\right)$	129.0	130.3	145.9	157.5
$\frac{N_L}{A}\left(\frac{\text{min.}}{A}\right)$	0.00795	0.0123	0.0109	0.0111

TABLE 3.11 COMPARISON OF DATA WITH VARIABLE RECORD LENGTH FOR TEST 4

Record Length (min.)	5	10	15	20
Section C:				
S_{RE} (ksi)	0.466	0.461	0.434	0.422
$N_M \left(\frac{\text{cycles}}{\text{min.}}\right)$	82.8	81.7	75.3	73.5
$\frac{N_L}{A} \left(\frac{\text{min.}}{A}\right)$	0.119	0.125	0.162	0.181
Section D:				
S_{RE} (ksi)	0.791	0.731	0.683	0.681
$N_M \left(\frac{\text{cycles}}{\text{min.}}\right)$	272.4	263.7	263.4	261.7
$\frac{N_L}{A} \left(\frac{\text{min.}}{A}\right)$	0.0074	0.00969	0.0119	0.0121

TABLE 3.12 COMPARISON OF DATA WITH VARIABLE RECORD LENGTH FOR TEST 5

Record Length (min.)	5	10
Section C:		
S_{RE} (ksi)	0.576	0.529
$N_M \left(\frac{\text{cycles}}{\text{min.}}\right)$	108.2	102.0
$\frac{N_L}{A} \left(\frac{\text{min.}}{A}\right)$	0.0664	0.0484
Section D:		
S_{RE} (ksi)	0.995	0.847
$N_M \left(\frac{\text{cycles}}{\text{min.}}\right)$	162.0	154.7
$\frac{N_L}{A} \left(\frac{\text{min.}}{A}\right)$	0.00625	0.0106

TABLE 3.13 COMPARISON OF DATA FOR VARIABLE RECORD LENGTH FOR TEST 6

Record Length (min.)	5	10
Section C:		
S_{RE} (ksi)	0.566	0.646
$N_M \left(\frac{\text{cycles}}{\text{min.}}\right)$	169.6	171.8
$\frac{N_L}{A} \left(\frac{\text{min.}}{A}\right)$	0.0326	0.0216
Section D:		
S_{RE} (ksi)	0.952	0.911
$N_M \left(\frac{\text{cycles}}{\text{min.}}\right)$	183.4	106.3
$\frac{N_L}{A} \left(\frac{\text{min.}}{A}\right)$	0.0063	0.0124

TABLE 3.14 COMPARISON OF DATA FOR VARIABLE RECORD LENGTH FOR TEST 7

Record Length (min.)	5	10	15	20
Section C:				
S_{RE} (ksi)	0.584	0.552	0.550	0.534
$N_M\left(\frac{\text{cycles}}{\text{min.}}\right)$	260.000	223.3	201.4	192.0
$\frac{N_L}{A}\left(\frac{\text{min.}}{A}\right)$	0.01935	0.0265	0.030	0.034
Section D:				
S_{RE} (ksi)	0.747	0.729	0.719	0.700
$N_M\left(\frac{\text{cycles}}{\text{min.}}\right)$	241.8	214.3	201.1	195.5
$\frac{N_L}{A}\left(\frac{\text{min.}}{A}\right)$	0.00990	0.0121	0.0134	0.0149

TABLE 3.15 COMPARISON OF DATA FOR VARIABLE RECORD LENGTH FOR TEST 8

Record Length (min.)	5	10
Section C:		
S_{RE} (ksi)	0.524	0.528
$N_M \left(\frac{\text{cycles}}{\text{min.}}\right)$	212.8	200.8
$\frac{N_C}{A}\left(\frac{N_L}{A}\right)$	0.03255	0.0338
Section D:		
S_{RE} (ksi)	0.648	0.859
$N_M \left(\frac{\text{cycles}}{\text{min.}}\right)$	222.2	210.8
$\frac{N_L}{A}\left(\frac{\text{min.}}{A}\right)$	0.0166	0.00748

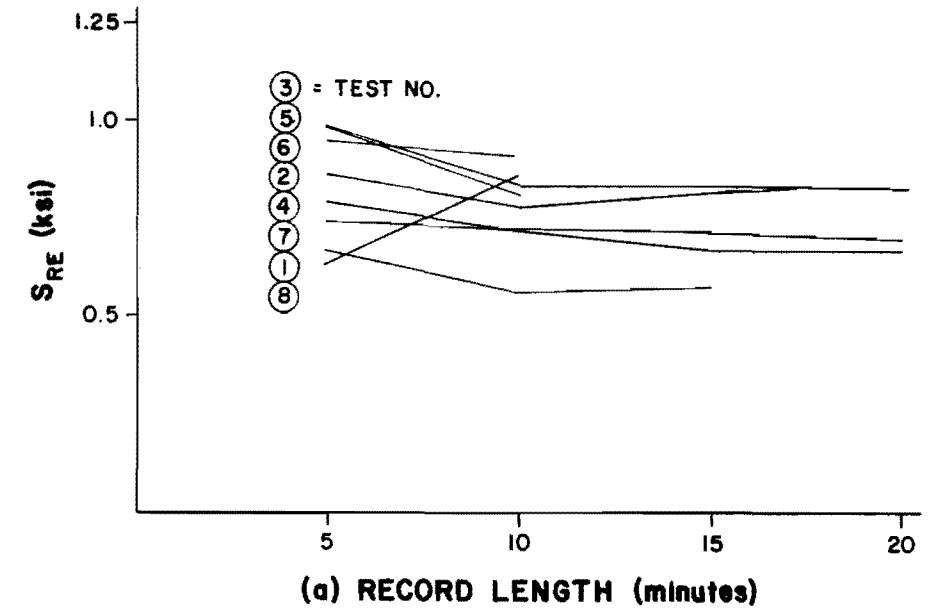

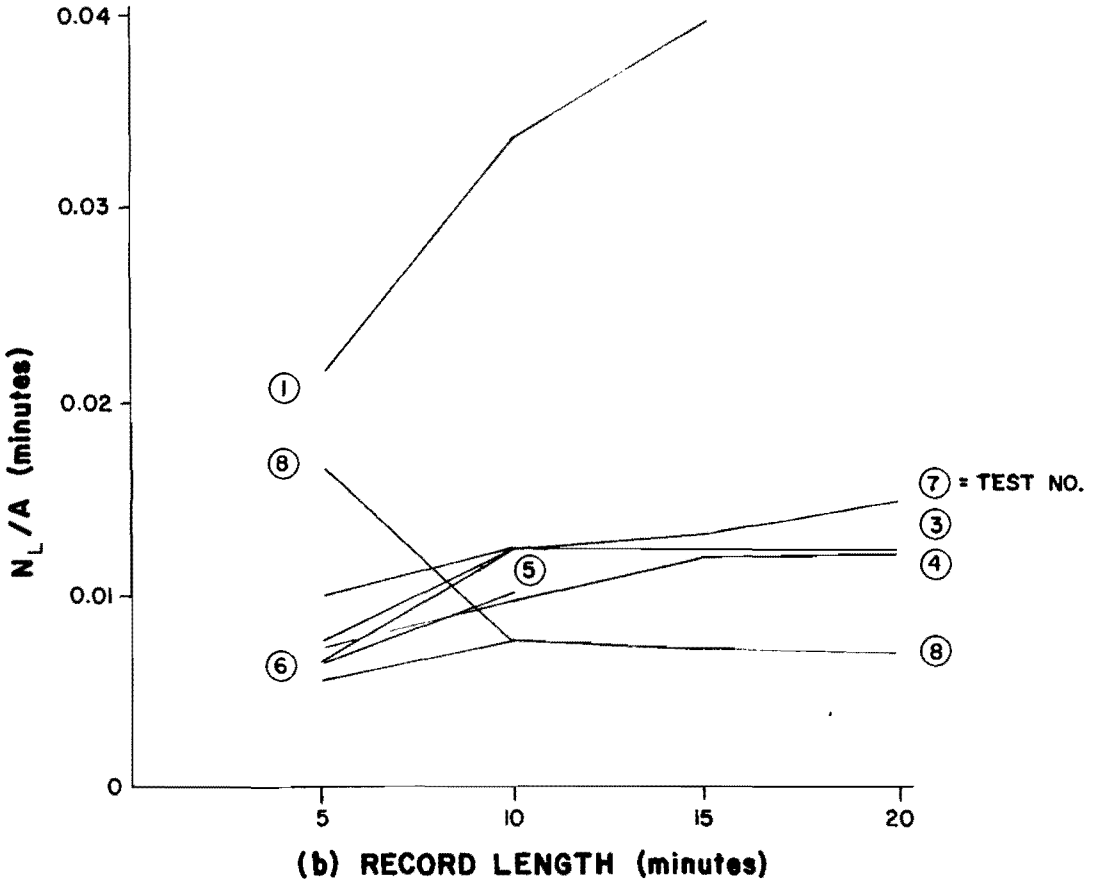

Fig. 3.17 Comparison of N_L and S_{RE} with record length for each test at section D

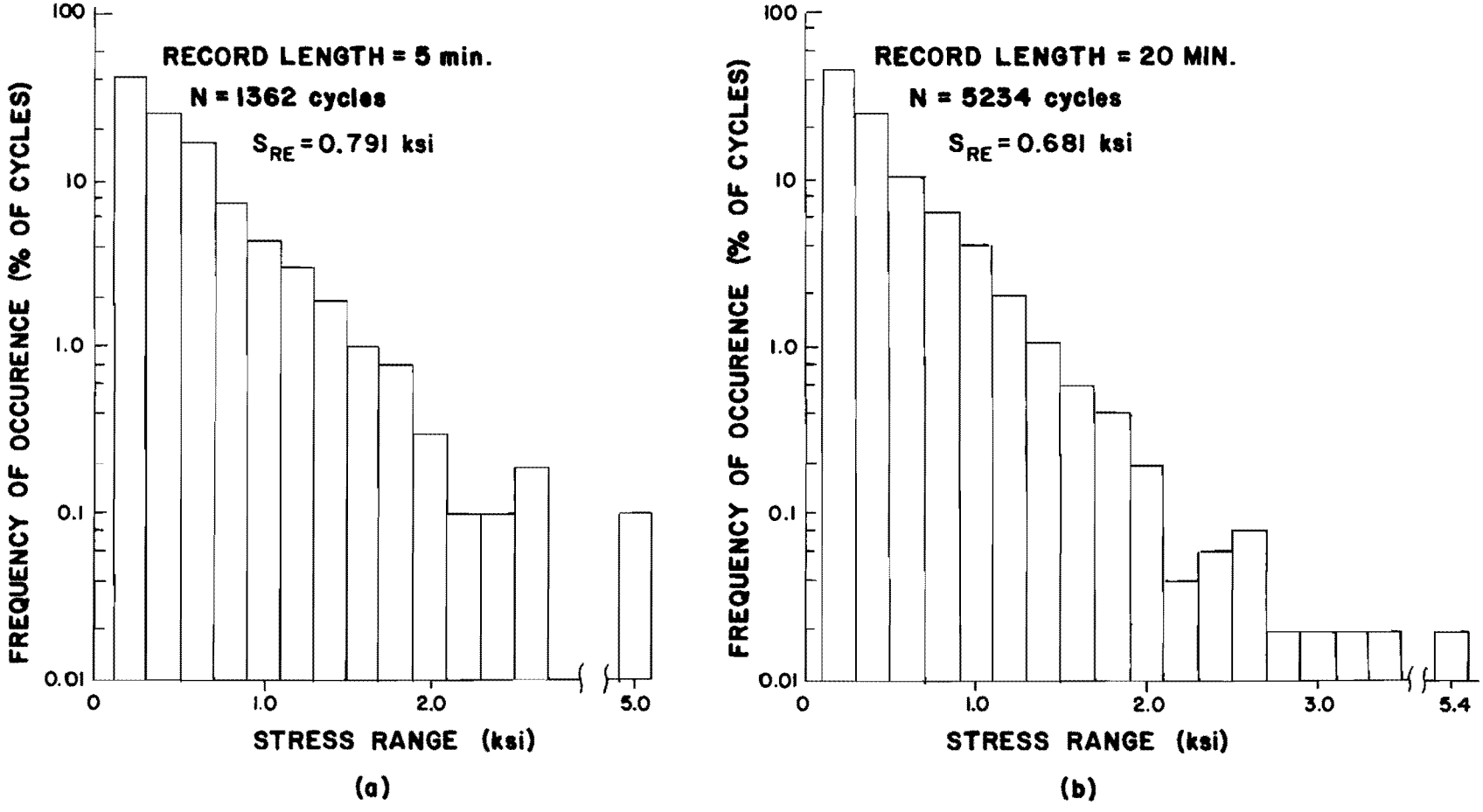

Fig. 3.18 Stress range histograms at section D for test 4

the stress histogram. Because the major stress range occurs early in the record, N_L and S_{RE} approach a constant value after a 15-minute record length as shown in Fig. 3.17.

If major stress ranges occur in the last 5 minutes of a record, then S_{RE} and N_L are significantly affected. Figure 3.19 shows stress-range histograms for record lengths of 5 and 10 minutes at section D for test 8. The major stress-range cycles occur within the last 5 minutes of the record. The addition of the large stress ranges increases S_{RE} and decreases N_L with increasing record length as shown in Fig. 3.17.

As the test record length approaches the total life of a structure, then S_{RE} and N_L will approach constant values which represent the total life of the structure. Figure 3.17 shows that a 10-minute record length or greater is sufficient to represent the stress history of the bridge for that period since S_{RE} and N_L approach constant values after a 10-minute record length for most tests. In the following chapter, fatigue-life estimates will be computed from record lengths equal to or greater than 10 minutes.

The fatigue life and effective stress range are plotted as a function of record length in Fig. 3.20a and 3.20b for section C for all tests. The effective stress range varies in the first 10 minutes of the record, but approaches a constant for each test after 10 minutes. This is similar to the behavior of S_{RE} found at section D in Fig. 3.17. The estimated fatigue life at section C is not similar to the behavior of N_L at section D. For example, N_L is constant at section C for test 8 while N_L sharply decreases with increasing record length at section D. Also, the fatigue-life estimates are longer at section C than at section D. Sections C and D are located on separate longitudinal girders. The difference between the behavior of N_L at sections C and D indicates that traffic patterns differ for each girder and that little interaction occurs between the two girders.

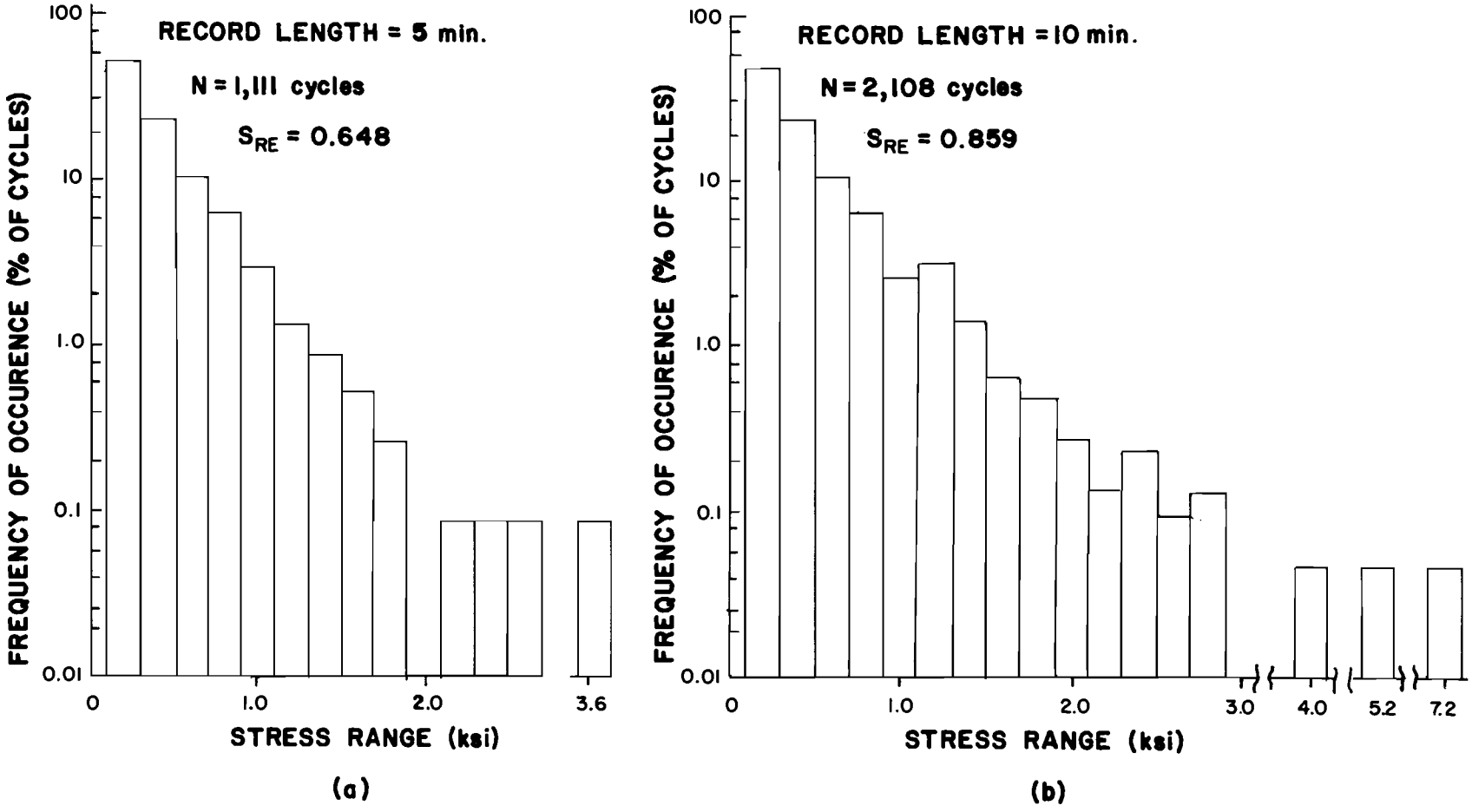

Fig. 3.19 Stress histograms at section D for test 8

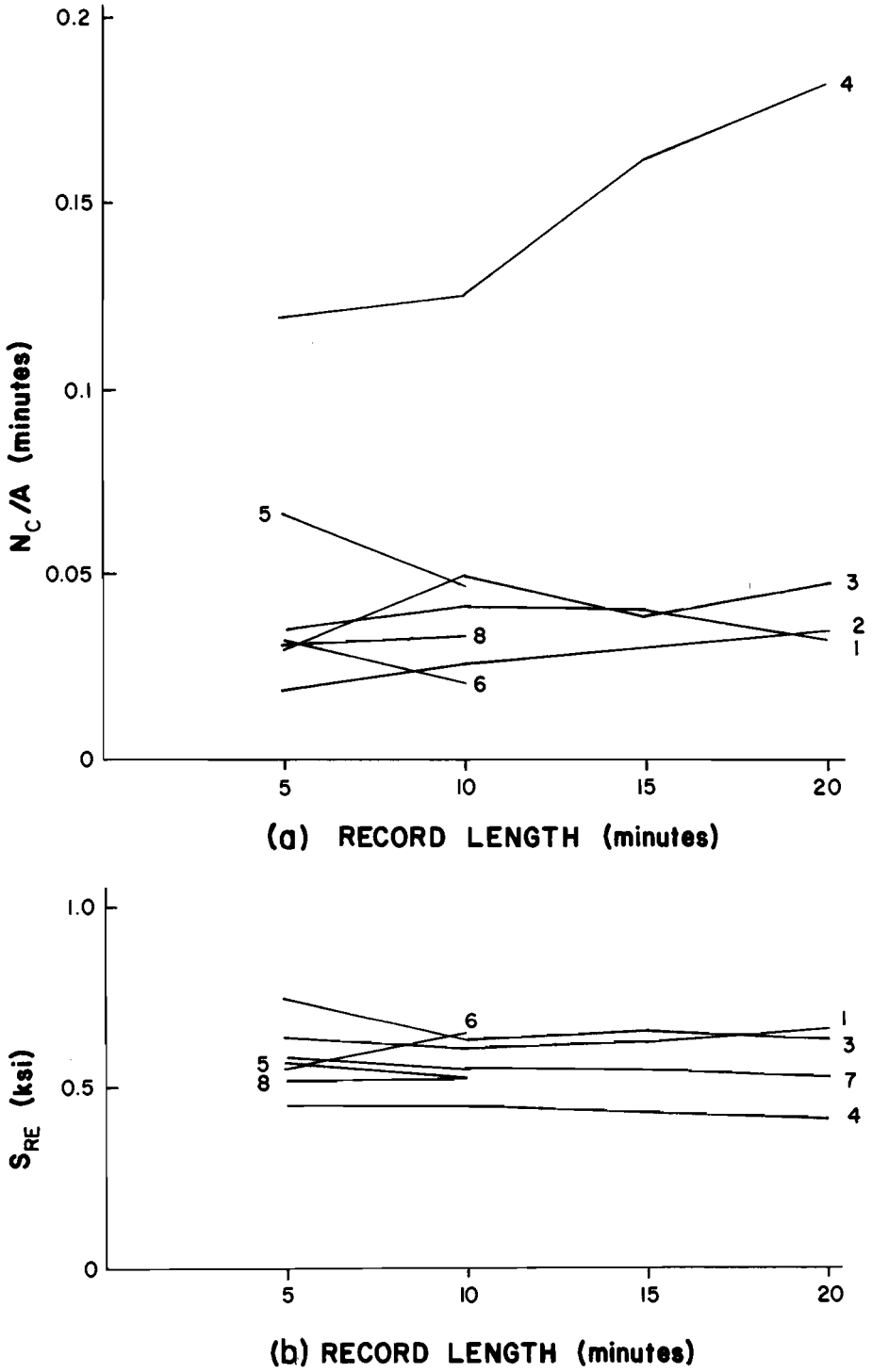

Fig. 3.20 Comparison of N_L and S_{RE} with record length for each test at section C

Table 3.16 shows a comparison of the data at sections C and D for different times of the day. In general, the data do not show any significant trends; however, the estimated fatigue life, N_L, was consistently lower on the second day of testing (Friday) relative to the first day of testing (Thursday). Figure 3.21 is a traffic count histogram for each day of the test. The traffic counts were consistently higher on the second day of the test as compared to the first. Therefore, calculations of fatigue life should be lower for the second day of testing because of the increase in traffic.

Figure 3.22 shows the trucks per hour during each test for each testing day. The truck traffic was greater on Friday during the first and last tests of the day. The truck traffic was greater on Thursday for the remaining tests; however, the difference in truck traffic between the two days is not as great during these tests than for the first and last tests of each day. The fatigue-life estimates at section D are much lower on Friday than on Thursday for the first and last tests of each day as shown in Table 3.16. The fatigue-life estimates at section D on Friday are similar to those on Thursday for the remaining tests. The differences in N_L at section D between testing days correspond to the differences in truck traffic between testing days while this pattern is not followed at section C. This indicates that most of the truck traffic traveled in the left-most lane over the girder which contains section D. Since most of the truck traffic traveled over the girder which contains section D, the fatigue-life estimates at section D should be lower than those at section C.

TABLE 3.16 COMPARISON OF DATA AT SECTIONS C AND D FOR DIFFERENT TIMES OF THE DAY. RECORD LENGTH = 10 MINUTES

Date	October 2, 1980				October 3, 1980			
Time of Day	10:30 am	1:40 pm	3:10 pm	4:20 pm	10:50 am	1:35 pm	3:00 pm	4:20 pm
Section C:								
S_{RE} (ksi)	0.614	--	0.625	0.461	0.529	0.646	0.552	0.528
$N_M \left(\frac{\text{cycles}}{\text{min.}}\right)$	104.1	--	82.9	81.7	102.0	171.8	223.3	200.8
N_L (min.)	0.0415	--	0.0494	0.1250	0.0664	0.0216	0.0266	0.0338
Section D:								
S_{RE} (ksi)	0.570	0.871	0.885	0.791	0.857	0.786	0.729	0.859
$N_M \left(\frac{\text{cycles}}{\text{min.}}\right)$	139.0	129.5	130.3	136.2	144.7	176.8	214.3	210.8
N_L (min.)	0.0339	0.0117	0.0123	0.0148	0.0106	0.0115	0.0121	0.0075

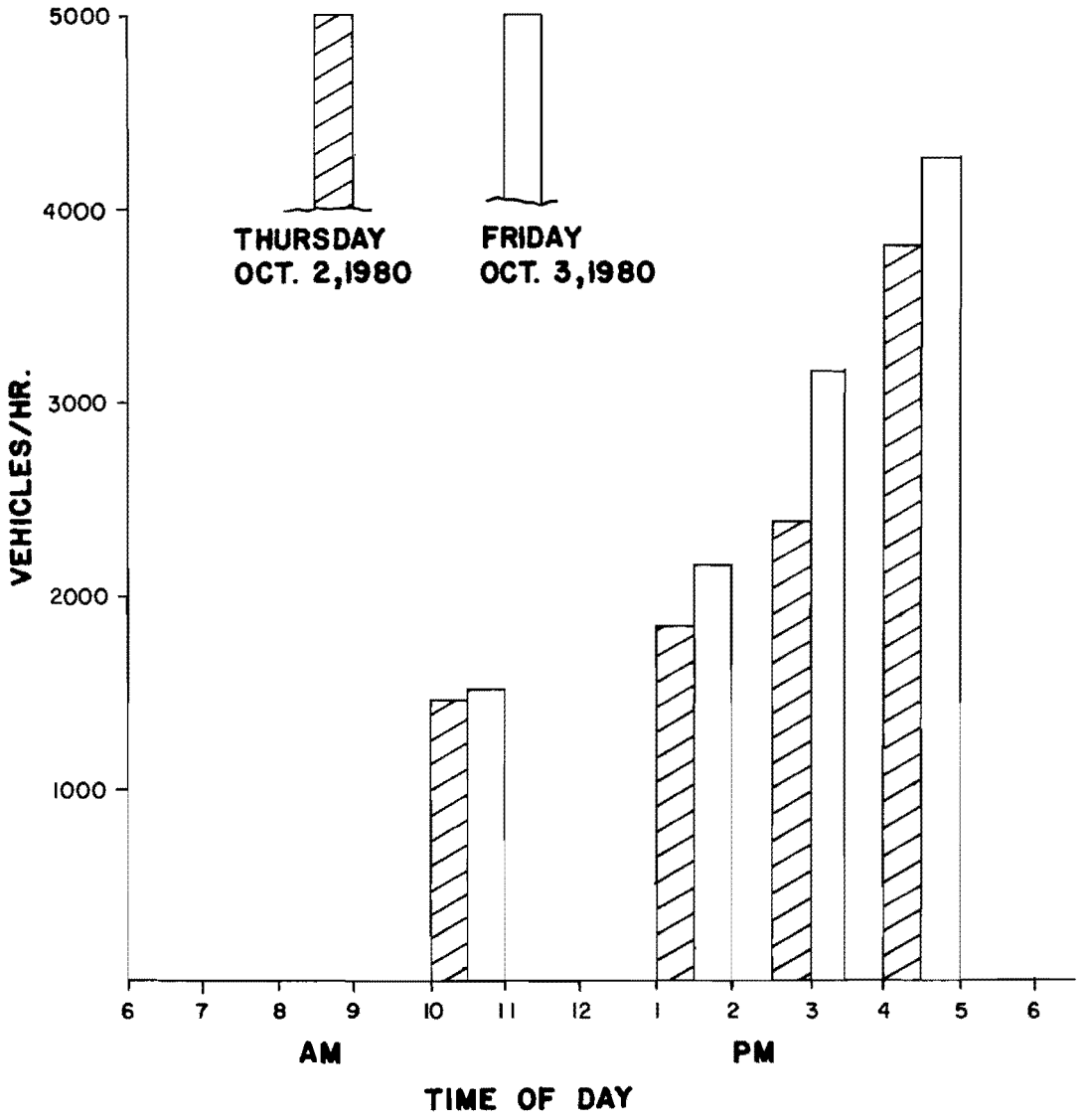

Fig. 3.21 Vehicles per hour during tests

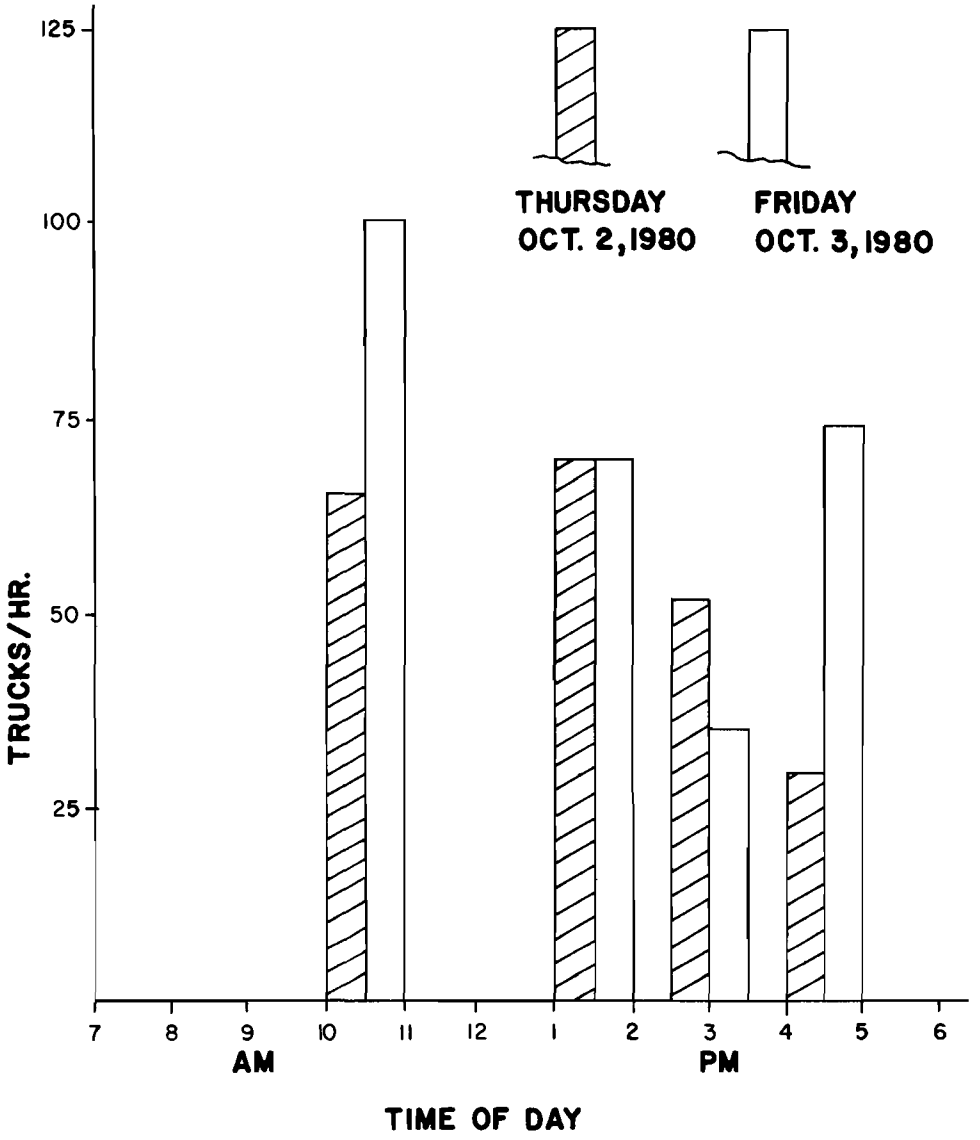

Fig. 3.22 Trucks per hour during tests

CHAPTER 4

ANALYSIS OF TEST DATA

4.1 Introduction

4.1.1 Fatigue life estimates from N_L and N_{LT}. The parameter N_L was calculated from tests conducted under normal traffic conditions. N_L represents the fatigue life of a detail. A fatigue life estimate, L, of a detail is given by

$$L = N_L \times A \tag{4.1}$$

where L is the fatigue life in units of time.

N_{LT} was computed from stress histories measured during the passage of the test truck. N_{LT} represents the number of times the test truck may pass over the bridge before failure occurs. The number of trucks required for fatigue failure is given by

$$T = N_{LT} \times A \tag{4.2}$$

where T is the number of trucks.

4.1.2 AASHTO Details for Fatigue. The parameter, A, is a function of the geometry and fabrication of a welded detail. The AASHTO specifications divide welded details into six categories with five categories labeled A through E and a sixth labeled E′. Category A, for example, includes base metal with rolled or cleaned surfaces and Category C includes the toe of transverse stiffener welds on girder webs or flanges. Each category of welded detail is associated with a S_R - N curve as shown in Fig. 1.1. The equation for each curve is given by

$$N = A \times S_R^{-n} \tag{4.3}$$

where n is approximately equal to 3. An average value of A for each category was computed using Eq. (4.3) and values of S_R at N equal to 2 million cycles and at N equal to 100,000 cycles. The computed values of A are shown in Table 4.1 for each category.

Figure 4.1 is an elevation of the longitudinal girder of the test bridge in the vicinity of the gaged sections. According to the AASHTO specifications the web-to-flange fillet weld is a Category B detail, the toe of the transverse stiffener fillet weld is a Category C detail, and the toe of the longitudinal stiffener fillet weld is a Category E detail. The intersection of the floor beam and longitudinal girder occurs at the midpoint between gaged sections on each girder.

4.1.3 Experimental Model of the Longitudinal-Transverse Stiffener Detail. Experimental studies of fatigue behavior have been performed on the termination of a longitudinal stiffener

TABLE 4.1 VALUES OF A FOR EACH AASHTO CATEGORY

A	2.46×10^{10}
B	1.04×10^{10}
C	3.84×10^{9}
D	1.98×10^{9}
E	9.75×10^{8}
E′	4.24×10^{8}

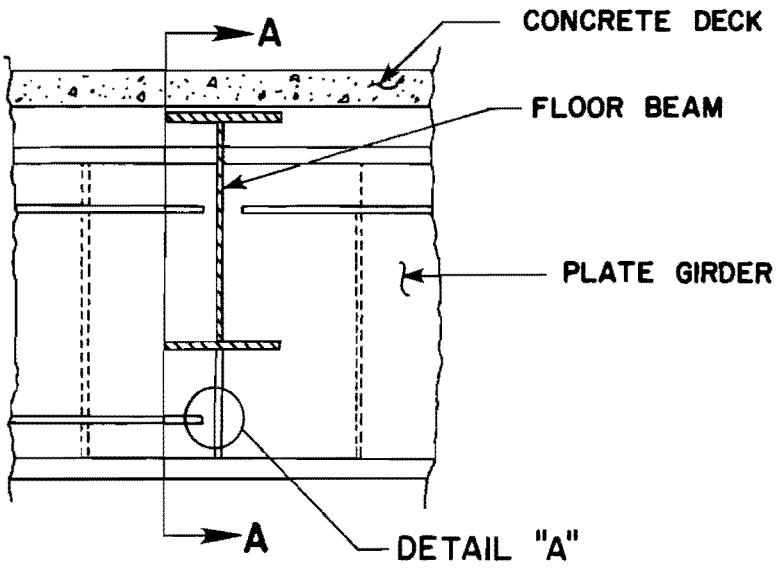

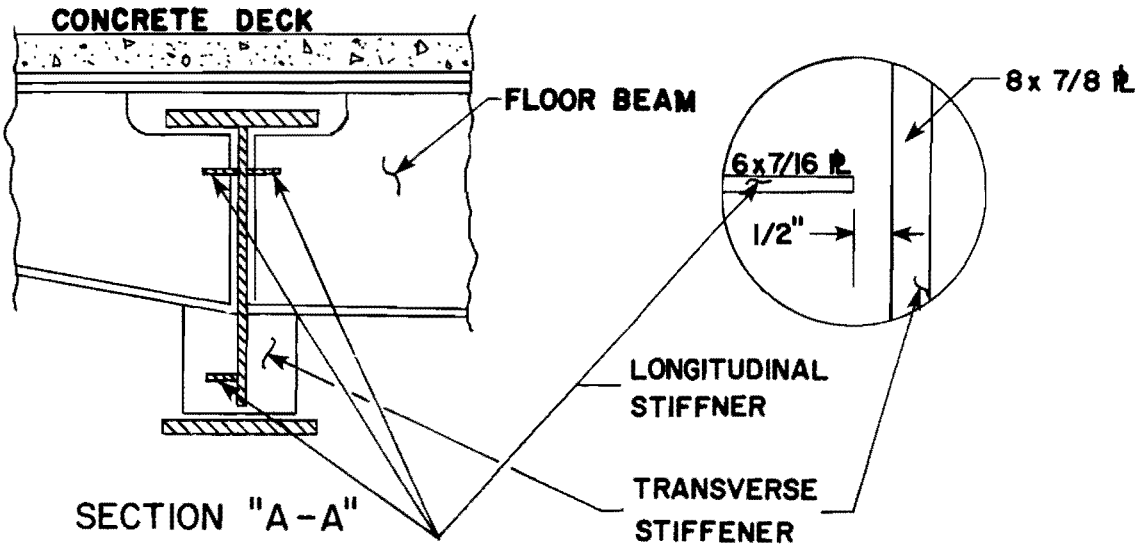

Fig. 4.1 Floor beam-to-plate girder connection

fillet weld near a transverse stiffener fillet weld.[16] This type of detail is found on the test bridge at the intersection of the longitudinal girder and floor beam as shown in Fig. 4.1. The data collected from the experimental studies are shown in Fig. 4.2 with a lower-bound S_R - N curve drawn for the data. This detail would be categorized as a Category E detail under the present AASHTO specifications. Figure 4.2 shows that the fatigue behavior of the longitudinal-transverse stiffener intersection detail, LTSI, is worse than a Category E detail at a given stress range. The fatigue life of the LTSI detail determines the fatigue life of the test bridge. Fatigue-life estimates of the bridge are computed in succeeding sections using the value of A from the data collected in the experimental study of the LTSI detail.

A modification of the LTSI detail was studied to determine if the fatigue behavior of this detail could be improved.[16] The modification, shown in Fig. 4.3, provides a smooth transition for the termination of the longitudinal stiffener fillet weld, and a connecting plate is welded between the longitudinal stiffener and the transverse stiffener. The data for the modified LTSI detail are presented in Fig. 4.2. The data show that the fatigue behavior of the LTSI detail is improved using the modifications described. The data indicate that the modified LTSI detail behaves similarly to a Category E detail. Fatigue-life estimates for the LTSI detail are compared with fatigue-life estimates for a Category E detail in succeeding sections to indicate the improvement of the fatigue life of the bridge using the modified LTSI detail.

4.1.4 Fatigue Parameters for the LTSI Detail from the Traffic Tests. The data obtained from the traffic tests were used to obtain values of S_{RE}, N_M, and N_L for each gaged section on the east and west longitudinal girders, measured at the flange-to-web intersection. These values are listed in Tables 3.6 and 3.7.

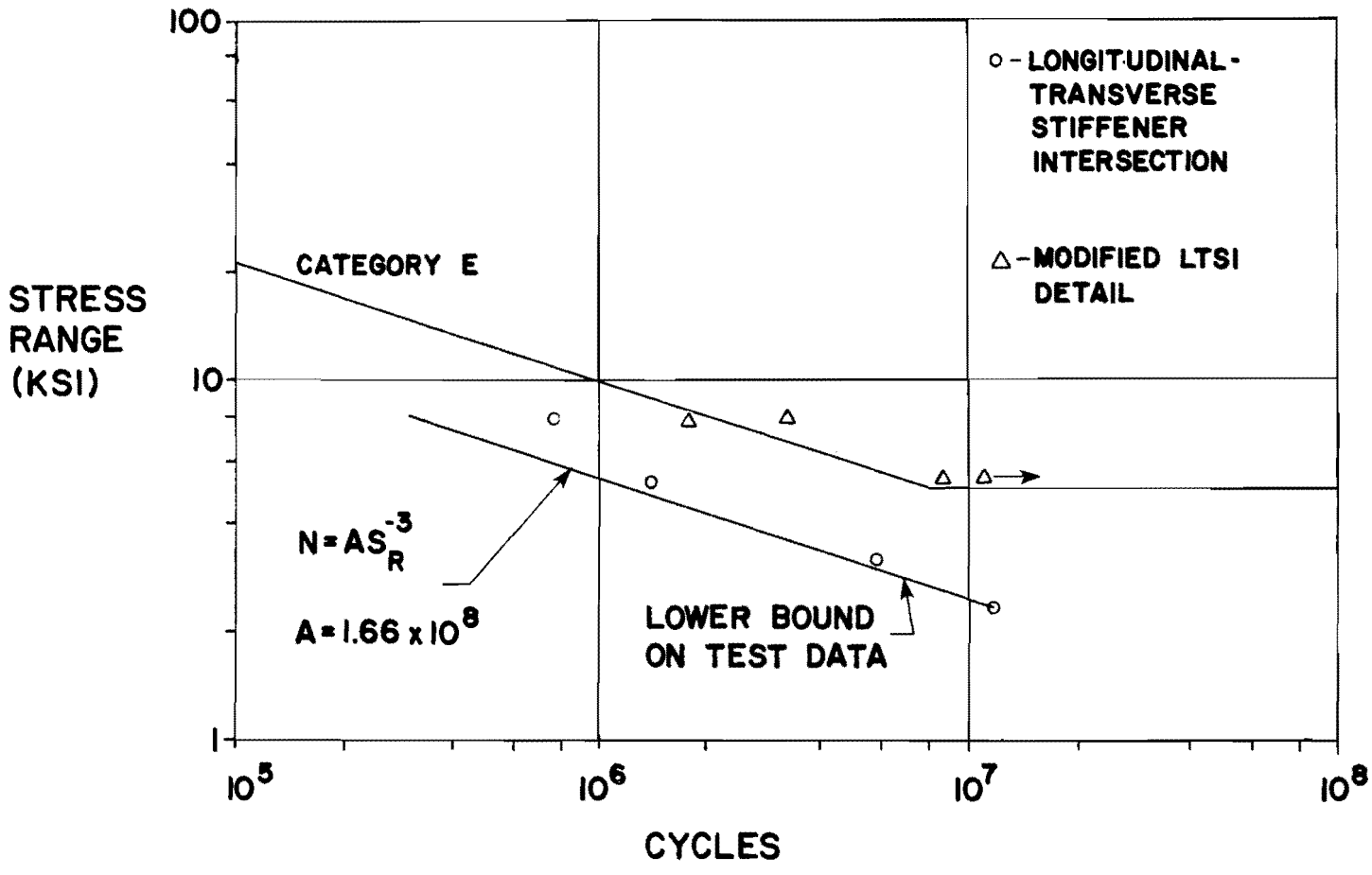

Fig. 4.2 Test data for the LTSI and modified LTSI detail

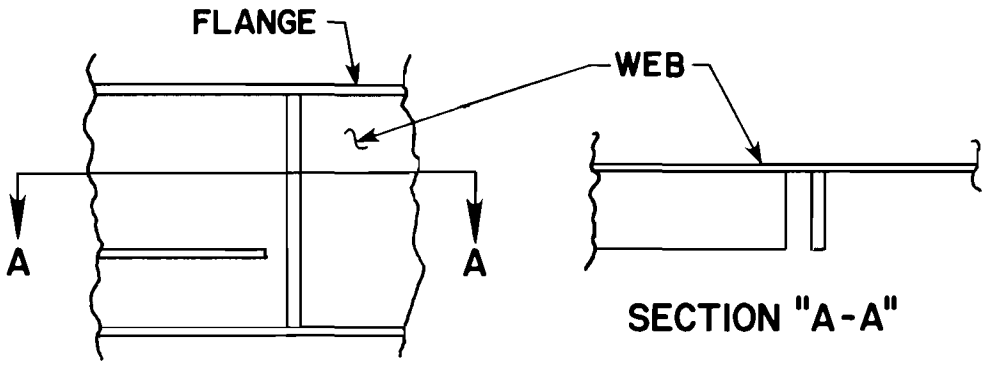

LONGITUDINAL-TRANSVERSE STIFFENER DETAIL

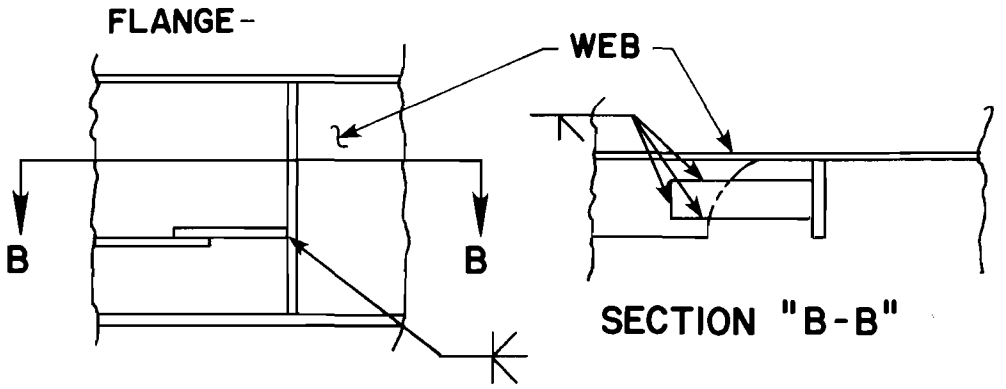

MODIFIED LONGITUDINAL-TRANSVERSE STIFFENER DETAIL

Fig. 4.3 Modification of a longitudinal-transverse stiffener intersection detail

The LTSI detail is located 15 in. above the gage level at the midpoint between gaged sections on each girder. Values of S_{RE} and N_M are computed at the LTSI detail assuming a linear relationship of S_{RE} and N_M between gaged sections on each girder, and plane sections are assumed to remain plane. The neutral axis is 36 in. above the gage level and 21 in. above the LTSI detail. Thus, the ratio of S_{RE} and N_M at the LTSI detail to S_{RE} and N_M at the gage level is 21/36. The values of S_{RE} and N_M at the LTSI detail were used to compute N_L at the LTSI detail using Eq. (3.4). The LTSI detail on the east longitudinal girder yields smaller values of N_L than the LTSI detail on the west longitudinal girder, and therefore, determines the fatigue life of the bridge. Values of S_{RE}, N_M, and N_L for the LTSI detail on the east longitudinal girder are listed in Table 4.2. Table 4.2 indicates that N_L for Traffic Test 6 yields the shortest fatigue-life estimate and N_L for Traffic Test 7 yields the longest fatigue-life estimate. These two values of N_L will be used in succeeding sections to compute a range of fatigue-life estimates for the test bridge. Average fatigue-life estimates will be computed using the average value of N_L from Table 4.2.

4.1.5 Fatigue Parameters for the LTSI Detail from the Test Truck Data. The data collected from the tests conducted with the test truck were used to compute values of S_{RE}, N_T, and N_{LT} at Sections A and D on the east longitudinal girder. These values are listed in Table 3.3. Values of S_{RE} and N_T were computed at the LTSI detail assuming a linear distribution of S_{RE} and N_T between gaged sections and adjusting for the difference in elevation of the gages and the detail. Values of N_{LT} for the LTSI stiffener were computed from S_{RE} and N_T using Eq. (3.3). Table 4.3 lists the values of S_{RE}, N_T, and N_{LT} at the LTSI detail. Only the 50 mph tests are listed because 50 mph is the normal speed of trucks traveling across the bridge. Furthermore,

TABLE 4.2 FATIGUE PARAMETERS AT THE TOE OF THE LONGITUDINAL STIFFENER FOR THE EAST LONGITUDINAL GIRDER FROM THE TRAFFIC TESTS

Test	1	2	3	4	5	6	7	8	Avg.
S_{RE} (ksi)	--	0.388	0.396	0.327	0.400	0.476	0.332	0.399	0.388
$N_M \left(\frac{\text{cycles}}{\text{min.}}\right)$	--	98.6	67.7	97.4	72.9	62.4	86.9	10.2	84.0
$\frac{N_L}{A}$ (minutes)	--	0.174	0.238	0.294	0.214	0.148	0.314	0.154	0.204

TABLE 4.3 FATIGUE PARAMETERS FOR THE LONGITUDINAL-TRANSVERSE STIFFENER DETAIL ON THE EAST LONGITUDINAL GIRDER FROM TEST TRUCK DATA

Test	50 mph	50 mph	50 mph	50 mph	Avg.
S_{RE} (ksi)	1.02	1.13	1.06	1.08	1.07
N_T $\frac{\text{cycles}}{\text{truck}}$	11.0	8.2	9.3	9.9	9.6
$\frac{N_{LT}}{A}$ $\frac{\text{trucks}}{\text{life}}$	0.0857	0.0845	0.0903	0.0802	0.0850

these tests yield shorter fatigue life estimates than tests at slower speeds. An average value of S_{RE}, N_T, and N_{LT} is also given in Table 4.3 and is used in succeeding sections to compute fatigue-life estimates.

4.1.6 Average Daily Truck Traffic for the Traffic Tests. The average daily traffic, ADT, and the average daily truck traffic, ADTT, for each traffic test are listed in Table 4.4. The ADTT and ADT were computed as follows:

$$ADT = \frac{\text{vehicles}}{\text{test record length}} \times \frac{60 \text{ min.}}{\text{hour}} \times \frac{24 \text{ hours}}{\text{day}} \qquad (4.4a)$$

$$ADTT = \frac{\text{trucks}}{\text{test record length}} \times \frac{60 \text{ min.}}{\text{hour}} \times \frac{24 \text{ hours}}{\text{day}} \qquad (4.4b)$$

where the test record length is in minutes. The vehicle and truck counts were obtained visually and recorded for each test period. The values of ADT and ADTT listed in Table 4.4 represent values required to produce a continuous stress history over the life of the structure similar to the stress history measured during each test.

TABLE 4.4 ADTT AND ADT FOR EACH TRAFFIC TEST

Test	ADTT	ADT
1	1584	38496
2	1680	46920
3	1272	60360
4	720	93264
5	2424	39984
6	1656	55368
7	864	78192
8	1776	104568
Average	1497	64644

4.2 Fatigue-Life Estimates from Traffic Data

4.2.1 Equation for Fatigue-Life Estimates. A fatigue-life estimate of the test bridge is computed from the measured traffic data using the following equation:

$$Y = N_L \times A \times \frac{1 \text{ hour}}{60 \text{ min.}} \times \frac{1 \text{ day}}{x \text{ hours}} \times \frac{1 \text{ week}}{y \text{ days}} \times \frac{1 \text{ year}}{52 \text{ weeks}} \qquad (4.5a)$$

or

$$Y = \frac{N_L \times A}{(x \text{ hours}) \times (y \text{ days})} \times \frac{1}{3120} \qquad (4.5b)$$

where Y is the fatigue life in years. The number of hours per day and days per week are left as variables in Eq. (4.5) to account for variations in fatigue damage during the day or week.

4.2.2 Variations in Fatigue Damage During the Day. Figure 4.4 shows the variation in traffic volume during the day at a location on the expressway near the test bridge.[18] The traffic volume during the early morning hours was considerably less than at midday. Therefore, it is reasonable to assume that fatigue damage is less during the early morning hours than at midday. One method of modeling the variation in fatigue damage during the day in a fatigue-life estimate is to assume there are fewer than 24 hours in a day. Table 4.5 is a list of fatigue-life estimates for the LTSI detail and a modified LTSI detail for different values of hours in a day. The fatigue life increases with decreasing number of hours in a day. Table 4.5 also lists the ADT and ADTT required to produce the corresponding fatigue lives. The daily traffic count given in Fig. 4.4 is within the range of the ADT's computed in Table 4.5 which indicates that these values are reasonable values of ADT to expect for the test bridge. Therefore, the fatigue-life estimates in Table 4.5 are reasonable estimates of the fatigue life of the bridge.

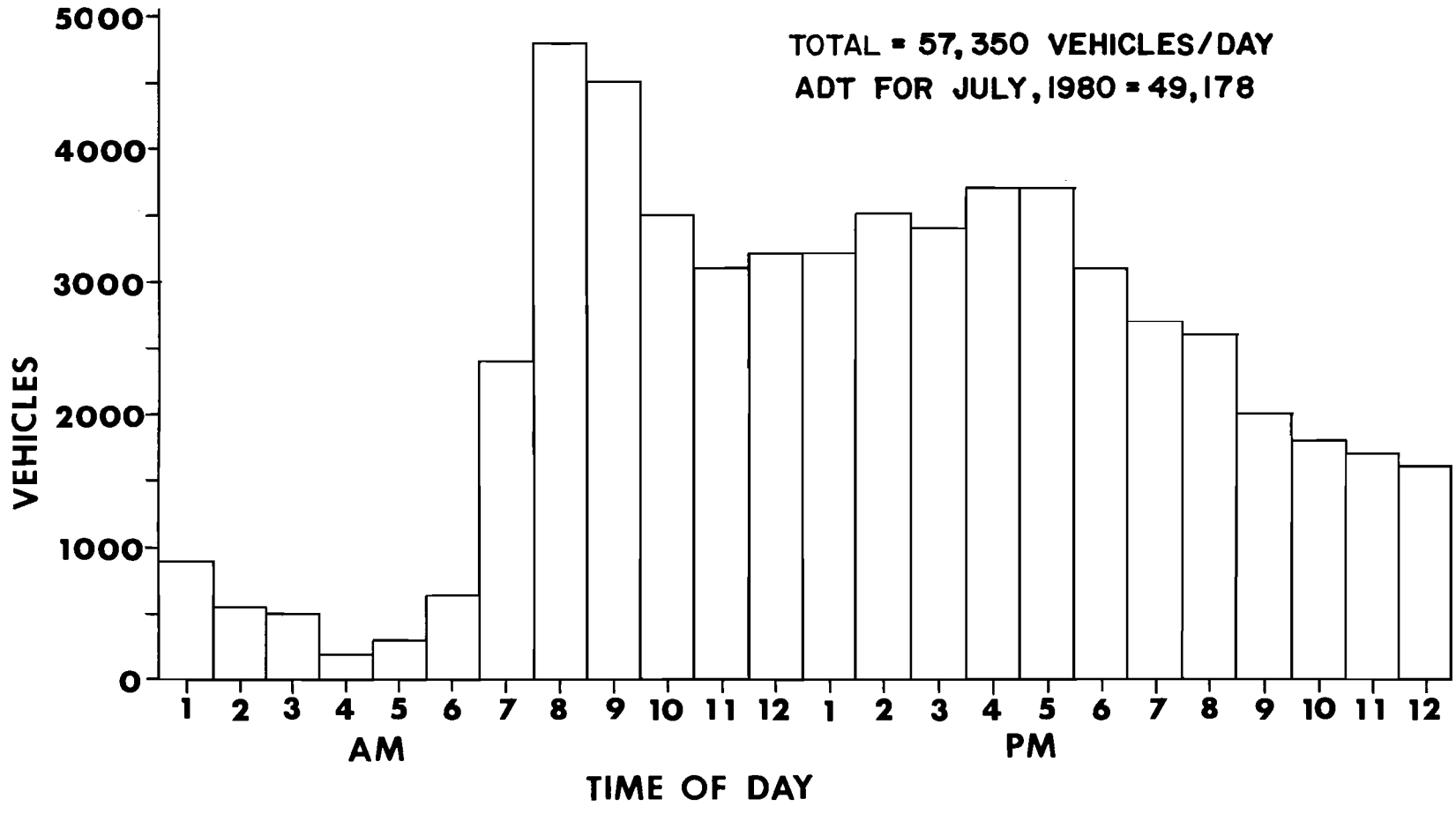

Fig. 4.4 Traffic data for July 11, 1980

TABLE 4.5 FATIGUE-LIFE ESTIMATES AS A FUNCTION OF HOURS/DAY

Variable		LTSI Detail			Modified LTSI Detail		
		Test 7	Test 6	Avg.	Test 7	Test 6	Avg.
24 hours/day	y*	99	47	65	584	275	379
	ADTT	864	1656	1497	864	1656	1497
	ADT	78192	55368	64644	78192	55368	64644
18 hours/day	y	132	62	86	779	367	506
	ADTT	648	1242	1123	648	1242	1123
	ADT	58644	41525	48483	58644	41525	48483
12 hours/day	y	199	94	129	1168	550	759
	ADTT	432	828	748	432	828	748
	ADT	39096	27684	32322	39096	27684	32322
6 hours/day	y	396	188	260	2336	1100	1516
	ADTT	216	414	374	216	414	374
	ADT	19548	13842	16161	19548	13842	16161

*y = fatigue life in years

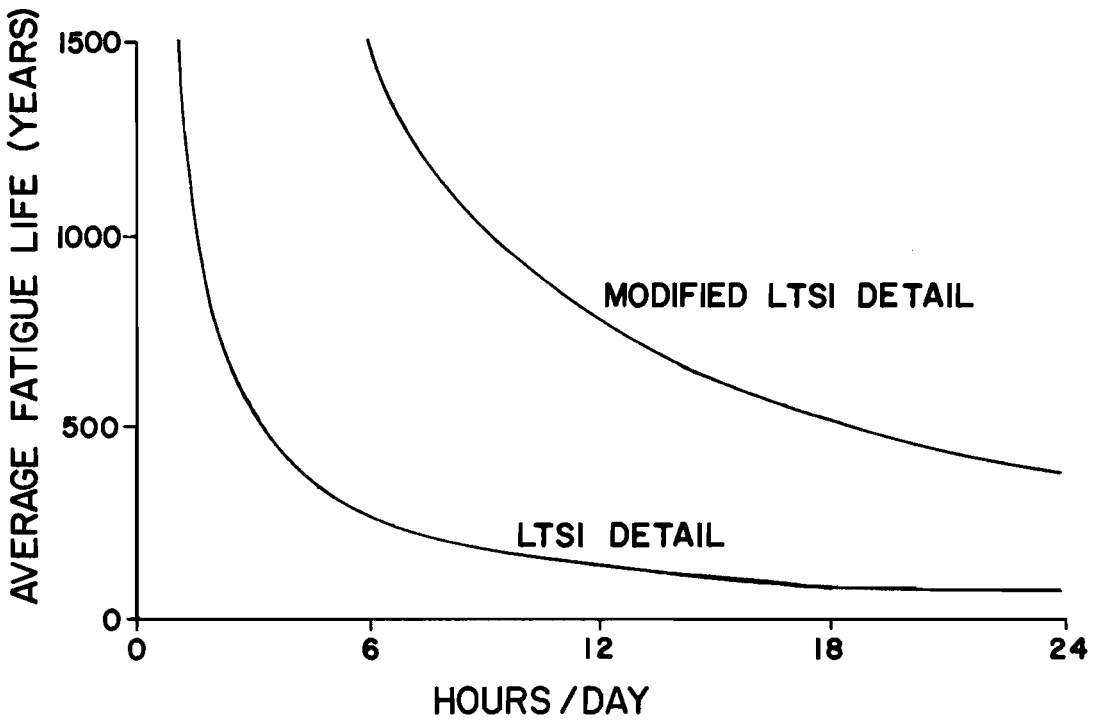

Fig. 4.5 Fatigue-life estimates as a function of hours/day

Figure 4.5 illustrates the variation of fatigue-life estimates for the LTSI and modified LTSI details with the number of hours per day and illustrates the longer fatigue lives of a modified LTSI detail as compared to a LTSI detail.

Based on the traffic count data presented in Fig. 4.4, fatigue damage from 6 p.m. to 6 a.m. is assumed to represent one-half of the fatigue damage which occurs from 6 a.m. to 6 p.m. Therefore, for purposes of this study, fatigue-life estimates will be computed in succeeding sections assuming 18 hours in a day.

4.2.3 Variation in Fatigue Damage During the Week. Figure 4.6 shows the variation in traffic volume during the week at a location on the expressway near the test bridge.[18] The traffic volume during the weekend was considerably less than during the week. Therefore, it is reasonable to assume that fatigue damage is less during the weekend than during the week. One method of modeling the variation in fatigue damage during the week in a fatigue-life estimate is to assume that there are fewer than 7 days in a week. Table 4.6 is a list of fatigue-life estimates for the LTSI detail and a modified LTSI detail for different values of days per week. The fatigue life increases as the number of days in a week decreases. Table 4.6 also lists the ADT and ADTT required to produce the corresponding fatigue lives. The daily traffic count given in Fig. 4.4 is within the range of ADT's computed in Table 4.6 which indicates that these values are reasonable values of ADT to expect for the test bridge. Therefore, the fatigue-life estimates listed in Table 4.6 are reasonable estimates of the fatigue life of the bridge.

Figure 4.7 illustrates the variation of fatigue-life estimates for the LTSI and modified LTSI details with the number of days in a week and illustrates the longer fatigue lives of a modified LTSI detail as compared to a LTSI detail.

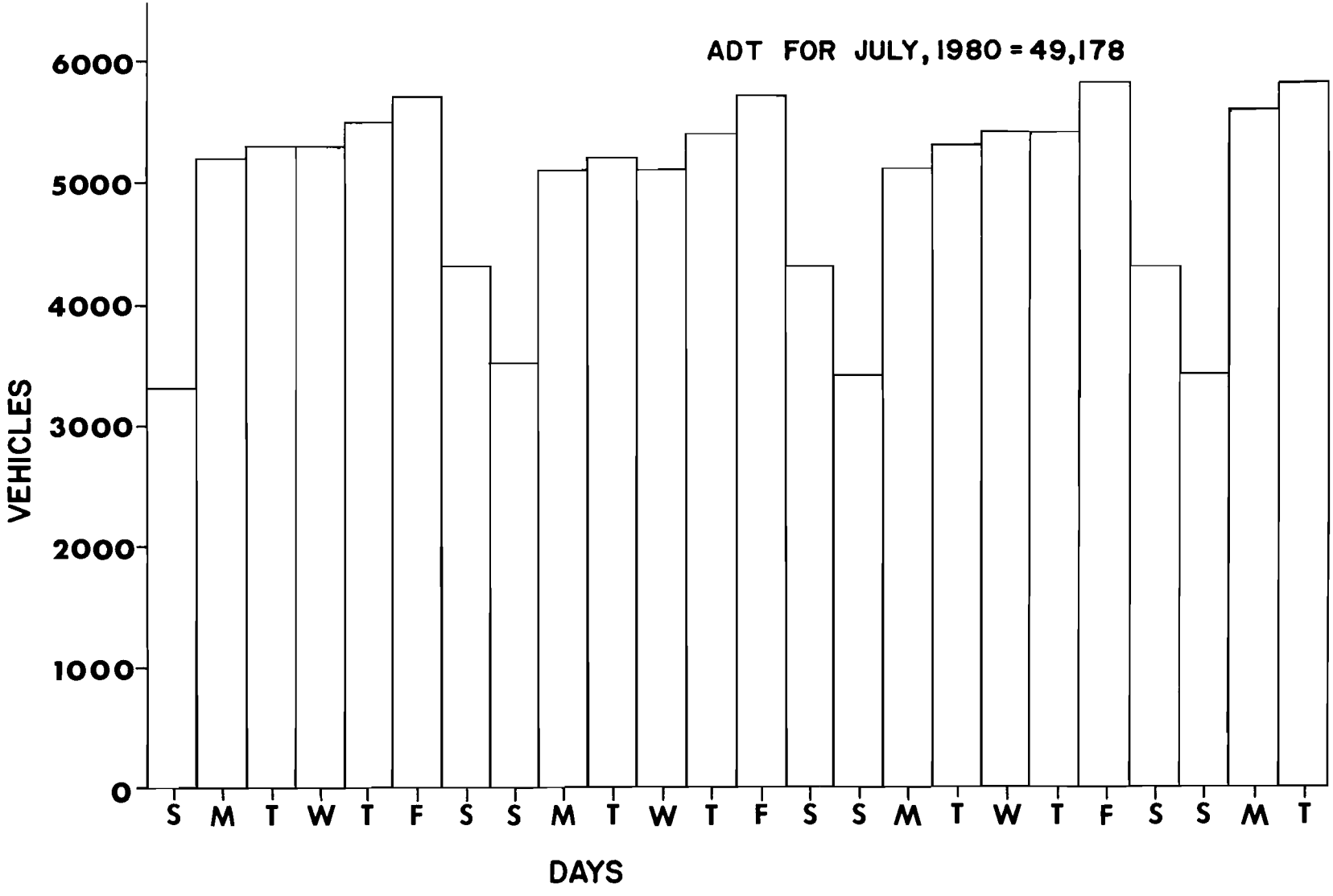

Fig. 4.6 Traffic data beginning July 6, 1980

TABLE 4.6 FATIGUE-LIFE ESTIMATES AS A FUNCTION OF DAYS/WEEK

Variable		LTSI Detail			Modified LTSI Detail		
		Test 7	Test 6	Avg.	Test 7	Test 8	Avg.
7 days/week	y*	132	62	86	779	367	506
	ADTT	648	1242	1123	648	1242	1123
	ADT	58644	41525	48483	58644	41525	48483
6 days/week	y	154	72	100	909	428	590
	ADTT	555	1064	962	555	1064	962
	ADT	50266	35593	41577	50266	35593	41557
5 days/week	y	185	87	120	1091	514	708
	ADTT	463	887	802	463	887	802
	ADT	41888	29661	34631	41888	29661	34631

*y = fatigue life in years

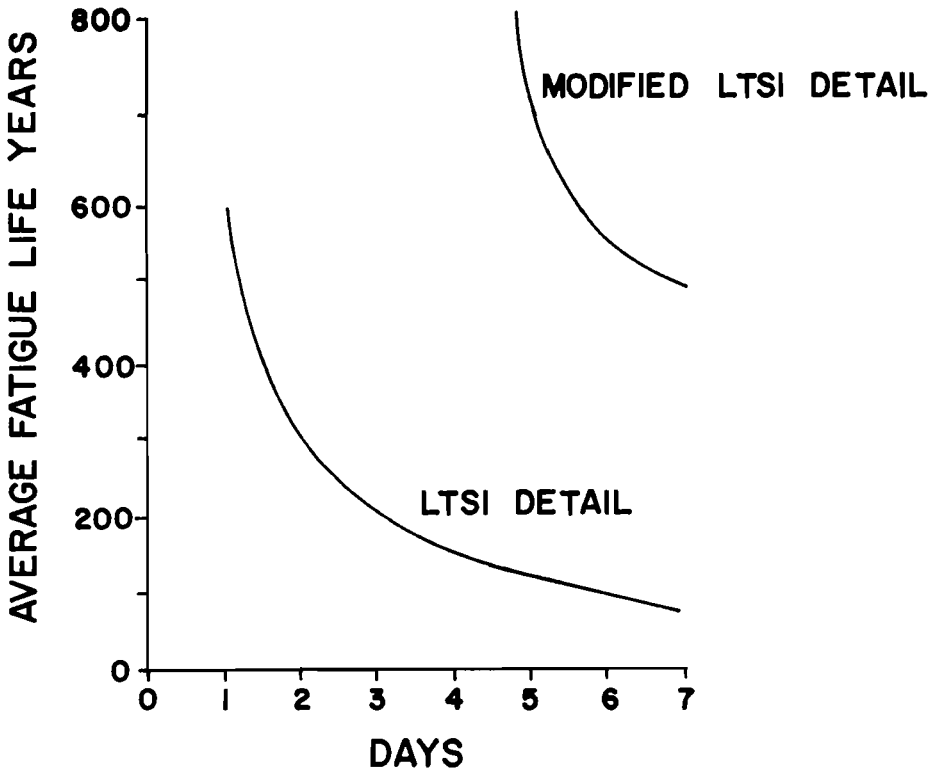

Fig. 4.7 Fatigue-life estimates as a function of days/week

Based on the traffic count data presented in Fig. 4.5, fatigue damage on weekends is assumed to equal the fatigue damage which occurs on one weekday. Therefore, for purposes of this study, fatigue-life estimates will be computed in succeeding sections assuming six days in a week.

4.2.4 Effect of Future Increases in Traffic on Fatigue-Life Estimates. All previous calculations assumed that observed traffic patterns will remain constant throughout the life of the structure. Figure 4.7 is the annual ADT at a location on the expressway near the test bridge for both directions and shows the traffic volume increasing by 43 percent in nine years.[18] The test bridge is located in the downtown section of a large city. The volume of traffic across the bridge will likely increase with the growth of the city. The probable increase in traffic across the bridge can be modeled in fatigue-life estimates by increasing the number of cycles per year to be experienced by the bridge.

The equation relating cycles to failure with effective stress range is

$$N = A \times S_{RE}^{-3} \tag{4.6}$$

The cycles to failure may be represented as the summation of cycles each year as follows:

$$N = \sum_{i=1}^{m} N_y \tag{4.7}$$

where

m = years to failure

N_y = cycles per year

The number of cycles per year is given by:

$$N_y = N_m \times \frac{60 \text{ min.}}{\text{hour}} \times \frac{18 \text{ hours}}{\text{day}} \times \frac{6 \text{ days}}{\text{week}} \times \frac{52 \text{ weeks}}{\text{year}} \tag{4.8a}$$

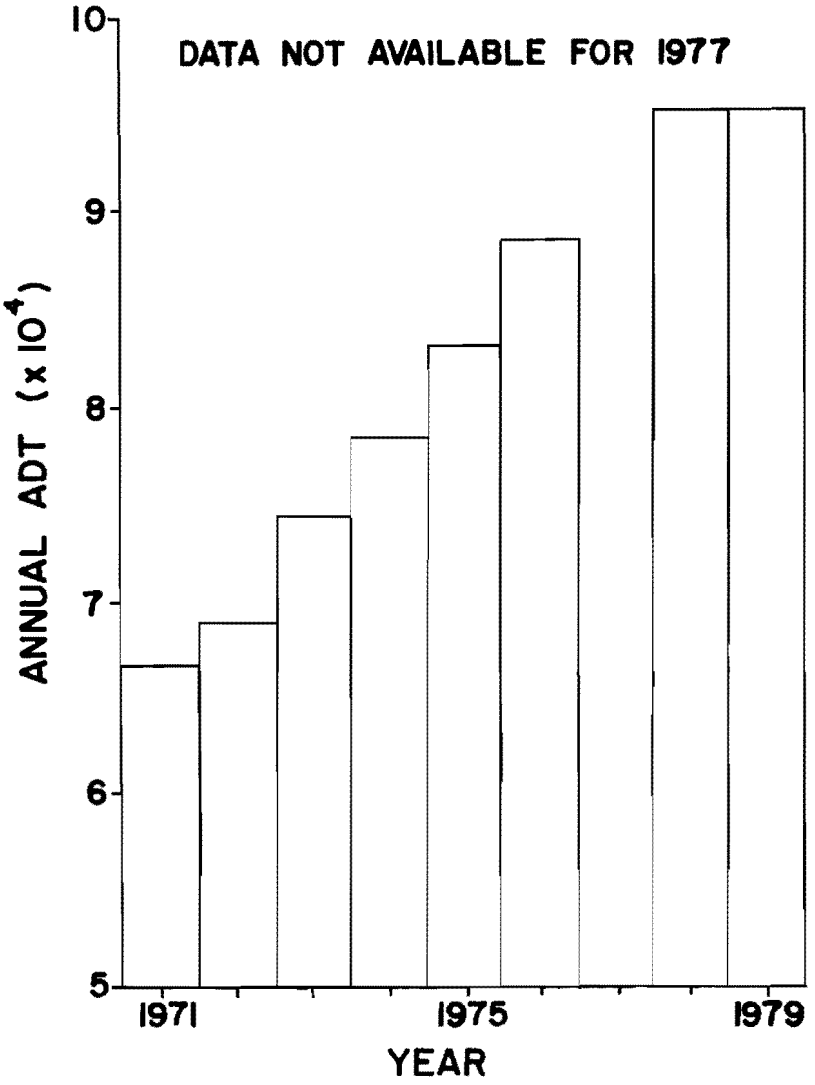

Fig. 4.8 Annual ADT for a location near the test bridge in both directions

or more simply

$$N_y = 336{,}960 \times N_m \tag{4.8b}$$

where N_m is the number of cycles per minute observed in the traffic tests. Substituting Eq. (4.7) and Eq. (4.8b) into Eq. (4.6) yields

$$\sum_{i=1}^{m} (336{,}960 \times N_m) = A \times S_{RE}^{-3} \tag{4.9}$$

Assuming N_m increases by some percentage rate each year, Eq. (4.9) becomes

$$336{,}960 \times \sum_{i=1}^{m} \left[N_m \times (1 + r)^{(m-1)} \right] = A \times S_{RE}^{-3} \tag{4.10}$$

where N_m is the cycles per minute the initial year and r is the decimal equivalent of the annual percentage increase in cycles. Rearranging Eq. (4.10) yields

$$\sum_{i=1}^{m} (1 + r)^{(m-1)} = \frac{A}{336{,}960 \times N_m \times S_{RE}^{-3}} \tag{4.11}$$

The parameter N_L is given by

$$N_L = \frac{1}{N_m \times S_{RE}^{-3}} \tag{4.12}$$

as described in Chapter 3. Substituting the definition of N_L into Eq. (4.11) yields

$$\sum_{i=1}^{m} (1 + r)^{(m-1)} = \frac{A \times N_L}{336{,}960} \tag{4.13}$$

The left side of Eq. (4.13) is a geometric progression. Its sum is given by

$$\sum_{i=1}^{m} (1 + r)^{(m-1)} = \frac{(1 + r)^{m} - 1}{r} \tag{4.14}$$

Substituting Eq. (4.14) into Eq. (4.13) and solving for m, the years to failure, yields

$$m = \frac{\log\left[\frac{A \times N_L \times r}{336,960} + 1\right]}{\log(1 + r)} \tag{4.15}$$

Figure 4.9(a) shows fatigue-life estimates of a LTSI detail and a modified LTSI detail for different values of r, the annual percent increase in cycles. The fatigue life decreases sharply for small percentage increases in cycles because the increases accumulate each year. Fagure 4.9a shows that the modified LTSI detail has a longer fatigue life than the LTSI detail.

Figure 4.9b shows the ADT in the last year of the fatigue life for the LTSI and modified LTSI details for different values of r. The ADT presented in Fig. 4.4 is also shown in Fig. 4.9b. Most of the ADT's in Fig. 4.9b are much larger than the ADT measured in July 1980 and may exceed the physical limitations of the bridge. Therefore, only a 1.0 percent annual increase in cycles will be considered in subsequent sections in fatigue-life estimates in order to model probable increases in ADT.

4.2.5 Effect of Increases in the Effective Stress Range on Fatigue-Life Estimates. Future increases in allowable axle loads can affect the fatigue life of the test bridge. The effective stress range can be varied in order to model future changes in axle loads.

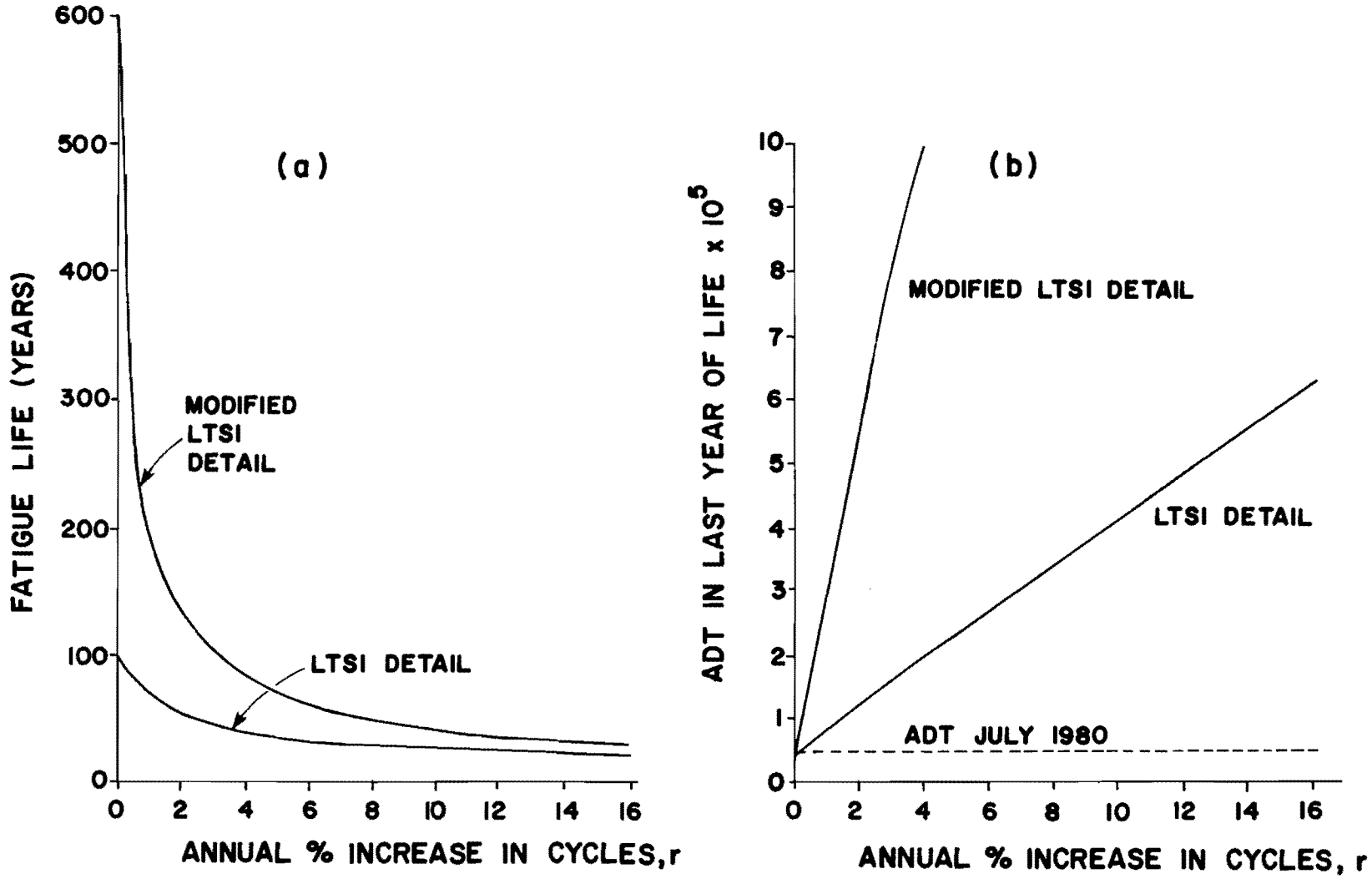

Fig. 4.9 Fatigue-life estimates and ADT with annual increase in cycles

The equation for N_L is

$$N_L = \frac{A}{N_m \times S_{RE}^{-3}} \tag{4.16}$$

Assuming S_{RE} changes by some percentage rate, q, yields a change in N_L as follows

$$N_L = \frac{A}{N_L \times \left[(1 + q) \times S_{RE}\right]^{\beta}} \tag{4.17}$$

Figure 4.10 shows fatigue-life estimates for the LTSI and modified LTSI details for different values of q. Small percent changes in S_{RE} do not significantly affect fatigue-life estimates. For example, a 5 percent increase in S_{RE} yields a 14 percent decrease in fatigue life. A 5 percent increase in S_{RE} does not mean a 5 percent increase in axle loads; only that some change in axle loads increases the effective stress range by 5 percent.

A 5 percent increase in S_{RE} will be considered in subsequent sections in fatigue-life estimates in order to model future increases in axle loads.

4.2.6 Fatigue-Life Estimates Combining All Variables Affecting Fatigue Life. The variables affecting fatigue life were combined to compute the fatigue-life estimates of the test bridge listed in Table 4.7. These estimates assume fatigue damage occurs 18 hours per day, 6 days per week. A 1 percent annual increase in cycles is assumed to account for future increases in traffic. A 5 percent increase in S_{RE} is assumed to account for future increases in axle load limits. The ADT and ADTT listed in Table 4.7 represent values in the last year of the fatigue life.

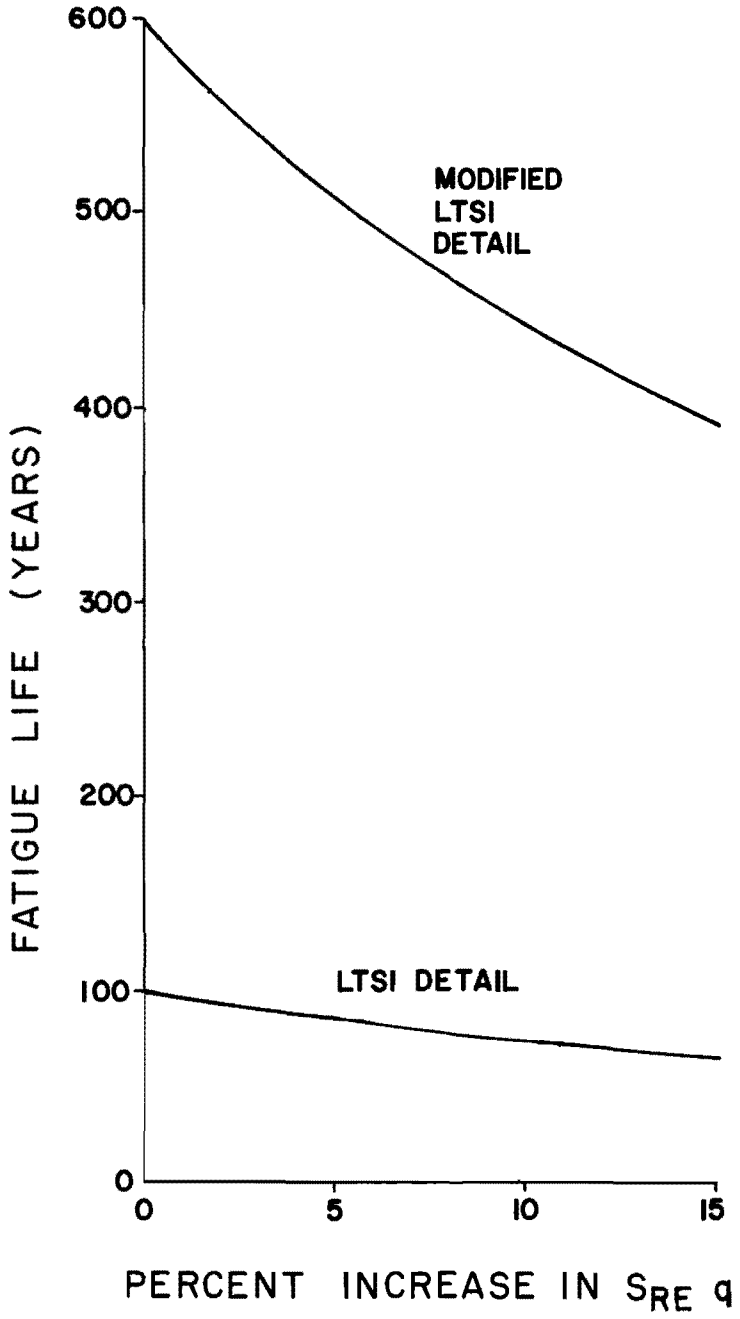

Fig. 4.10 Variation of fatigue life with a percent increase in S_{RE}

The fatigue-life estimates for the LTSI detail indicate that a fatigue failure could occur in 49 to 85 years. The ADT for Test 6 is 17 percent greater than the ADT in July 1980 listed in Fig. 4.4, which is a smaller percent increase than the case shown in Fig. 4.8. The ADTT for the LTSI detail represents a maximum of 1.2 trucks per minute which is a reasonable value to expect for a busy highway bridge. This data indicate that a fatigue failure could occur in the LTSI detail during the probable service life of the structure.

The fatigue-life estimates for the modified LTSI detail indicate that a fatigue failure could occur in 155 to 219 years. The ADT's for the modified LTSI detail probably exceed the physical limitations of the bridge. This data indicate that a fatigue failure will not occur in a modified LTSI detail during the expected service life of the structure.

TABLE 4.7 FATIGUE-LIFE ESTIMATES COMBINING ALL VARIABLES AFFECTING FATIGUE LIFE

	LTSI Detail			Modified LTSI Detail		
	Test 7	Test 6	Avg.	Test 7	Test 6	Avg.
y*	85	49	63	219	155	182
ADT**	115,950	57,384	77,014	439,880	164,762	251,659
ADTT**	1,280	1,715	1,783	4,857	4,925	5,826

*y = Fatigue life in years

**Values in the last year of life

4.3 Fatigue-Life Estimates from Test Truck Data

The parameter N_{LT} was computed from tests conducted with a test truck and represents the number of test trucks required to cause a failure of a particular detail on the test bridge. The values of N_{LT} for the LTSI detail are listed in Table 4.3.

The number of test trucks, T, required to cause a fatigue failure in a particular detail is given by

$$T = A \times N_{LT} \tag{4.18}$$

and the number of test trucks required each day, TTD, is given by

$$TTD = \frac{T}{D} \tag{4.19}$$

where D is the number of days in the service life of the bridge. Values of TTD from the test-truck data can be compared with values of ADTT from the traffic test data given in Table 4.7 to indicate if the corresponding fatigue-life estimates are valid.

An average value of T for the 50 mph tests is presented in Table 4.8 for the LTSI detail. Values of TTD are computed using the fatigue-life estimates for the LTSI detail from Table 4.7 and represent the required number of trucks per day similar to the test truck needed to yield the corresponding service life. For example, if 805 test trucks cross the test bridge daily, then the fatigue life of the bridge is 49 years.

The test truck represents the worst loading case for the test bridge. Therefore, only a fraction of the ADTT will be similar to the test truck. The maximum values of the ADTT corresponding to the expected service lives are listed in Table 4.8. The values of the TTD are between 35 percent and 47 percent of the corresponding ADTT. The exact proportion of test trucks to the ADTT is not known for the test bridge, however, because the TTD's are only a

TABLE 4.8 FATIGUE-LIFE ESTIMATES FROM TEST-TRUCK DATA

Expected Service Life (years)	LTS Detail		
	T (trucks)	TTD	ADTT*
49	1.41×10^7	805	1715
63	1.41×10^7	634	1783
85	1.41×10^7	477	1200

*ADTT in the last year of life

fraction of the ADTT, then the corresponding fatigue-life estimates are reasonable estimates for the test bridge. If the TTD's were greater than the ADTT, then the corresponding fatigue-life estimates would be questionable.

4.4 Design Application of Traffic Test Data

The test data presented in this study may be used to estimate the fatigue life of a bridge in the design phase. Values of S_{RE} and N_m computed from traffic test data and the ADTT and the design stress range, S_{RD}, for the test bridge are used with the ADTT and S_{RD} for the design bridge to compute cycles per minute and an effective stress range for the bridge being designed. In order to simplify this procedure, average values of S_{RE} and N_m at the web-to-flange fillet weld at Section D will be used. The average values of S_{RE} and N_m at Section D are computed from the data in Table 3.6, and are listed below with the ADTT and S_{RD} at the web-to-flange fillet weld for the test bridge.

$$S_{RE} = 0.781 \text{ ksi} \tag{4.20a}$$

$$N_m = 182 \tag{4.20b}$$

$$ADTT = 1497 \tag{4.20c}$$

$$S_{RD} = 13.7 \text{ ksi} \tag{4.20d}$$

The effective stress range for a bridge in the design phase, S'_{RE}, is given by

$$S'_{RE} = \frac{S_{RE}}{S_{RD}} \times S'_{RD} = \frac{0.781 \text{ ksi}}{13.7 \text{ ksi}} \times S'_{RD} \tag{4.21}$$

where S_{RE} and S_{RD} are given in Eq. (4.20a) and Eq. (4.20d) for the test bridge and S'_{RD} is the design stress range at the web-to-flange fillet weld for the design bridge. The number of cycles per minute for a bridge in the design phase, N'_m, is given by

$$N'_m = \frac{N_m}{ADTT} \times ADTT' = \frac{182}{1497} \times ADTT' \tag{4.22}$$

where N_m and ADTT are given in Eq. (4.20b) and Eq. (4.20c) for the test bridge, and ADTT′ corresponds to the design bridge. A fatigue-life estimate, Y, for a bridge in the design phase is given by

$$Y = \frac{A}{N'_m \times S'^{3}_{RE}} \times \frac{1 \text{ hr.}}{60 \text{ min.}} \times \frac{1 \text{ day}}{24 \text{ hrs.}} \times \frac{1 \text{ yr.}}{365 \text{ days}} \tag{4.23}$$

where A is the value for a Category B detail, a web-to-flange fillet weld, given in Table 4.2, and Y is the fatigue-life estimate in years assuming damage occurs 24 hours a day, 365 days a year. Substituting Eq. (4.21) and Eq. (4.22) into Eq. (4.23) yields

$$Y = \frac{ADTT}{ADTT'} \times \frac{S^3_{RD}}{S'^{3}_{RD}} \times \frac{A}{N_m \times S^3_{RE}} \times \frac{1}{525{,}600} \tag{4.24a}$$

or more simply,

$$Y = \frac{8.78 \times 10^8}{ADTT' \times S'^{3}_{RD}} \qquad (4.24b)$$

An example follows.

Example 1. Let,

$$S'_{RD} = 10 \text{ ksi}$$

and

$$ADTT' = 1000$$

The estimated fatigue life using Eq. (4.24b) is

$$Y = \frac{8.78 \times 10^8}{1000 \times 10^3} = 878 \text{ years}$$

The process of estimating a fatigue life for a bridge in the design phase can be summarized in two steps: (1) compute the ADTT and the design stress range at the web-to-flange fillet weld; and then (2) substitute the ADTT and S_{RD} into Eq. (4.24b) to compute a fatigue-life estimate.

The estimates given by Eq. (4.24b) assume that the design bridge is similar in material and structural configuration to the test bridge. Also, future traffic patterns on the design bridge are assumed to be similar to traffic patterns on the test bridge, and the web-to-flange fillet weld is assumed to control the fatigue life. Therefore, fatigue-life estimates given by Eq. (4.24b) are only an indication of the fatigue life of the design bridge and should only be considered as an order of magnitude estimate.

CHAPTER 5

SUMMARY AND CONCLUSIONS

Stress histories were obtained from a welded steel girder highway bridge. Two types of stress histories were measured, the first measured during the passage of a truck of known weight and the second measured during normal traffic conditions. Stress ranges and stress range cycles were obtained from these stress histories using the Rainflow Cycle Counting method. This method was chosen over other cycle counting methods because the Rainflow method:

(1) adequately counts stress-range cycles in a constant amplitude stress history;

(2) uses all parts of a modified stress history; and

(3) includes both the major and minor stress-range cycles.

Miner's law was used in conjunction with the Rainflow Cycle Counting method to compute the effective stress range, S_{RE}. The effective stress range concept was used to reduce a variable amplitude stress history to a constant amplitude stress range for use in predicting fatigue lives of welded steel details under a variable amplitude load. The effective stress range and number of cycles were used to compute fatigue-life estimates of the test bridge. Fatigue-life estimates were expressed in terms of years to failure and number of test trucks to failure. Variables affecting the fatigue life of the structure, including variable amount of fatigue damage per day and per week, probable increases in traffic and allowable loads, were incorporated in the fatigue-life estimates.

The longitudinal transverse stiffener intersection, LTSI, detail controls the fatigue life of the test bridge. Fatigue-life

estimates of the LTSI detail range from 49 years to 85 years, which indicates that a fatigue failure could occur within the probable service life of the structure.

A modification of the LTSI detail significantly improves its fatigue life.[16] Fatigue-life estimates of a modified LTSI detail on the test bridge ranged from 155 years to 219 years, which indicates that a fatigue failure would not occur during the probable service life of the structure if a modified LTSI detail is employed. It is the recommendation of this study that the modified LTSI detail be used on the test bridge to increase the fatigue life.

The parameter, N_L, derived from the traffic test data, represents the fatigue life of a detail under normal traffic loading. This parameter can be used with the ADTT to estimate the fatigue life of a similar type bridge during the design phase.

A P P E N D I X A

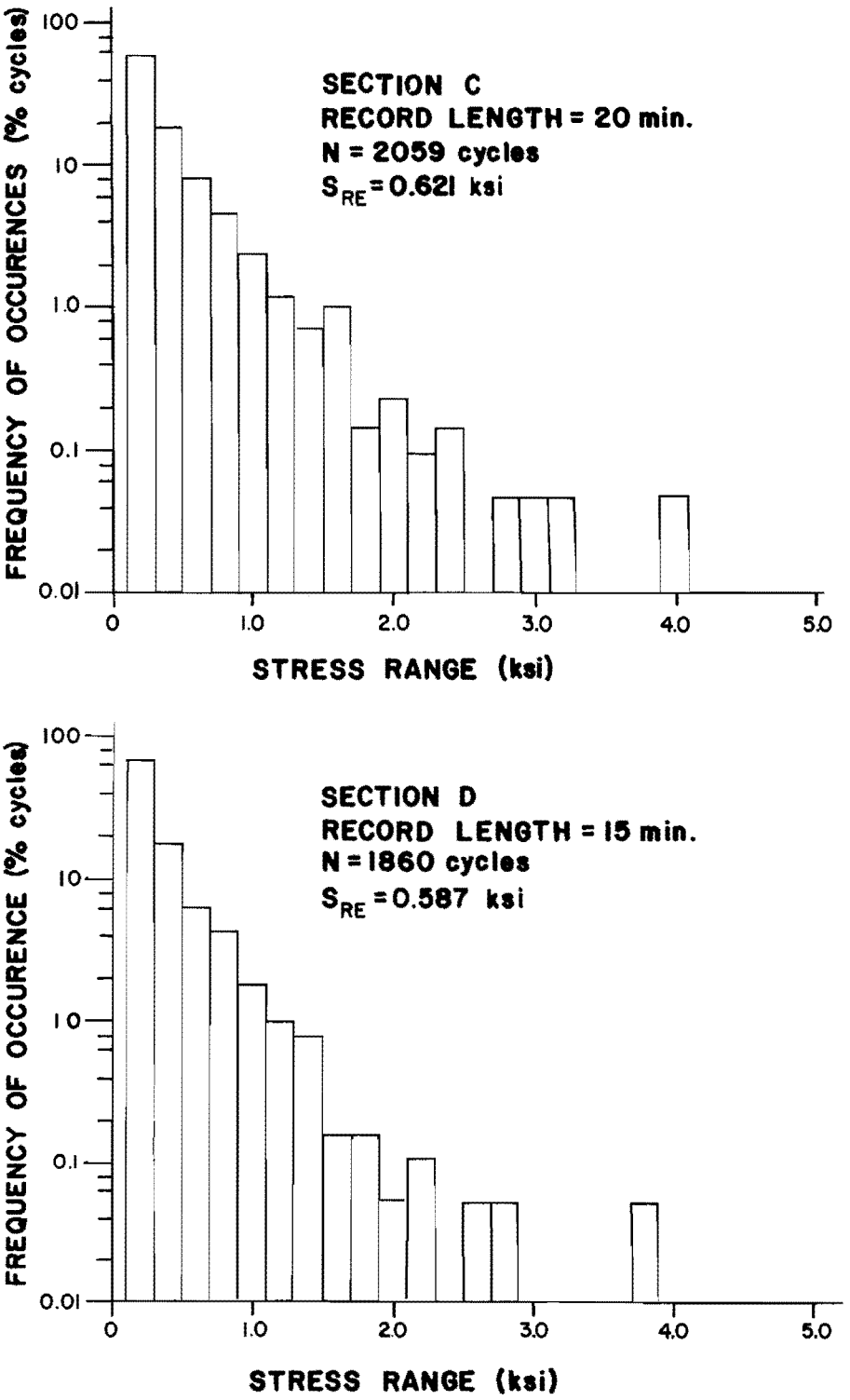

Fig. A.1 Stress histograms for Test 1

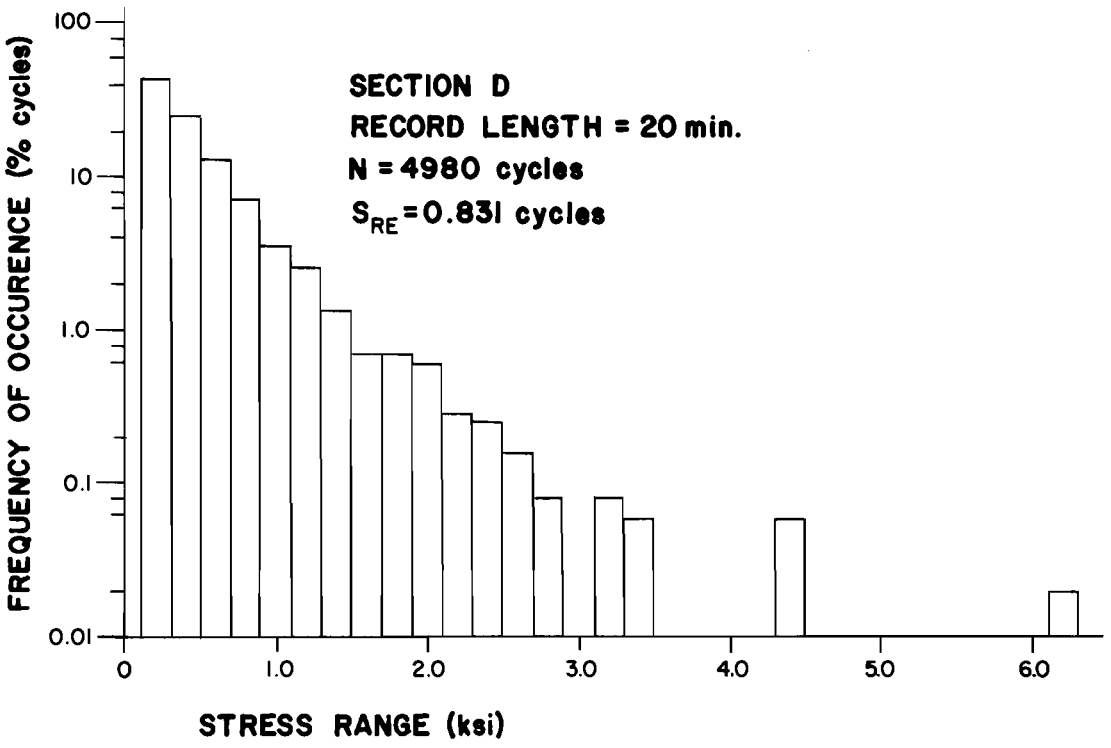

Fig. A.2 Stress range histogram for Test 2

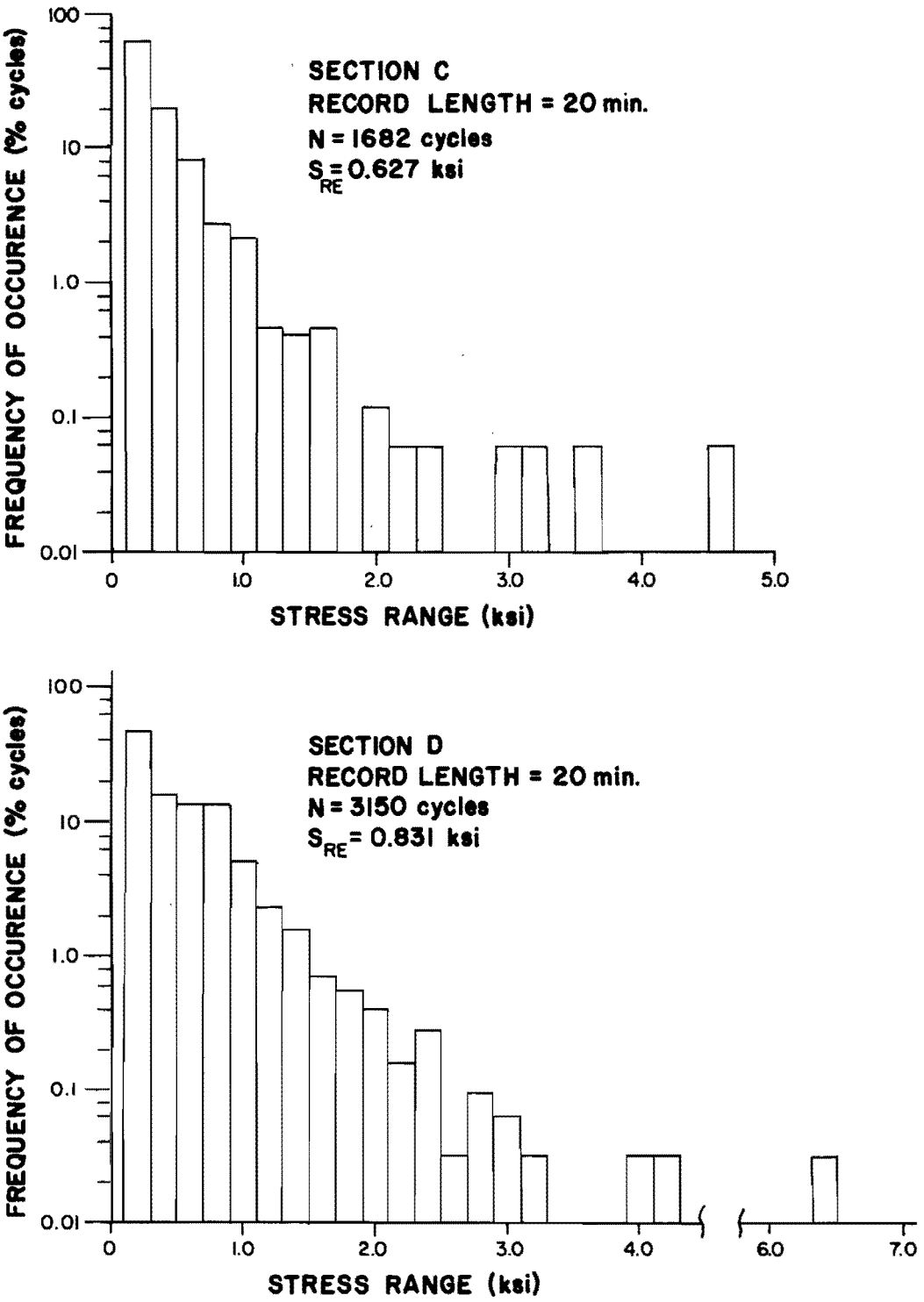

Fig. A.3 Stress histograms for Test 3

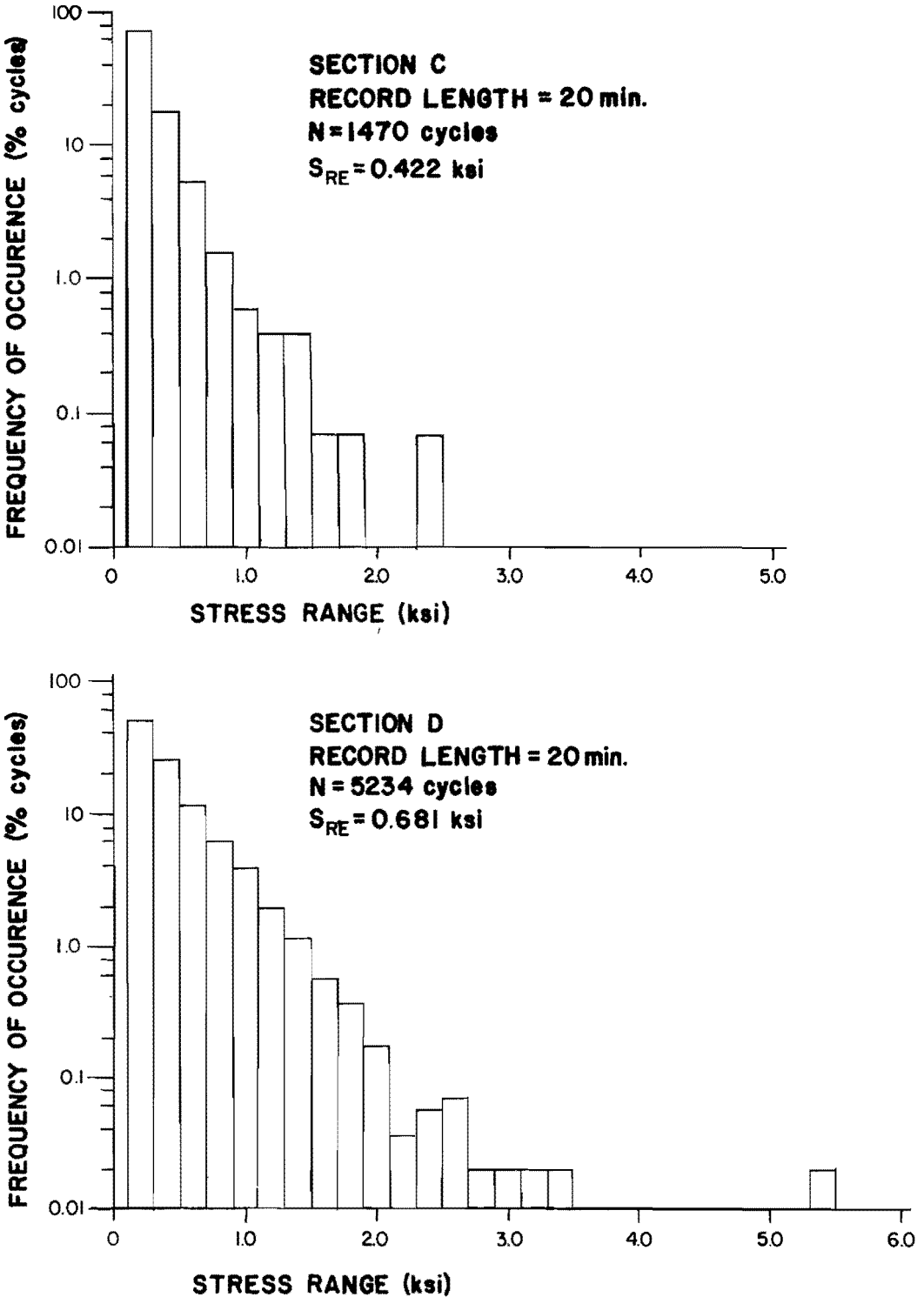

Fig. A.4 Stress range histograms for Test 4

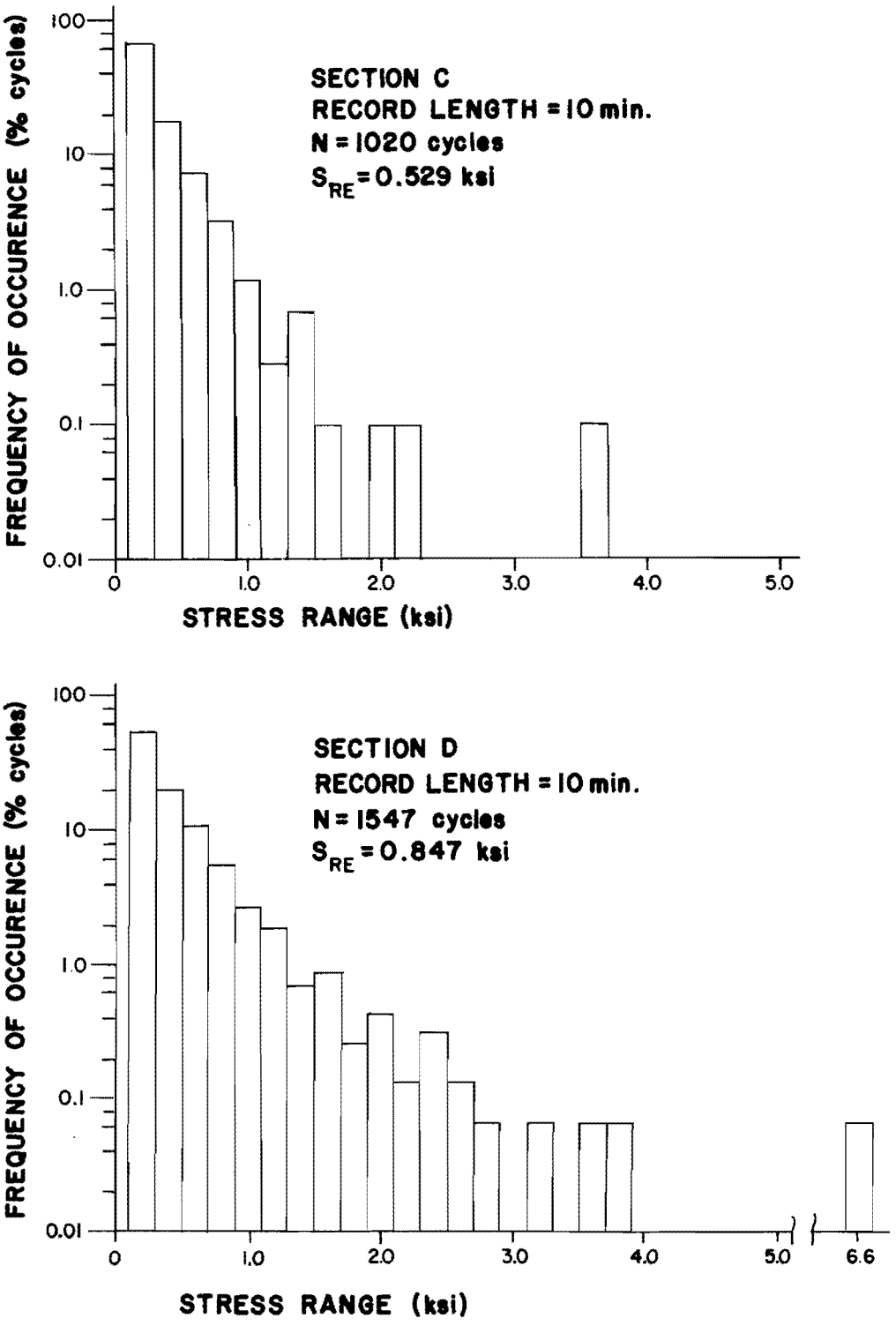

Fig. A.5 Stress range histograms for Test 5

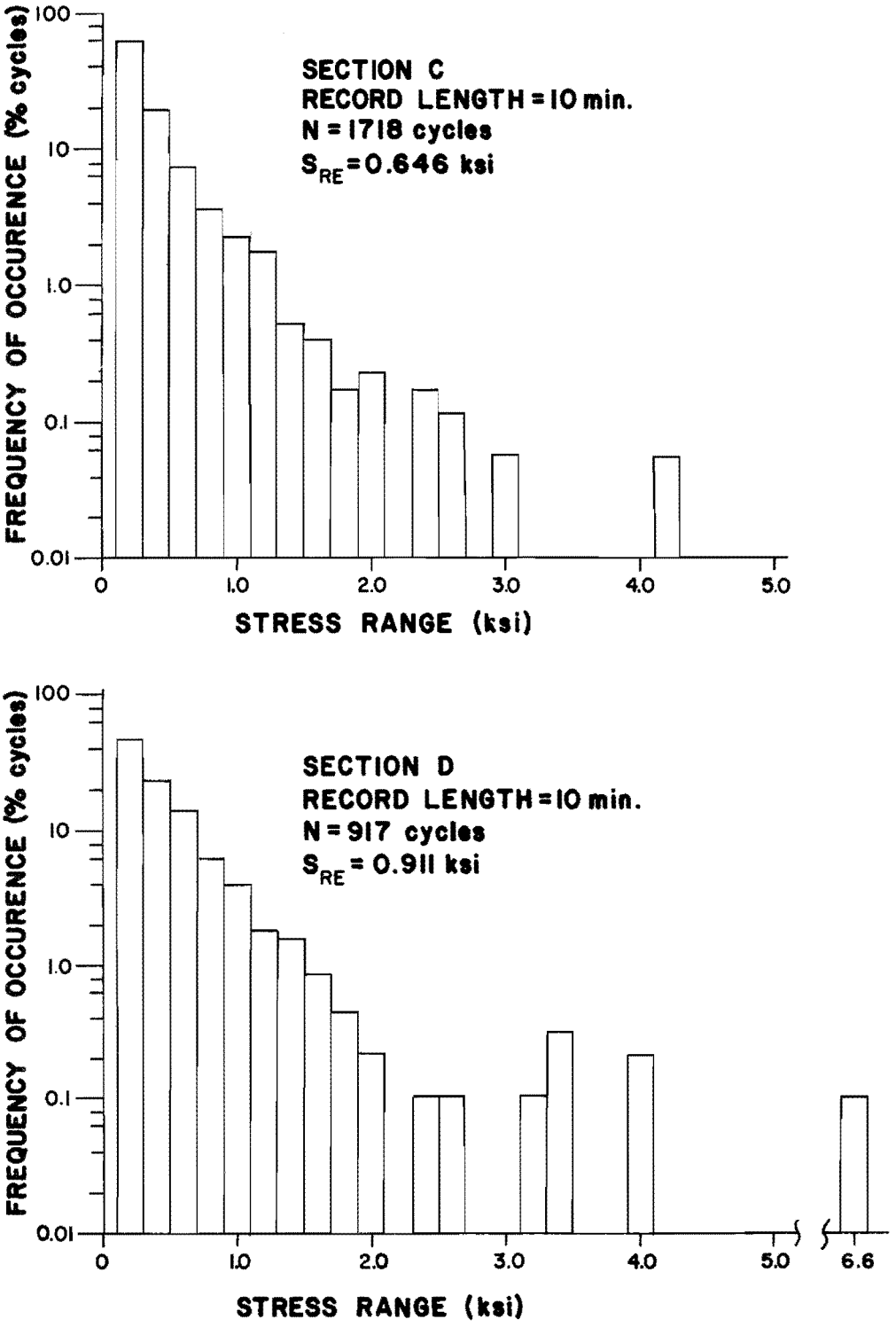

Fig. A.6 Stress range histograms for Test 6

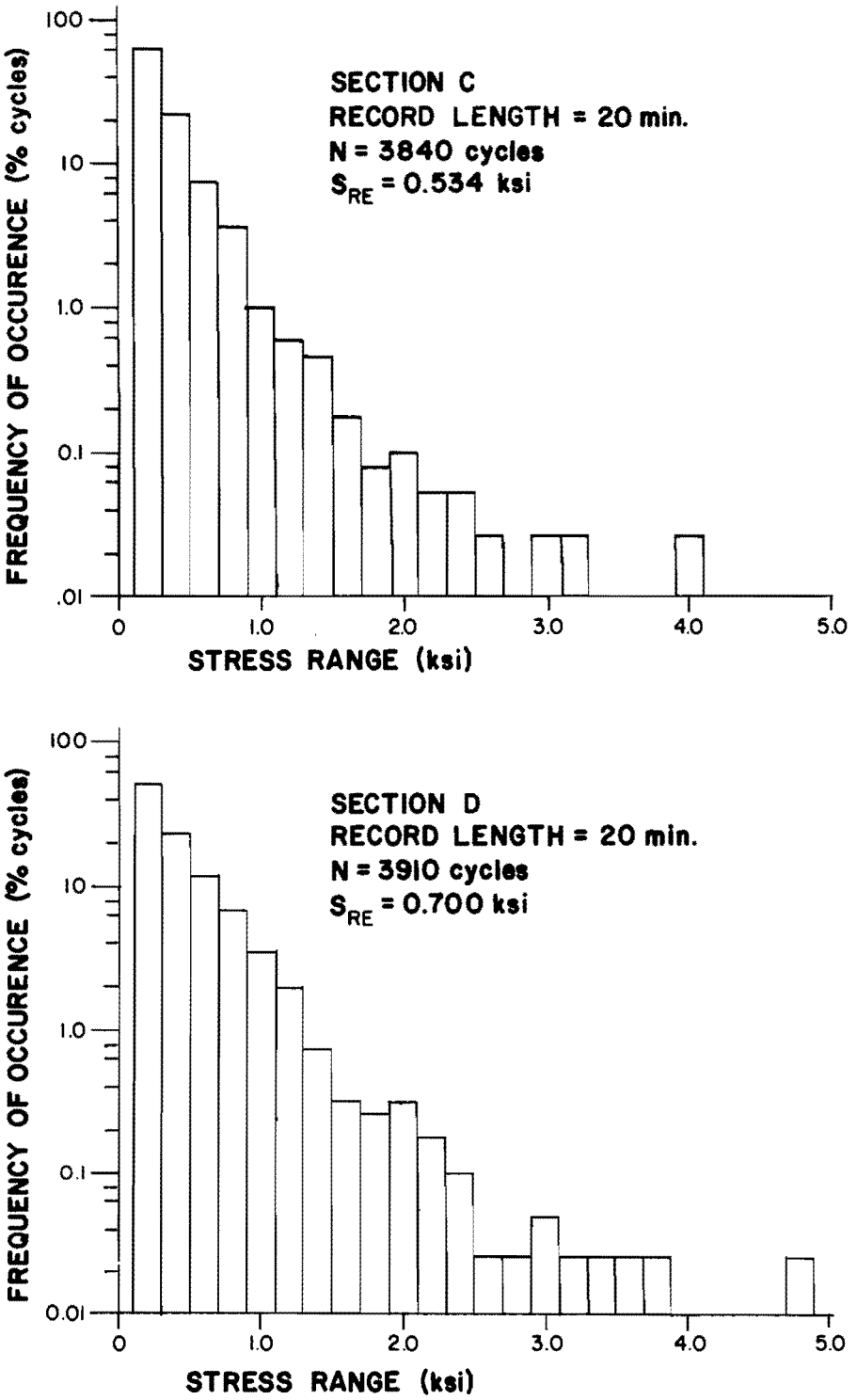

Fig. A.7 Stress range histograms for Test 7

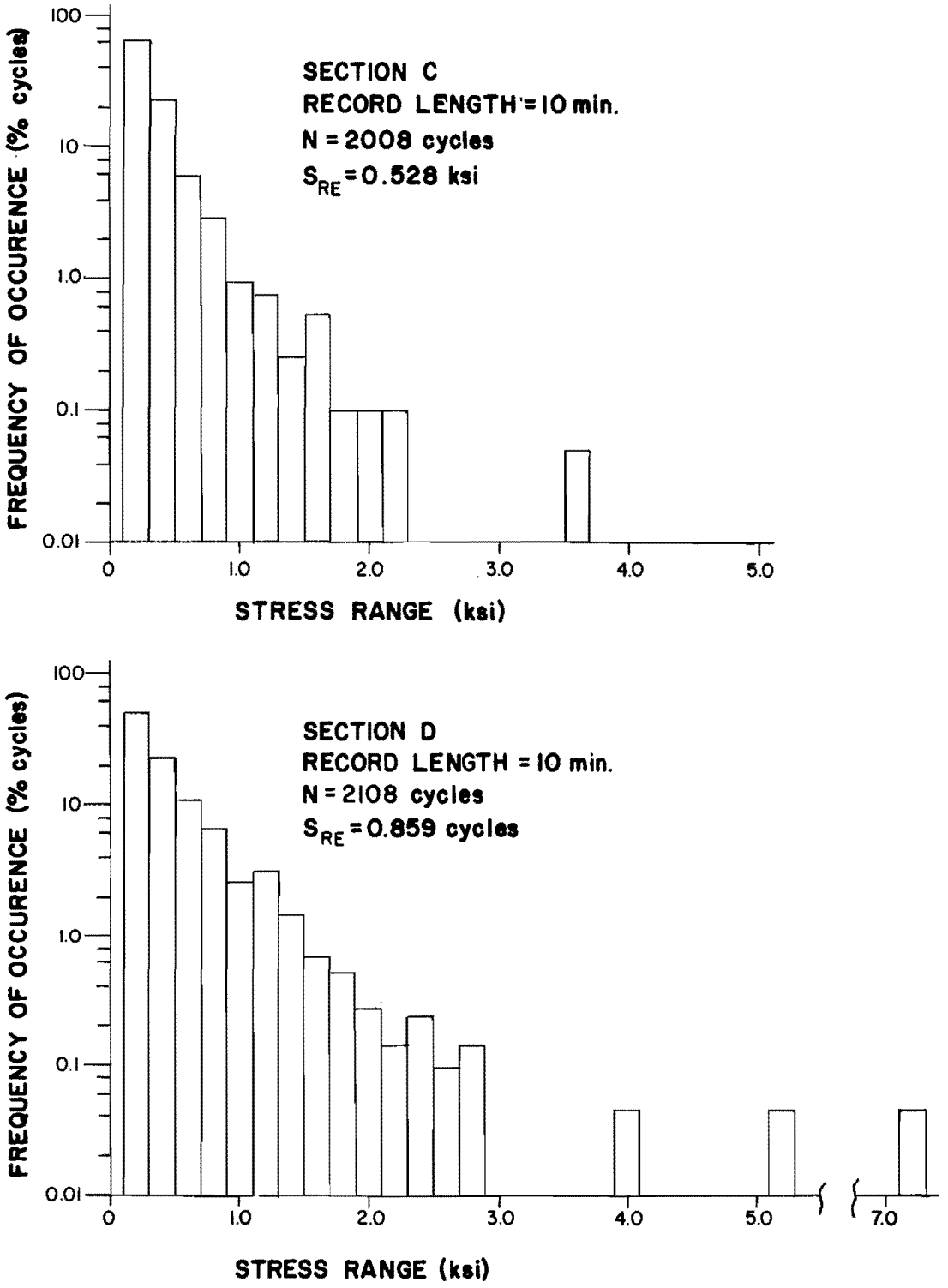

Fig. A.8 Stress range histograms for Test 8

REFERENCES

1. Fisher, J. W., K. H. Frank, M. A. Hirt and B. M. McNamee, Effect of Weldments on the Fatigue Strength of Steel Beams," NCHRP Report 102, Highway Research Board, 1970.

2. Fisher, J. W., P. A. Albrecht, B. T. Yen, D. J. Klingerman, and B. M. McNamee, "Fatigue Strength of Steel Beams, with Transverse Stiffeners and Attachments," NCHRP Report 147, Highway Research Board, 1974.

3. Standard Specifications for Highway Bridges, American Association of State Highway and Transportation Officials, Washington, D.C., 1977.

4. Miner, M. A., "Cumulative Damage in Fatigue," Journal of Applied Mechanics, Vol. 12, Sept. 1945.

5. Schilling, C. G., K. H. Klippstein, J. M. Barson and G. T. Blake, "Fatigue of Welded Steel Bridge Members under Variable-Amplitude Loadings," Final Report, NCHRP Project 12-12, Transportation Research Board, Aug. 1975.

6. Bowers, D. G., "Loading History, Span No. 10 Yellow Mill Pond Bridge I-95, Bridgeport Connectivut," Research Project NPR 175-332, Dept. of Transportation, Conn., May 1972.

7. Yen, B. T., N. M. Marchica and J. W. Fisher, "Stress Measurements and Behavior of the Lehigh Canal Bridge," Fritz Engineering Laboratory Report 386.1, Lehigh University, Dec. 1973.

8. Fisher, J. W., Bridge Fatigue Guide--Design and Details, American Institute of Steel Construction, 1221 Avenue of the Americas, New York, N.Y. 10020, 1977.

9. Wirshing, P. H. and A. M. Shehata, "Fatigue under Wide Band Random Stresses Using the Rain-Flow Method," Journal of Engineering Materials and Technology, July 1977, pp. 205-211.

10. Wirshing, P. H. and M. C. Light, "Fatigue under Wide Band Random Stresses," Journal of the Structural Division, ASCE, July 1980, pp. 1593-1607.

11. Mercer, C. A. and J. Livesey, "Statistical Counting Methods as a Means of Analysing the Load Histories of Light Bridges," Journal of Sound and Vibration (1973) 27(3), pp. 399-410.

12. British Standards Institution, "Steel Concrete and Composite Bridges," Port 10 Code of Practice for Fatigue, BS5400, London, 1980.

13. Tilly, G. P. and J. Page, "A Review of Traffic Loads and Stresses in Steel Bridges," Transport and Road Research Laboratory, Supplementary Report 596, 1980.

14. Schijive, J., "The analysis of Random Load-Time Histories with Relation to Fatigue Tests and Life Calculations," Fatigue of Aircraft Structures, Symposium on Fatigue of Aircraft Structures, Paris 1961, edited by W. Barrois and E. L. Ripley, MacMillan, 1963.

15. Dowling, N. E., "Fatigue Failure Predictions for Complicated Stress-Strain Histories," Journal of Materials, Vol. 7, No. 1, March 1972, pp. 71-87.

16. Pass, J., K. H. Frank, and J. A. Yura, "Experimental Fatigue Behavior of Longitudinal-Transverse Stiffener Intersection," Research Report 247-5F, Center for Transportation Research, Bureau of Engineering Research, The University of Texas at Austin, September, 1982.

17. Yura, J. A., K. H. Frank, and A. K. Gupta, "Field Tests of a Continuous Twin Girder Steel Bridge," Research Report 247-2, Center for Transportation Research, Bureau of Engineering Research, The University of Texas at Austin, November 1981.

18. Texas State Department of Highways and Public Transportation, Traffic Recorder Record, Transportation Planning Division, unpublished data received from R. L. Reed, State Department of Highways and Public Transportation.